UNIVERSITY OF CALIFORNIA,
IRVINE

Immunomodulatory Effects of Engineered Biomimetic Materials

DISSERTATION

Submitted in partial satisfaction of the requirements
for the degree of

DOCTOR OF PHILOSOPHY

in Chemical and Biomolecular Engineering

by

Esther Yu-Tin Chen

Dissertation Committee:
Professor Wendy F. Liu, Chair
Professor Andrea J. Tenner
Professor Szu-Wen Wang

2019

TABLE OF CONTENTS

page

TABLE OF CONTENTS *I*

LIST OF FIGURES *IV*

ACKNOWLEDGMENTS *VI*

CURRICULUM VITAE *VII*

ABSTRACT *VIII*

1. Chapter 1: Background Information *1*

1.1 Foreign body response **1**

1.2 Approaches to reduce the foreign body response **5**

1.3 CD200 as an immunomodulatory molecule **7**

1.4 Poly(lactic-co-glycolic acid) (PLGA) as a biomaterial **10**

1.5 Immunomodulatory PLGA with different geometries **12**

2. Chapter 2: CD200-coated PLGA materials for tissue engineering *13*

2.1 Introduction **13**

2.2 Experimental Design **15**

2.2.1 Production of CD200 from mammalian cells 15

2.2.2 Fabrication of PLGA film and microparticles 17

2.2.3 Conjugation of CD200 on PLGA (Biotin-streptavidin conjugation) 17

2.2.4 Characterization of CD200-coated PLGA 18

2.2.5 Isolation of bone marrow-derived macrophages (BMDM) 19

2.2.6 Isolation of human monocytes and macrophages 19

2.2.7 BMDM viability assay 20

2.2.8 BMDM cytokine secretion assay 20

2.2.9 BMDM phagocytosis of PLGA microparticles 21

2.2.10 Phagocytosis of opsonized erythrocytes 21

2.2.11 Statistical analysis 22

2.3 Results and Discussions 23

2.3.1 Characterization of PLGA film and microparticles 23

2.3.2 Characterization of CD200-coated PLGA 25

2.3.3 BMDM viability 27

2.3.4 BMDM cytokine secretion 29

2.3.5 BMDM phagocytosis of PLGA microparticles 33

2.3.6 Human BMDM phagocytosis of PLGA microparticles 36

2.3.7 Human monocyte and macrophage phagocytosis of opsonized targets 37

2.4 Summary 39

3. Chapter 3: CD200-coated PLGA nanoparticles and their immunomodulatory effects 41

3.1 Introduction 41

3.2 Experimental Design 42

3.2.1 Production of CD200 42

3.2.2 Fabrication of PLGA and PEGylated PLGA nanoparticles 42

3.2.3 Conjugation of CD200 on PLGA nanoparticles 44

3.2.4 BMDM culture 44

3.2.5 BMDM phagocytosis assay 44

3.2.6 BMDM cytokine secretion 45

3.2.7 CD200R1 siRNA knock-down 45

3.2.8 Intraperitoneal (IP) injection of PLGA nanoparticles 46

3.2.9 Statistical analysis 46

3.3 Results and Discussions 47

3.3.1 Characterization of PLGA-PEG copolymer 47

3.3.2 Characterization of PLGA and PLGA-PEG nanoparticles 48

3.3.3 Characterization of CD200-coated PLGA nanoparticles 50

3.3.4 BMDM viability with PLGA nanoparticles 52

3.3.5 CD200R expression of BMDM 53

3.3.6 BMDM cytokine secretion 56

3.3.7 CD200R1 siRNA knock-down 58

3.3.8 The effect of CD200-coated nanoparticles on CD200R knock-down BMDM 59

3.3.9 Intraperitoneal (IP) injection of PLGA nanoparticles 63

3.4 Summary 66

4. Chapter 4. Conclusions and Future Directions 68

REFERENCE 72

LIST OF FIGURES

		page
Figure 1.1	Schematic depicting parallels between the foreign body response after implantation of biomaterials and the wound healing process after injury.	**2**
Figure 1.2	The foreign body response to biomaterial implants.	**3**
Figure 1.3	Macrophage phenotype diagram.	**4**
Figure 1.4	Regulation of myeloid cells by self-proteins.	**6**
Figure 1.5	The expression pattern of CD200 and CD200R.	**8**
Figure 1.6	Modulation of macrophage phenotype by self-protein modified biomaterials.	**9**
Figure 1.7	Hydrolysis of PLGA.	**11**
Figure 1.8	Experimental design and hypothesis of the study.	**12**
Figure 2.1	Illustration of experimental design.	**14**
Figure 2.2	Size distribution of PLGA dissolved in either dimethyl carbonate (DMC) or dichloromethane (DCM).	**23**
Figure 2.3	Characterization of PLGA microparticles and films.	**24**
Figure 2.4	Bright field and fluorescent images of PLGA microparticles.	**25**
Figure 2.5	Modification of PLGA surfaces with CD200.	**26**
Figure 2.6	Viability of BMDM with cytokine and microparticle treatment.	**28**
Figure 2.7	The effect of PLGA microparticles on TNF-alpha secretion by BMDM.	**29**
Figure 2.8	CD200 modulates macrophage cytokine secretion in response to PLGA particles and films.	**31**
Figure 2.9	CD200 modulates macrophage cytokine secretion in response to modified polystyrene and glass surfaces.	**32**
Figure 2.10	The confirmation of microparticles internalization.	**34**
Figure 2.11	Phagocytosis of CD200-coated PLGA microparticles by BMDM.	**35**
Figure 2.12	Phagocytosis of CD200-coated PLGA microparticles by human monocytes.	**37**
Figure 2.13	Modulation of human phagocytic activity by CD200.	**38**
Figure 3.1	Characterization of PLGA-PEG copolymer.	**48**
Figure 3.2	Characterization of PLGA and PLGA-PEG nanoparticles.	**49**

Figure 3.3	Characterization of PLGA nanoparticles with different modifications.	**51**
Figure 3.4	Viability of BMDM cells incubated with PLGA nanoparticles of different modifications.	**52**
Figure 3.5	CD200R expression of different BMDM phenotypes.	**53**
Figure 3.6	BMDM phagocytosis of PLGA nanoparticles.	**55**
Figure 3.7	BMDM TNF-alpha and IL-10 secretions after incubation with cytokines and nanoparticles.	**57**
Figure 3.8	CD200R expression after CD200R siRNA transfection.	**58**
Figure 3.9	Representative immunofluorescent images of BMDM.	**60**
Figure 3.10	Quantification of CD200R knock-down study.	**62**
Figure 3.11	F4/80 and CD11b population of peritoneum cavity cells.	**64**
Figure 3.12	F4/80 and CD200R population of peritoneum cavity cells.	**65**
Figure 4.1	Illustration of osteoarthritis (OA) and proposal of using CD200-coated microparticles for synovial inflammation treatment.	**71**

ACKNOWLEDGMENTS

Completing a Ph.D. thesis requires physical and mental support from everyone around me. I sincerely thank my advisor Dr. Wendy Liu for the continuous support on my research, and her patience, motivation, enthusiasm, and immense knowledge. Her guidance provided me a handful of resources to accomplish this study. Besides my advisor, I would also like to thank my thesis committee members, Dr. Andrea Tenner, and Dr. Szu-Wen Wang, for their insightful comments and suggestions to the project. My sincere thanks also go to Dr. Jered Haun and Dr. Abe Lee, who provided quite a bit of guidance and tips toward success in the experiments.

Nothing is better than working in a laboratory such as Liu lab. I want to thank Ann Fain and Linda McCarthy for coordinate and manage our core facility. My thank is beyond words to my sweet labmates in Liu lab: France McWhorter, Tim Smith, Yoon Kyung Kim, Thuy Luu, Jessica Hsieh, Vijay Meli, Hamza Atcha, Joe Hsu, Raji Nagalla, Praveen Veer, and of course to all the undergrads who worked with me: Anthony Han, Xiuhui Gao, Ci Ren, Sien Tam, Arian Cano and all others! I would not enjoy this work without your support and all the fun that we had. I also thank my collaborators for giving me opportunities working on diverse subjects: Dr. Blanka Sharma's lab, Dr. Shelly Peyton's lab, Dr. Angie Louie's lab, and Dr. Ming-Lin Ma's lab.

Last but not least, my family. Without Mom and Dad, everything is impossible. I am one lucky person to be born and raised in the family with you two. Thank you both for supporting me spiritually throughout my life. Also, I thank all of my friends around the world and all the strangers who cheered me up.

CURRICULUM VITAE

Esther Yu-Tin Chen

2011	**R&D Intern,** Development Center for Biotechnology	*Taipei, Taiwan*
2011-2012	**Research Assistant**, W.S. Wu Laboratory, University of Minnesota	*Minneapolis, MN*
2012	**BS** in Chemical and Materials Engineering, Chang Gung University	*Taoyuan, Taiwan*
2017	**MS** in Chemical Engineering, University of California, Irvine	*Irvine, CA*
2018-2019	**NSF Intern at Beckman Coulter**	*Brea, CA*
2019	**Ph.D.** in Chemical and Biomolecular Engineering, University of California	*Irvine, CA*

FIELD OF STUDY

Macrophage responses to immunomodulatory biomaterials

PUBLICATIONS

Kyung Kim Y., **Chen EY,** Liu WF. Biomolecular strategies to modulate the macrophage response to implanted materials. Journal of Materials Chemistry B. 2016;4(9):1600-9.

Chen EY, Chu SH, Gov L, Kim YK, Lodoen MB, Tenner AJ, Liu WF. CD200 modulates macrophage cytokine secretion and phagocytosis in response to poly (lactic-co-glycolic acid) microparticles and films. Journal of Materials Chemistry B. 2017;5(8):1574-84.

Smith TD, Nagalla RR, **Chen EY,** Liu WF. Harnessing macrophage plasticity for tissue regeneration. Advanced drug delivery reviews. 2017 May 15;114:193-205.

Chen EY, Liu WF, Megido L, Díez P, Fuentes M, Fager C, Olsson E, Gessner I, Mathur S. Understanding and utilizing the biomolecule/nanosystems interface. Nanotechnologies in Preventive and Regenerative Medicine 2018 Jan 1 (pp. 207-297). Elsevier.

Jansen LE, Amer LD, **Chen EY**, Nguyen TV, Saleh LS, Emrick T, Liu WF, Bryant SJ, Peyton SR. Zwitterionic PEG-PC hydrogels modulate the foreign body response in a modulus-dependent manner. Biomacromolecules. 2018 Apr 26;19(7):2880-8.

Chen EY, "CD200-coated PLGA nanoparticles inhibit macrophage activation." BMES 2017, Phoenix, Arizona.

Chen EY, "Modification of PLGA microparticles with the immunomodulatory protein promotes phagocytosis and anti-inflammatory cytokine secretion by macrophage." BMES 2016, Minneapolis, Minnesota.

Chen EY, "Immunomodulatory effects of CD200-coated PLGA microparticles on the macrophage response." UC Systemwide Bioengineering Symposium 2016, San Francisco, California.

Chen EY, "Immunomodulatory protein-conjugated PLGA" BMES 2015, Tampa, Florida.

Chen EY, "Regulation of macrophage response by immunomodulatory hydrogels." BMES 2014, San Antonio, Texas.

Chen EY, "The effect of immunomodulatory protein, CD200, on macrophage activation." UC Systemwide Bioengineering Symposium 2014, Irvine, California.

ABSTRACT

Immunomodulatory Effects of Engineered Biomimetic Materials

by

Esther Yu-Tin Chen

Doctor of Philosophy in Chemical and Biomolecular Engineering

University of California, Irvine, 2019

Professor Wendy Liu, Chair

Biocompatibility is an essential parameter to evaluate when designing the biomaterial in order to induce an appropriate host response in its specific application. Generally, biocompatibility refers to the lack of foreign body response to an implanted or injected material. The foreign body response involves activation of various immune cells and leads to severe inflammation, and eventually device failure. Modulation of the foreign body response to biomaterials therefore is a key to translating medical devices into the clinic. There have been various chemical and physical approaches to overcome the foreign body response. However, these methods do not provide any specific biological signal to immune cells, such as macrophages, who have diverse functionalities at different stages of inflammation. Therefore, a biological approach to mitigate the foreign body response to the biomaterials is essential.

This Ph.D. dissertation utilizes a biomolecular design of biomaterials to mimic the host tissue by displaying an immunomodulatory molecule on the surface, providing a specific inhibitory signaling to the immune cells. The immunomodulatory molecule that we exploit is CD200, which has been shown to interact with its inhibitory receptor, CD200R on myeloid cells, suppressing the activation of myeloid cells. In this study, we focus on a biomaterial that has been widely used in

FDA-approved devices, poly (lactic-co-glycolic) acid (PLGA). Even though PLGA is relatively biocompatible, as a foreign material, it initiates inflammation. This dissertation focuses on the fabrication of CD200-coated PLGA materials and their immunomodulatory effects on macrophages. We synthesize CD200-coated PLGA in different geometries and study macrophage behaviors including cytokine secretion and phagocytosis.

In Chapter 1, we provide background in the foreign body response, and introduction of CD200 as an immunomodulatory molecule and PLGA as a biomaterial. The fabrication of CD200-coated PLGA microparticles and films and the influences of CD200 coating on macrophage behaviors are discussed in Chapter 2. Chapter 3 demonstrates the effects of CD200-coated PLGA nanoparticles on macrophage phagocytosis *in vitro* and *in vivo,* and examines the translational potential of CD200-coated materials. Lastly, Chapter 4 provides conclusions on work performed in this study and presents future directions.

This Ph.D. study suggests that immunomodulatory coating of CD200 on PLGA mitigates macrophage activation and the effect of CD200 is geometry-dependent. Specifically, CD200-coated PLGA films and microparticles exhibit anti-inflammatory property, while the effect of CD200-coated PLGA nanoparticles on macrophage cytokine secretion is minimum. Additionally, macrophages phagocytose more CD200-coated microparticles, whereas they uptake less CD200-coated nanoparticles, when compared to the unmodified particles. This dissertation suggests that CD200-coated microparticles and films can be used as implantable biomaterials to silence inflammation, while CD200-coated nanoparticles propose an improved drug delivery system.

Chapter 1: Background Information

1.1 Foreign body response

Biomaterials are a cornerstone of modern medicine, used in a wide range of applications including implanted and extracorporeal devices, vehicles for drug delivery, and scaffolds for tissue engineering or regenerative medicine [1]. Implantation of medical devices within the body initiates a series of reactions, collectively called the foreign body response, which aims to eliminate or isolate the implanted foreign materials from the host immune system. This response limits the longevity and functionality of implanted or injected biomaterials [2]. The physical and chemical properties of the biomaterial play an essential role in governing the adsorbed protein species, including serum components involved in the complement and coagulation cascades, as well as their conformation (Figure 1.1 A) [3]. These events in turn influence downstream interactions with blood clotting factors and inflammatory cells, including platelets, neutrophils, macrophages, and dendritic cells (Figure 1.1 B) [4]. These immune cells are important for mediating the overall host response, and also help orchestrate wound healing and tissue repair processes (Figure 1.1 C) [5]. This final phase involves resident tissue cells, including fibroblasts that lay down a new matrix to form scar tissue (Figure 1.1 D).

Overcoming this foreign body response is essential for reducing fibrosis, which ultimately prevents the functional integration of the device with the surrounding host tissue. Native tissue, on the other hand, expresses self-proteins such as CD200[6], CD47[7], heparin sulfate proteoglycan [8], etc., to prevent immune cell adhesion and activation (Figure 1.1 E). Inflammation can be triggered by injury and the subsequent wound healing. Wound healing is a complex process involving a cascade of events, including coagulation, acute inflammatory response, regeneration, and remodeling. In both the wound healing process or implantation inflammation, immune cells such as macrophages play a crucial role in maintaining the dynamic balance between inflammatory

and pro-healing signals. Cell-material interaction, therefore, becomes an engineering approach to manipulate the outcome of implantation.

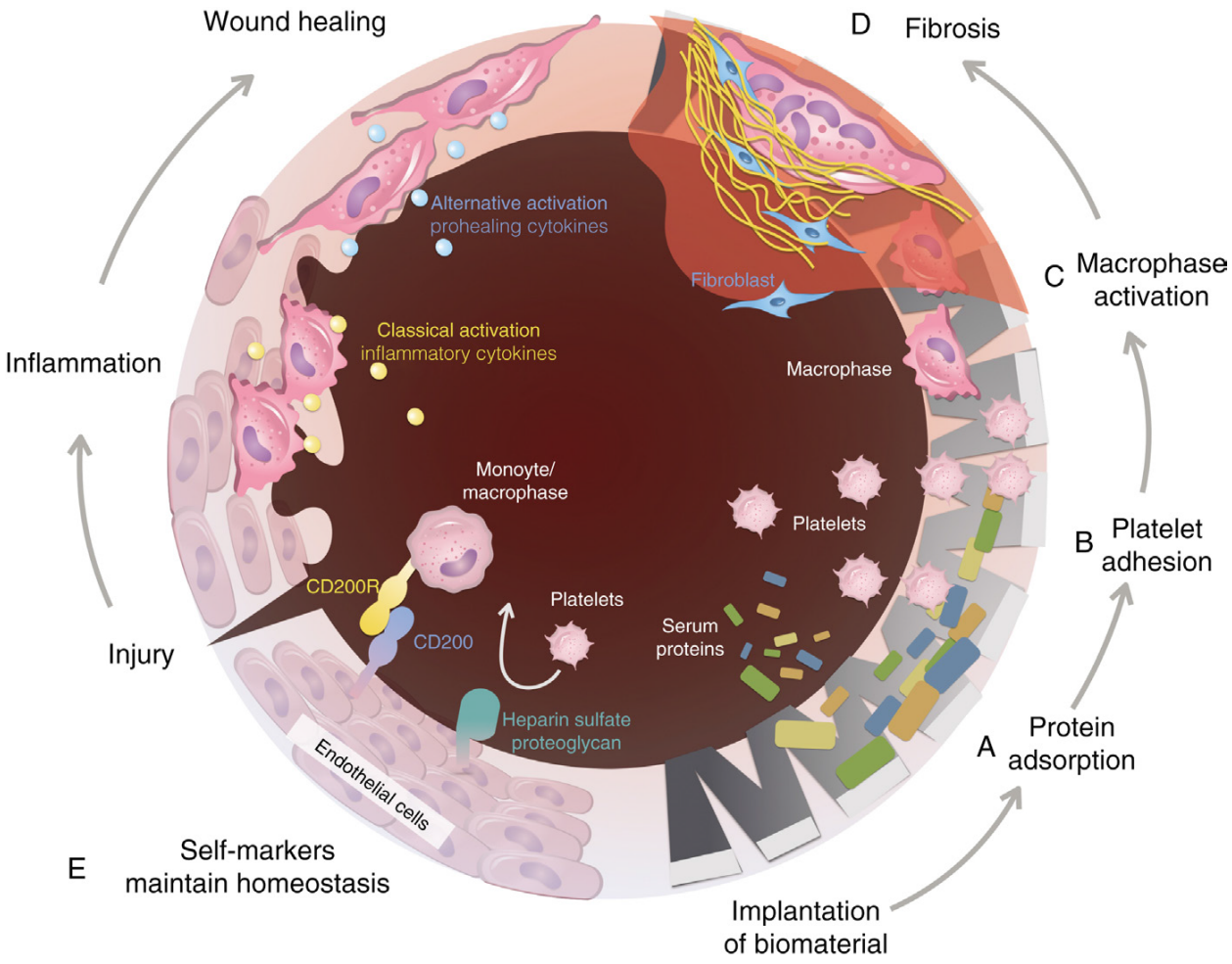

Figure 1.1 Schematic Depicting Parallels Between the Foreign Body Response. *After Implantation of Biomaterials (Right) and the Wound Healing Process After Injury (Left). Following implantation, proteins adsorb to the surface of the biomaterial (A). The adsorbed proteins, along with injury to the tissue, lead to recruitment and activation of immune cells (B), followed macrophages, and dendritic cells (C). Macrophages fuse to form giant cells, and fibroblasts proliferate and become activated forming a fibrous connective tissue (D). Eventually, the fibrous capsule of the implant isolates the implant from the local tissue. During homeostasis, host cells express a variety of self-markers that prevent immune cells from adhesion and activation, including CD200 [6], CD47 [7], and heparin sulfate proteoglycan [8] (E). Adapted from [9].*

1.2 The role of macrophages in the foreign body response

While the foreign body response is a coordinated response involving many different cell types, macrophages are thought to be a major determinant of the overall fibrotic outcome (Figure 1.2) [10]. Macrophages, originating from circulating monocytes, are mononuclear phagocytic cells which have been demonstrated to be involved in phagocytosis, clearance, inflammation, and tissue repair [2, 11]. They produce various types of chemokines and cytokines and play a major role as a communicator in the immune response.

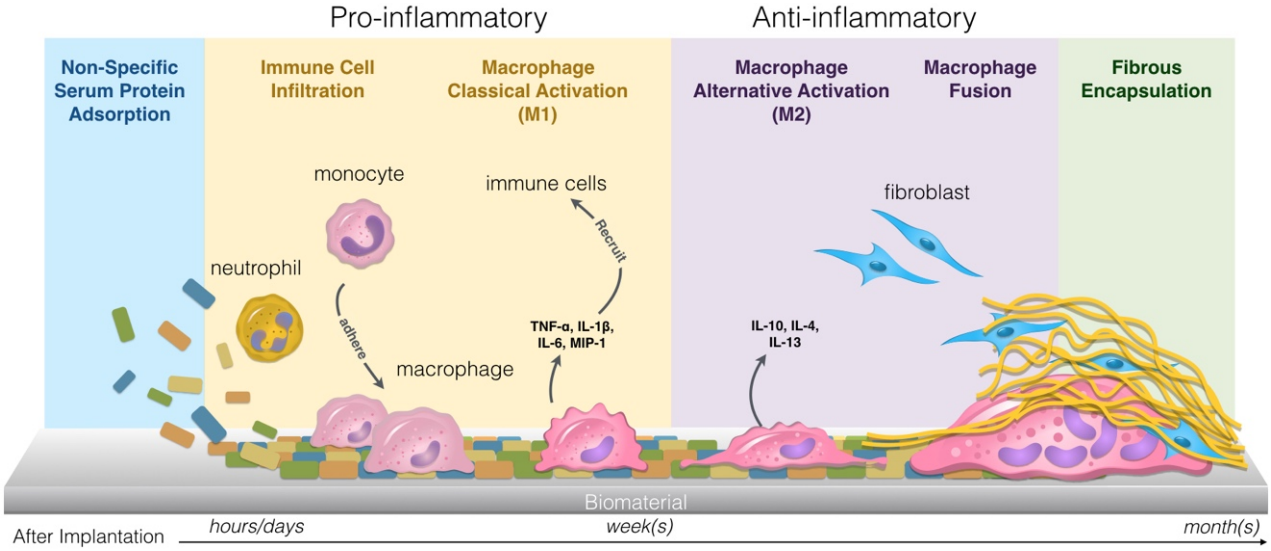

Figure 1.2 The foreign body response to biomaterial implants. *Schematic of the host response that follows implantation of a biomaterial. Proteins from serum adsorb to the surface of the biomaterial, and inflammatory cells including neutrophils and monocyte-derived macrophages infiltrate in response to the injury. Macrophages are initially classically activated (M1) and secrete pro-inflammatory cytokines, recruiting additional immune cells. After several days, macrophages polarize towards a pro-healing, alternatively activated (M2) phenotype and release IL-10, IL-4, and IL-13. The final stages of the response include fusion of macrophages to form giant cells, fibroblast recruitment, collagen deposition, and fibrous capsule formation. Adapted from [10].*

Macrophages can polarize towards a spectrum of phenotypes in response to their microenvironment to facilitate wound healing and tissue repair [12-14]. Initially, in response to the implantation, macrophages adopt a classically activated, pro-inflammatory (M1) phenotype and secrete cytokines and chemokines to recruit additional immune cells (Figure 1.2). These cytokines include tumor necrosis factor-alpha (TNF-alpha), interleukin-6 (IL-6), and interleukin-

1beta (IL-1beta), etc. TNF-alpha and IL-1beta dominate the initiation and maintenance of the inflammatory response and modulate immunosuppressive mechanisms. The primary function of M1 macrophages is to mediate tissue damage, defend against intracellular pathogens and upregulate pro-inflammatory cytokines in addition to inducible nitric oxide synthase (iNOS) (Figure 1.3). Over the course of wound healing, macrophages polarize towards an alternatively activated (M2) phenotype and secrete a different milieu of cytokines to promote healing (Figure 1.2), which include transforming growth factor beta (TGF-β) and interleukin-10 (IL-10), and have enhanced arginase (Arg1) activity (Figure 1.3) [15, 16].

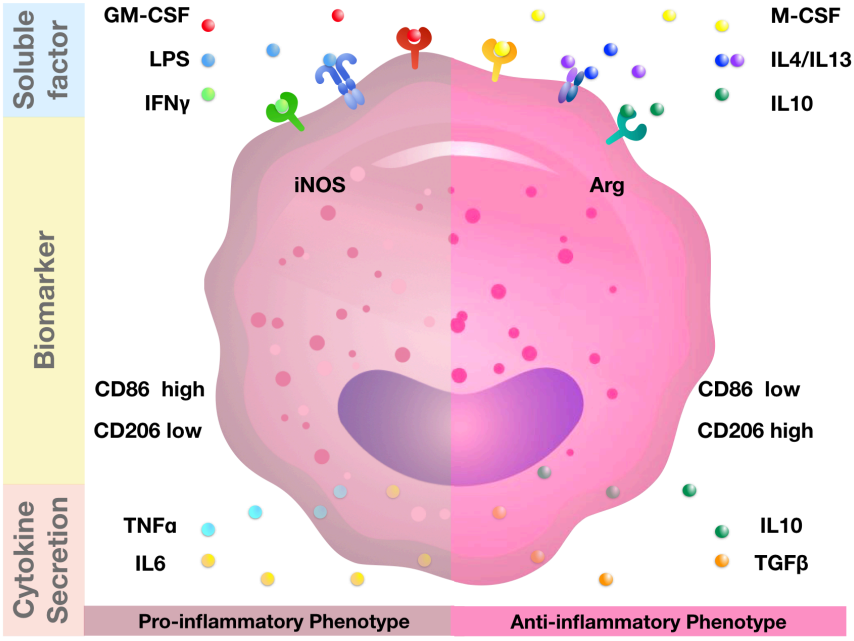

Figure 1.3 Macrophage phenotype diagram. *Lipopolysaccharide (LPS) and interferon-gamma (IFNy) stimulation usually leads to pro-inflammatory macrophages (left). They express high nitric oxide synthase (iNOS) and CD86, and secret cytokines including TNF-alpha and IL-6. Anti-inflammatory macrophages, on the other hand, secrete anti-inflammatory cytokine IL-10 and TGF-beta, and express high arginase (Arg) level and CD206.*

The diversity of macrophages is not limited to two phenotypes. Several studies have reported macrophage subsets and their diverse functions [17, 18]. In addition, there is plasticity in macrophage polarization, suggesting fluidity among different subsets of macrophages. Upon

completion of tasks, M1 macrophages were observed to transform into alternative phenotype to present tissue remodeling [14]. Given that different subsets of macrophages facilitate the immune response at different stages, manipulation of macrophage phenotype becomes one of the strategies to resolve the foreign body response [19]. The polarization of macrophages can be assessed by identifying surface receptors/markers, as well as the amount of cytokine secreted. Therefore, cytokine secretion, and protein expression of macrophages provide an approach to studying macrophage activation and potentially offering predictions of implantation outcomes.

1.3 Approaches to reduce the foreign body response

Many recent advances in biomaterial engineering have focused on designing surfaces to actively modulate local immune cells to control the foreign body response [20]. Physical approaches utilize material microgeometry [21], topography [22], stiffness [23], or hydrophobicity [24, 25], while chemical approaches focus on surface chemistry [26] to modulate macrophage phenotype. These techniques may reduce overall inflammation but do not manipulate immune cells toward pro-healing phenotype. Thus, an emerging strategy in immunomodulatory materials is to incorporate biomolecules that directly target immune cells and naturally control their activities [27]. These biomolecules may be proteins thought to mitigate the inflammatory response, such as extracellular matrix (ECM) components, cytokines, or self-proteins. Upon contacting ECM, macrophage integrins bind to proteins including fibrinogen, fibronectin, and vitronectin, and this binding mediates cell adhesion and activation. One study showed that adhesion to ECM is involved the formation of foreign body giant cells on material surfaces [28]. Therefore, numerous strategies have emphasized on either engaging or preventing integrin binding site with the tri-peptide sequence, Arg-Gly-Asp (RGD) [28-32]. Cytokines are the critical soluble mediators that lead to the recruitment and the activation of various cell types. Local delivery of cytokines from biomaterials has been used to polarized macrophages toward desired phenotypes, including IL-4

and IL-10 [33, 34]. Another approach to modulate immune cell response is through self-proteins. Immune cells can distinguish dangerous from non-dangerous objectives by the recognition of molecular cell surface patterns. Self-proteins provide inhibition signals towards the activation of the immune cells and prevent autoimmunity. The self-proteins that have been engineered on biomaterials are CD47 and CD200.

CD47 is an immunomodulatory self-protein involved in the inhibition of phagocytosis [35] (Figure1.4). It is highly expressed on normal red blood cells to prevent clearance of these healthy erythrocytes. The inhibitory signal is transported through the binding of CD47 and its inhibitory receptor, SIRP-a, expressed on macrophages. Taking the advantage of CD47 immunomodulatory properties, a study showed that immobilization of recombinant CD47 on nanoparticles prolonged circulation of these modified nanoparticles after I.V. injection in the mouse model [36]. CD47-coated surfaces also diminished adhesion and activation of platelets and neutrophils [37]. Additionally, a vascular stent coated with CD47 inhibited platelet and inflammatory cell adhesion, and further reduced restenosis [38].

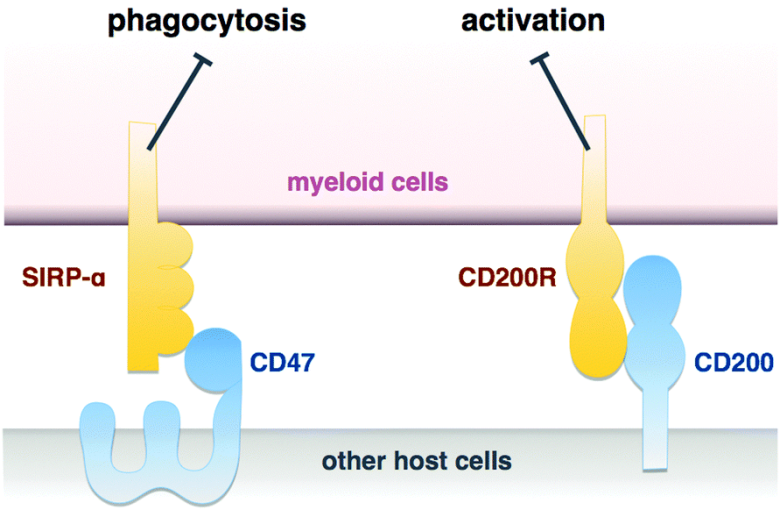

Figure 1.4 Regulation of myeloid cells by self-proteins. *Interaction between CD47 on host cells and its receptor SIRP-α, expressed on myeloid cells, minimizes phagocytosis. The interaction between CD200 on host cells and CD200R, expressed on myeloid cells, inhibits inflammatory activation. Adapted from [10].*

1.4 CD200 as an immunomodulatory molecule

Another immunomodulatory protein that has been incorporated in biomaterial design is CD200 (OX2) (Figure1.4). CD200 is a membrane glycoprotein broadly expressed on a variety of cell types, including myeloid cells (mast cells, neutrophils, macrophages, and dendritic cells), lymphoid cells (B cells, a subset of T cells, and dendritic cells), neuron, and endothelial cells. The CD200 receptor, CD200R, is restricted to myeloid cells such as dendritic cells and macrophages [39]. Both CD200 and CD200R contain two immunoglobulin(Ig)-like domains (V and C), a single transmembrane region, and a cytoplasmic tail. CD200R has an additional long cytoplasmic domain (67aa) containing signaling motifs that are involved in the suppression of myeloid cell activation, while CD200 has a short intracellular domain (19aa) [40].

The ligation of CD200 and CD200R triggers the intracellular inhibitory pathway in myeloid cells. Briefly, upon ligation, CD200R becomes phosphorylated on its tyrosine residues, which is associated with an induction of the inhibitory adaptor proteins Dok1 and Dok2 (down-stream of tyrosine kinase) (Figure 1.5) [41]. Dok1 and 2 are involved in Ras GTPase phosphorylation/activation and also recruit SH2-containing inositol phosphatase (SHIP) [41, 42]. Eventually, the signaling cascade results in decreased synthesis of cytokines (TNF-alpha, IFNγ, MCP-1, IL-1, IL-17, IL-6, and IL-8), decreased activation of inducible nitric oxide synthase (iNOS) and increased synthesis of anti-inflammatory cytokines (IL-10 and TGF-β) [43].

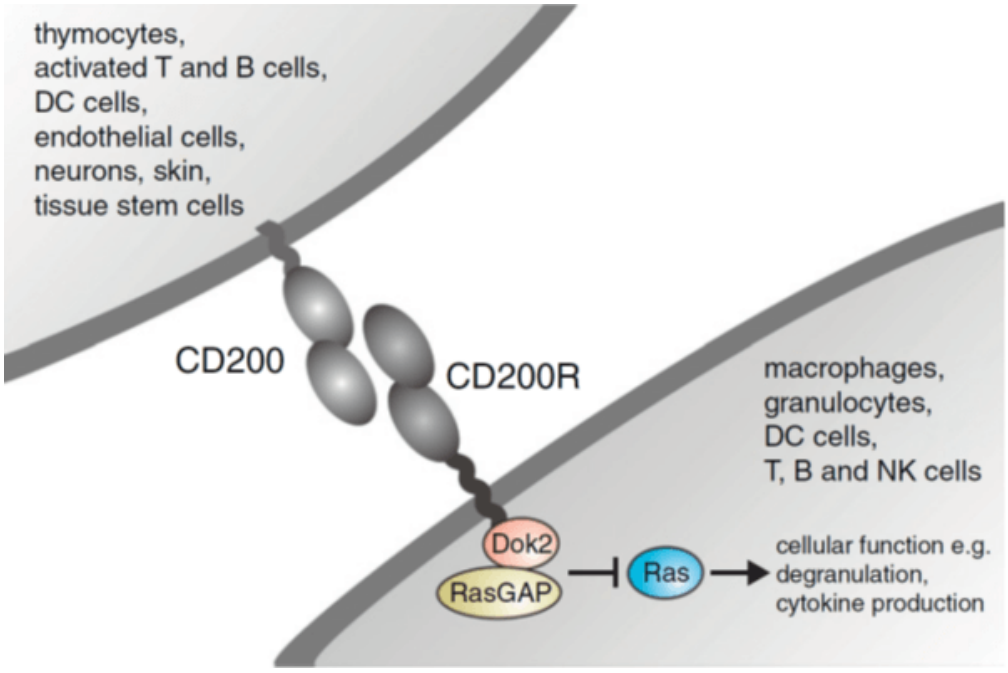

Figure1.5 The expression pattern of CD200 and CD200R [44].

The significance of CD200 as critical regulators of inflammation has been shown in several studies. In mice lacking CD200, macrophage lineage cells were more numerous and exhibited an activated phenotype in the spleen [45]. Inhibitory effect of CD200 was further demonstrated using two autoimmune models. In an experimental autoimmune encephalomyelitis (EAE) model, activated inflammatory macrophages and microglia (with iNOS and CD68 expression) were found in the central nervous system of CD200-deficient mice but not wild type mice. Additionally, blockage of CD200-CD200R interaction, using either soluble CD200R protein or blocking Ab, augmented collagen-induced arthritis (CIA) in mice and exacerbated EAE in rats [45, 46]. After the discovery of the importance of CD200-CD200R interaction, the role of CD200 has been studied in many immune conditions, including cancer [44], arthritis [40, 47, 48], and brain diseases [49]. CD200 has also been shown to play a role in inflammatory lung disease. Mice lacking CD200 exhibited more macrophage activity and enhanced sensitivity to influenza infection, which ultimately lead to death [50].

Taking advantage of the interaction between CD200 and CD200R, Kim *et al.* showed that a biomaterial coated with CD200 not only inhibited pro-inflammatory cytokine secretions (TNF-alpha and IL-6) effectively but also decreased macrophage infiltration in the subcutaneous injection of the modified microbeads (Figure 1.6) [51].

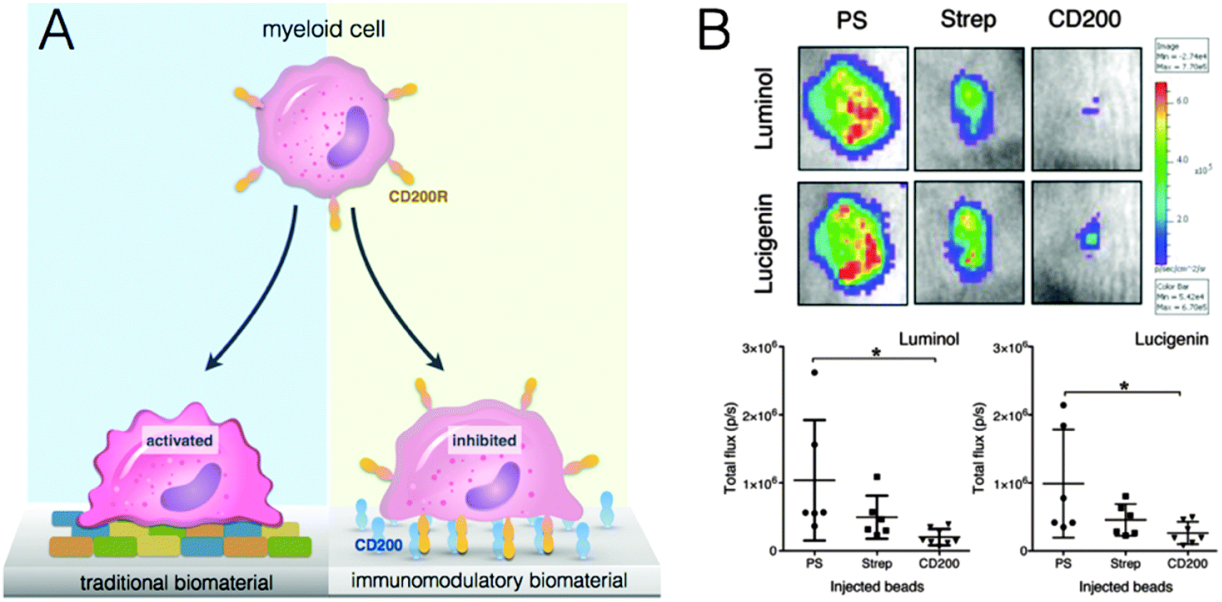

Figure 1.6 Modulation of macrophage phenotype by self-protein modified biomaterials. *(A) Strategy conferring immune inhibition using CD200. Myeloid cells become activated on traditional biomaterial due to non-specific serum protein adsorption, while CD200-coated biomaterial inhibits myeloid cell activation. (B) In vivo imaging of luminol and lucigenin bioluminescence in mice implanted with uncoated (PS), streptavidin- (Strep), or CD200- (CD200) coated polystyrene microspheres (top) and quantification of photon flux (bottom). Adapted from [51].*

1.5 Poly(lactic-co-glycolic acid) (PLGA) as a biomaterial

Selection and design of materials for biomedical applications is highly dependent on the chemical and mechanical properties of materials and their purposes. These properties include but are not limited to biocompatibility, bio-functionality, toxicology, tensile strength, elastic modulus, corrosion, resistance, permeability, and hydrophobicity, etc. In order to develop a biomaterial that fits its applications, the compositions and properties of materials and how they interact with the environment must be considered. Polymeric materials have been widely studied as a biomaterial, due to its diverse application, over metallic or ceramic materials. Their unique properties include flexibility, biocompatibility, lightweight, tunable physical and mechanical properties.

Poly(lactic-co-glycolic) (PLGA) is an FDA-approved biocompatible polymer used in many applications due to its tunable properties and its wide range of possible erosion times. It is degradable by hydrolysis into two endogenous monomers: lactic acid and glycolic acid (Figure 1.7). Both monomers can be metabolized in cells via the Krebs cycle, which makes PLGA relatively biocompatible. Owing to its biodegradability and biocompatibility, PLGA is considered to be a good candidate for tissue engineering applications and drug delivery systems. PLGA has been used as a biodegradable scaffold for bone repair in tissue engineering [52, 53]. More specifically, three-dimensional PLGA scaffolds have been applied in cartilage engineering to provide structural support and to stimulate repair [54]. Cardiovascular stents coated with drug-loaded PLGA nanoparticles were found to limit plaque progression and restenosis [55-57]. Additionally, PLGA nano-/micro-particles have been employed as drug delivery systems for growth factors [58, 59] and various medications, including vaccine delivery, cancer treatment, and cardiovascular disease treatment, reviewed in [60]. However, as a foreign body to the host, PLGA still triggers an immune response. Dexamethasone is an anti-inflammatory drug that has been encapsulated in PLGA microparticles to suppress inflammatory responses [61-65]. However, the

anti-inflammatory drug often leads to undesirable side effects and fails to improve wound healing. In order to unlock the full spectrum of applications of PLGA, further modifications to PLGA may be necessary.

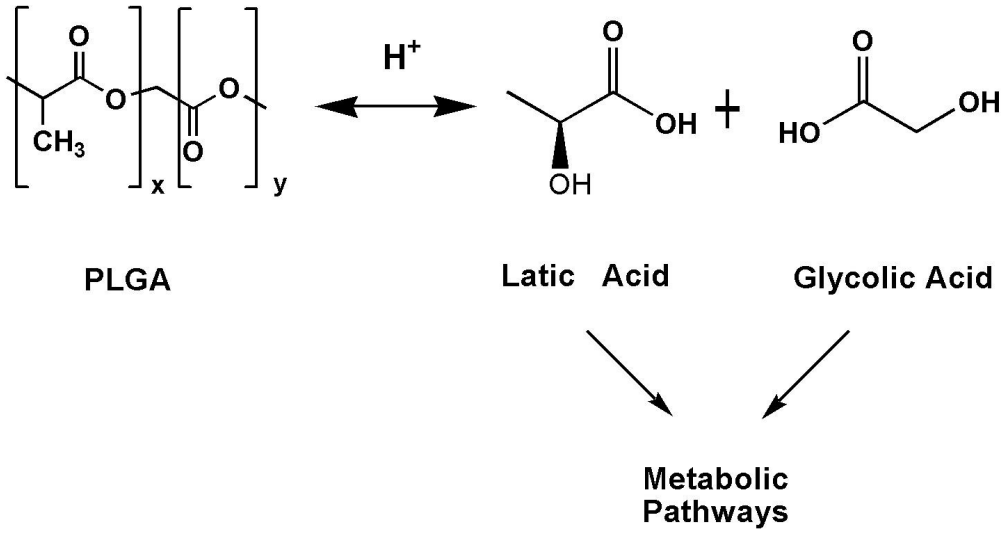

Figure 1.7 Hydrolysis of PLGA *[66]*

1.6 Immunomodulatory PLGA with different geometries

In this study, we fabricate PLGA biomaterials with different geometries and coat the surfaces with a recombinant immunomodulatory protein, CD200, for the modulation of the material-induced host response. We hypothesize that CD200 coating provides specific interaction between immune cells and biomaterials and reduces inflammation caused by materials, and the effect might be geometry dependent (Figure 1.8). We examine and discuss the size-dependent immunomodulatory effects of CD200 on macrophage response, including cell viability, cytokine secretion, phagocytosis, as well as *in vivo* uptake evaluation. The study suggests that modified PLGA microparticles and PLGA films can potentially be applied in tissue engineering as a locally implanted biomaterial, while PLGA nanoparticles can be an immunomodulatory drug delivery system.

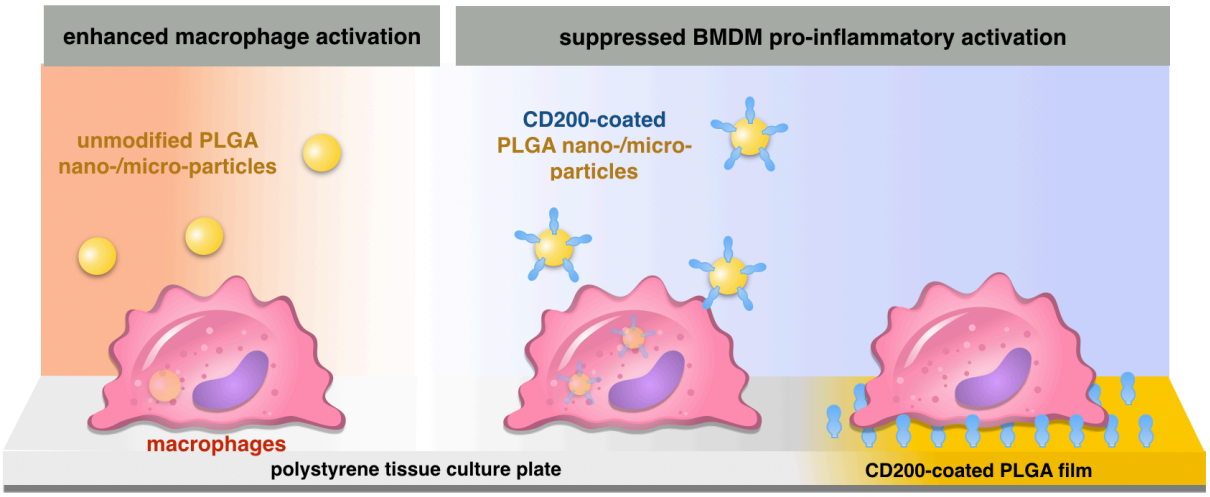

Figure 1.8 Experimental design and hypothesis of the study.

Chapter 2: CD200-coated PLGA materials for tissue engineering

2.1 Introduction

Poly (lactic-co-glycolic acid) (PLGA) is a biodegradable polymer which has been approved by the FDA for many applications, including sutures, bone screws, and surgical meshes. However, the foreign body response to PLGA still limits its potential uses in many other tissue engineering or drug delivery applications. Extensive studies have focused on incorporating anti-inflammatory drugs into PLGA biomaterials to modulate inflammation, such as dexamethasone [61, 63-65, 67-69]. However, the effect of anti-inflammatory drugs is non-specific, and they often lead to undesirable side effects and fail in wound healing. To guide immune cells for proper responses, a more specific interaction between biomaterials and the immune system must be established.

CD200 (OX2) is a membrane glycoprotein broadly expressed on a variety of cell types, including myeloid cells, lymphoid cells, neuron, and endothelial cells. The CD200R is restricted to myeloid cells such as dendritic cells and macrophages [39]. The ligation of CD200 and CD200R triggers the intracellular inhibitory pathway in myeloid cells and inhibits the pro-inflammatory activities of myeloid cells. A considerable amount of literature emphasizes the significance of CD200 as a critical regulator of inflammation [40, 47, 48], making CD200 a possible candidate for immunomodulatory biomaterial engineering. We hypothesize that CD200 potentially enables the immune system to recognize foreign material as a host and it provides appropriate signals to the immune system.

Taking advantage of the interaction between CD200 and CD200R, we developed immunomodulatory biomaterials for tissue engineering and drug delivery purposes. Previously in our laboratory, Dr. Kim used recombinant protein technology to produce the extracellular domain of CD200 and coated the protein on the model surface. We found significant suppression of TNF-

alpha and IL-6 cytokine secretion of bone marrow-derived macrophages (BMDM) on the CD200-coated surface [27]. This proof-of-concept is further carried down in this study. This study aims to develop immunomodulatory PLGA biomaterial for tissue engineering and drug delivery purposes. Herein, we fabricated PLGA with different geometry (microparticle and film), modified PLGA with CD200, and investigated the ensuing pro-inflammatory and anti-inflammatory responses to PLGA (Figure 2.1). We examined BMDM cytokine secretion and phagocytosis in response to different geometries and different modifications of PLGA. We hypothesize that CD200-coated PLGA inhibits the pro-inflammatory activities of BMDM and the effect of CD200 on BMDM might be geometry-dependent.

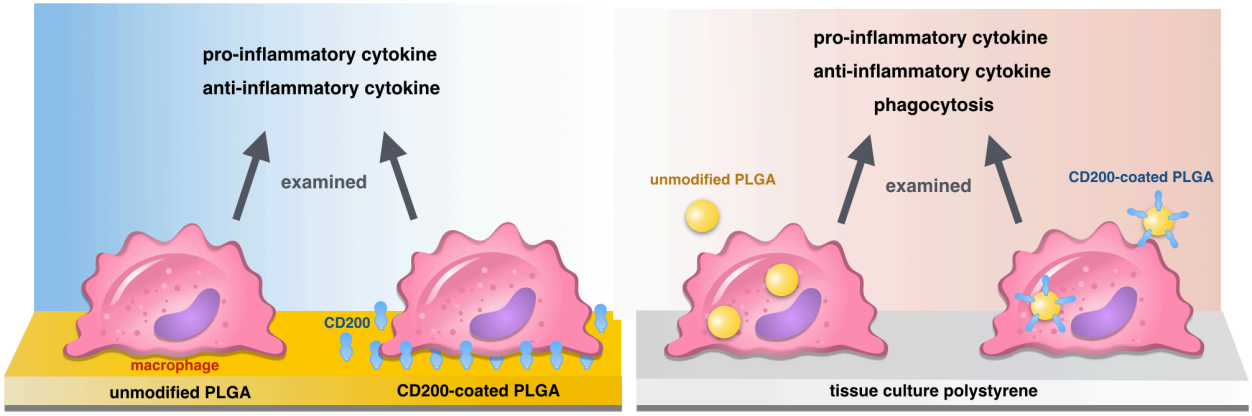

Figure 2.1 Illustration of experimental design.

2.2 Experimental Design

2.2.1 Production of CD200 from mammalian cells

2.2.1.1 Expression of CD200 in CHO-K.1 cells

The CD200-AviTag recombinant protein was constructed previously in our laboratory by Dr. Yoon Kyung Kim [51]. Briefly, the extracellular domain of mouse CD200 (GenBank Accession Number AAB93980; amino acids 1-121), a 15-amino acid stiff linker sequence (SLSTPPTPSPSTPPT), an AviTag amino acid sequence (GLNDIFEAQKIEWHE), and a 6x His sequence were constructed from N- to C- termini. For protein expression in mammalian cells, the constructed gene was then transferred to a pEE14 expression vector that contains the glutamine synthase minigene as a selectable marker (kindly provided by A. Yap at the University of Queensland, Brisbane, Australia).

The mammalian cell line, Chinese Hamster Ovary (CHO-K1, ATCC, Manassas, VA) was employed for protein expression. CHO-K1 cells were cultured in glutamine-free DMDM media containing dialyzed fetal bovine serum (FBS) (Gibco, Carlsbad, CA), 50U/mL penicillin, 50 μg/mL streptomycin, 60 μg/mL glutamate, 60 μg/mL asparagine, 7 μg/mL adenosine, 7 μg/mL guanosine, 7 μg/mL cytidine, 7 μg/mL uridine, 7 μg/mL thymidine, 1x non-essential amino acids (Sigma, Louis, MO), and 1mM sodium pyruvate (Invitrogen, Grand Island, NY).

CHO-K1 cells were transfected with pEE14 plasmid DNA containing CD200-AviTag-6x His using Lipofectamine LTX (Invitrogen) according to the manufacturer's instructions. Transfected cells were incubated in the 5% CO_2 incubator at 37°C for 4 hours before changing into serum-containing media. 24 hours after transfection, cells were selected in a glutamine-free media with 50 μM L-methionine sulfoximine (MSX) (Sigma, Louis, MO). Once successfully transfected colonies formed, several colonies were trypsinized in cloning cylinders (VWR, Visalia, CA).

Selected colonies were further expanded in media containing 250μM MSX for 2 weeks. Among colonies, a transfected CHO-K1 colony with the highest expression of CD200-AviTag-6x His was determined by Western blot after supernatant concentration using Amicon filter unit (Sigma, Louis, MO).

2.2.1.2 Production, purification, and biotinylation of CD200

For protein production, CHO-K1 cells transfected with "CD200-AviTag-6xHis" pDNA were cultured in protein-free chemically-defined media, Pro CHO-AT (Lonza, Verviers, Belgium) containing 1% HT supplement (Gibco), 50U/mL penicillin, and 50 μg/mL streptomycin. Upon passaging, cells were incubated in 4% FBS -contained media for 4 hours (for attachment) before changing into serum-free media. Transfected cells were expanded into 10 T150 culture flasks and cultured for 8 days in serum-free media for protein expression. After 8-day culture, the supernatant containing CD200 protein was collected and condensed using a Pellicon XL Device (Sigma) with Labscale Tangential Flow Filtration system (Sigma). Concentrated protein was then purified using a HisSpin Ni Column (GE Healthcare, Uppsala, Sweden) following the manufacturer's manual. The condensed and purified protein was detected by Western blot. The purified protein was then buffer exchanged with 10mM Tris-HCl, pH 8, using Amicon filter unit. For biotinylation, protein in 10mM Tris-HCl was incubated with biotin and BirA enzyme at 30℃ for 2 hours following the manufacturer's protocol (Avidity, Aurora, CO). The final concentration of the protein was determined using μBCA Protein Assay Kit (ThermoFisher, Rockford, IL). 500 mL of cell culture media yielded approximately 500μg of final product (biotinylated CD200). Endotoxin level was determined by the *Limulus* Amebocyte Lysate Gel Clot Endotoxin Assay Kit (GenScript, Piscataway, NJ).

2.2.2 Fabrication of PLGA film and microparticles

2.2.2.1 Fabrication of PLGA film

10%w/v PLGA was dissolved in dimethyl carbonate (DMC) (Fisher Scientific, Hampton, NH). 100µL of PLGA solution was placed on top of 12mm-diameter sterile FisherBrand cover glass (Fisher Scientific). The Solvent was allowed to evaporate under vacuum overnight for film formation. PLGA film was further sterilized using 70% EtOH followed by three PBS washes. The surface topography of PLGA film was determined by Scanning Electron Microscopy (SEM).

2.2.2.2 Fabrication of PLGA microparticles

We fabricated PLGA microparticles using single emulsion evaporation techniques. For PLGA microparticles, 1 mL of 10% w/v PLGA dissolved in dimethyl carbonate (DMC) (Fisher Scientific, Hampton, NH) was pipetted into continuously stirred 50 mL 1% poly(vinyl alcohol) (PVA) (Sigma) at 700 rpm. All the reagent was sterile filtered using a 0.22 µm syringe filter unit. Once the PLGA droplets were formed, the solvent was allowed to evaporate under continuous stirring for 5 min. Solid PLGA particles formed when the solvent evaporated completely. We further size-selected PLGA particles using cell strainers (1, 6, 10, 20, 30, and 40 µm) for better characterization. PLGA particles were washed with sterile PBS thre times followed by centrifugation. Particle size and morphology were determined by SEM imaging and analysis.

2.2.3 Conjugation of CD200 on PLGA (Biotin-streptavidin conjugation)

To conjugate CD200 on PLGA surface through biotin-streptavidin interaction, we first modified PLGA surface with streptavidin via an amide bond. Carboxylic acid-terminated PLGA films or particles were prewashed with 50 mM MES, pH5.4 (Fisher Scientific). With 10 mg of PLGA, 10 mg of EDC was dissolved in 500 µL 50 mM MES buffer, followed by 5 min incubation at RT. 10 mg of sulfo-NHS (Fisher Scientific) in 500 µL 50 mM MES buffer was then added into the reaction. The reaction was incubated at RT for 20 min on a rotator or a shaker. After the reaction,

PLGA films were washed quickly 2 times with MES buffer, while PLGA particles were washed with the same condition and centrifuged. Immediately after washes, 10 μg of streptavidin in 500 μL PBS solution was dropped on top of PLGA film. 10 mg of PLGA particles were mixed with 10 μg of streptavidin in 1 mL PBS solution. The streptavidin conjugation through NHS-amine reaction was carried out at RT for 4 hours. The streptavidin-coated PLGA was then washed 3 times with PBS (centrifugation for particles). After washes, 10 μg of biotinylated CD200 in 100 μL PBS was dropped on top of a 12mm-diameter PLGA film, while 10 mg PLGA particles were resuspended in 1mL PBS containing 10 μg of biotinylated CD200. The biotin-streptavidin reaction was incubated for 4hr at RT on a rotator or shaker.

2.2.4 Characterization of CD200-coated PLGA

The conjugation of CD200 was confirmed by PE-conjugated anti-CD200 antibody using microscopic techniques. PLGA microparticles coated with or without CD200 were incubated with 20 mg/ml PE monoclonal anti-mouse CD200 antibody (BioLegend) for 2hr on a rotator, and then washed 3 times with PBS. PE signal was detected using an Olympus inverted microscope. To quantify the amount of CD200 conjugated on the microparticles, we used a QuantibriteTM PE kit (BD Biosciences), which contains a set of beads conjugated with four different levels of PE molecules/bead to generate a standard curve. The amount of PE anti-CD200 antibody conjugated on the surfaces was determined using the standard curve of known levels of PE molecules per bead, and the amount of CD200 per particle was calculated assuming a ratio of one antibody bound to one CD200 molecule.

2.2.5 Isolation of bone marrow-derived macrophages (BMDM)

All protocols involving animals were approved by the Institutional Animal Care and Use Committee at the University of California Irvine before initiation of the study. Bone marrow-derived macrophages (BMDM) were harvested from the femurs of 6-8-week-old C57BL/6 mice (Jackson Laboratories). Femurs were harvested, and bone marrow was flushed with DMEM supplemented with 3% heat-inactivated FBS (both from Invitrogen) to collect bone marrow cells. To isolate and differentiate BMDM, cells were treated with ACK lysis buffer (Invitrogen), centrifuged, and resuspended in D-10 media, which consists of Dulbecco's modified Eagle medium (DMEM) supplemented with 2 mM L-glutamine, 100 units per ml penicillin-streptomycin, 10% heat-inactivated FBS, and 10%media collected from the supernatant of CMG 12–14 cells ectopically expressing recombinant mouse macrophage colony stimulating factor (M-CSF). BMDM were cultured at 37℃ in a humidified incubator with 5% CO2. BMDM were dissociated using cell dissociation buffer (Invitrogen) on day 7 and seeded on the tissue culture plates (Olympus Plastics) in fresh D-10 culture media.

2.2.6 Isolation of human monocytes and macrophages

All blood samples were collected into CPDA1 at the UCI Institute for Clinical and Translational Science in accordance with guidelines and approval of the University of California, Irvine (UCI) Institutional Review Board. Human peripheral blood lymphocytes and monocytes were isolated from peripheral blood mononuclear cells (PBMCs) by countercurrent elutriation. All experimental samples were 90-98% CD11b+ in the monocyte fraction by flow cytometry. Human monocyte-derived macrophages were generated from monocytes by culture at $5*10^5$ cells per ml for 7 days in RPMI1640 (Invitrogen), 10% FBS (HyClone), 2 mM L-Glutamine (Invitrogen) and 1% penicillin/streptomycin (complete media) containing 25 ng/ml recombinant human M-CSF (rhM-CSF) (PeproTech) with addition of fresh media with rhM-CSF at day 3. The adherent human

monocyte-derived macrophages were harvested at day 7-8 by washing twice with 1X PBS and incubating with non-enzymatic CellStripper (CellGro) for 20-30 min. After washing twice with 1X PBS, viable cells were counted using a 0.4% Trypan blue solution, a hemocytometer chamber, and an optical microscope.

2.2.7 BMDM viability assay

BMDM were seeded on tissue culture plates at 100,000 cells/cm^2. At 6hr after cell seeding, the culture media was replaced with D-10 media containing different combinations of the following stimuli: 0.3 ng/mL lipopolysaccharide (LPS), 1.0 ng/mL interferon-gamma (IFNγ), 20 ng/mL interleukin-4 (IL-4), and 20 ng/mL interleukin-13 (IL-13). PLGA microparticles with different surface modifications were introduced to the cells together with culture media containing different stimuli. After 36hr of incubation, the viability of BMDM was analyzed by MTT cell proliferation assay kit (ThermoFisher) following the manufacturer's protocol and reading absorbance at 570 nm.

2.2.8 BMDM cytokine secretion assay

BMDM were seeded on the tissue culture plates or PLGA films with different surface modifications at a cell density of 100,000 cells/cm^2. At 6hr after cell seeding, the culture media was replaced with D-10 media containing different combinations of stimuli as described in the previous section. For particle experiments, the PLGA microparticles with different surface modifications were introduced to the cells at 8% projected surface coverage together with culture media containing different stimuli. After 36hr of incubation, the supernatants were collected and analyzed for TNF-alpha and IL-10 secretion by enzyme-linked immunosorbent assay (ELISA) following the manufacturer's instructions (BioLegend).

2.2.9 BMDM phagocytosis of PLGA microparticles

BMDM or human monocytes were seeded in 8-well Lab-Tek Chamber slides (Thermo Scientific) at 62,500 cells/well in their respective media. PLGA microparticles were seeded at a ratio of 10 particles to 1 cell. After 12hr incubation, the cells were fixed with 4% paraformaldehyde (Electron Microscopy Sciences) for 5 min and washed carefully with PBS. To permeabilize cells, we treated the samples with 0.1% Triton X-100 (Sigma-Aldrich) (in PBS) for 5 min. BMDM were then stained with Alexa Fluor-594 conjugated phalloidin (Invitrogen) and Hoechst 33342 dye (Invitrogen) for 1hr, followed by thorough washes with PBS. Human monocytes were stained with Vybrant DiI cell-labeling solution (Thermo Scientific) and Hoechst. Finally, the chamber slide was mounted using Fluoromount-G (Southern Biotech). Fluorescence images were obtained using an Olympus inverted microscope. For flow cytometric analysis, cells with phagocytosed fluorescein-containing PLGA microparticles were collected after 12hr (for BMDM) or 3hr (for human monocytes) of particle incubation. The un-phagocytosed particles were washed out with PBS. The cells were then collected using a cell scraper and suspended in PBS. Phagocytosed cell acquisition and analysis were performed using a BD LSR II flow cytometer and FlowJo software.

2.2.10 Phagocytosis of opsonized erythrocytes

Sheep erythrocytes (Colorado Serum Co., Denver, CO) were suboptimally opsonized using rabbit anti-sheep erythrocyte immunoglobulin (EA) and the phagocytosis assays were performed as described [70, 71]. Briefly, 8-well LabTek chambers (Nunc) were UV ozone treated for 15 min and then silanized with a 4% (3-mercaptopropyl)trimethoxysilane solution (Sigma Aldrich) at RT for 1hr. Meanwhile, streptavidin was crosslinked using sulfo-SMCC (Life Technologies) at RT for 30 min, and unreacted sulfo-SMCC was removed using a 7 kDa Zeba desalting column (Thermo Scientific). Silanized chambers were washed thoroughly with 100% ethanol and dried with an N_2 stream. The maleimide-activated streptavidin was diluted to 0.1 mg/mL and incubated on the

silanized chambers at RT for 1hr. Streptavidin-modified chambers were then coated with different concentrations of CD200-biotin in PBS and incubated at room temperature for 2hr. After washing chambers twice with PBS, 250 µl of monocytes or human monocyte-derived macrophages (0.25M cell/mL) suspended in phagocytosis buffer (RPMI with 2 mM of glutamine, Pen/Strep and 5 mM of $MgCl_2$), were added to chambers. After spinning down at 700 rpm for 3 min, chambers were placed at 37℃ in 5% CO_2 air for 30 min. Target particles (EA) were then added (100 µl/well, $1*10^8$ EA/mL) and spun down at 700 rpm for 3 min and incubated for 30 min at 37℃ in 5% CO_2. After removing erythrocytes that were not cell-associated by washing, non-ingested erythrocytes were further removed by hypotonic lysis. Slides were then fixed in 1% glutaraldehyde (Sigma-Aldrich), stained with Giemsa, and scored by microscopic examination. A minimum of 200 cells per experimental condition in duplicate was quantified by individuals blinded to the experimental design. Percent phagocytosis was defined as the number of monocytes/macrophages ingesting at least one target divided by the total number of monocytes/macrophages counted, multiplied by 100. The phagocytic index was defined as the number of ingested targets per 100 cells counted.

2.2.11 Statistical analysis

Statistical analysis was performed using ordinary two-way ANOVA, followed by Tukey's post hoc test, and $p < 0.05$ was considered statistically significant.

2.3 Results and Discussions

2.3.1 Characterization of PLGA film and microparticles

To fabricate the PLGA film, we dissolved PLGA (50:50) in dimethyl carbonate (DMC) solvent at 10%w/v and dropped on top of a 12 mm coverslip. The PLGA film formation happened upon solvent evaporation. On the other hand, PLGA microparticles were generated by a single emulsion (oil-in-water) technique followed by solvent evaporation. Briefly, 1% PLGA was dissolved in an organic solvent (oil phase) and poured into a 1% PVA solution (water phase) under the stirring condition to create a single emulsion, followed by solvent evaporation for particle formation. Dimethyl carbonate (DMC) was used as a solvent because of the broad range of microparticle sizes it yielded. The Different solvent was found to yield different particle size distribution (Figure 2.2).

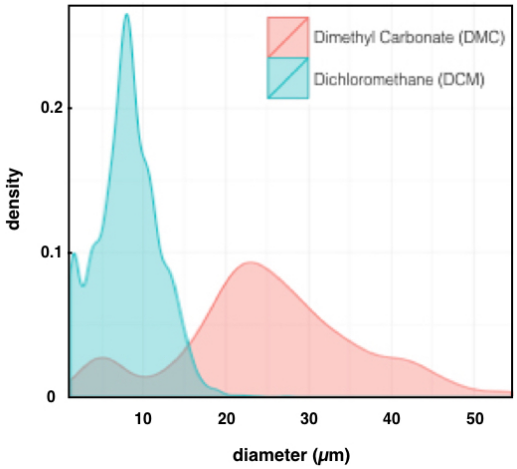

Figure 2.2 Size distribution of PLGA dissolved in either dimethyl carbonate (DMC) or dichloromethane (DCM). *For both cases, 1% PLGA was dissolved in either solvent, and the single emulsion was formed in 1% PVA at constant stirring condition (1000 rpm). Particles were collected for microscopic size analysis.*

Several studies have shown the effects of size on different cell activation [72-74]. Indeed, studies have found that macrophages recognize the size and shape of their targets [75, 76]. To better understand the effect of CD200 on different sizes, we separated the particles using cell

strainers with 1, 6, 10, 20, 30, and 40 µm membrane sizes. After size-selection, we obtained a different population of homogeneous PLGA microparticles, as illustrated by the scanning electron microscopy (SEM) imaging (Figure 2.3 A). PLGA film formed on top of the coverslip exhibited a smooth surface, as suggested by SEM imaging. Quantification of microparticle diameters revealed that particles passing through the 6 µm cell strainer were 2 µm to 13 µm in diameter, with a median diameter of 7 µm. The particles collected between the 10 µm and 20 µm strainers had a median diameter of 21 µm, while the 20 µm and 30 µm strainers yielded a median size of 28 µm. Notably, PLGA microparticles selected between the 30 µm and 40 µm strainers are less spherical and more concave compared to the 10-20 µm particles (Figure 2.3 B). We selected a phagocytose-able population 7 µm (from 1-6 µm cell strainers) of microparticles and a non-phagocytose-able population 28 µm of (from 20-30 µm cell strainers) to continue the study.

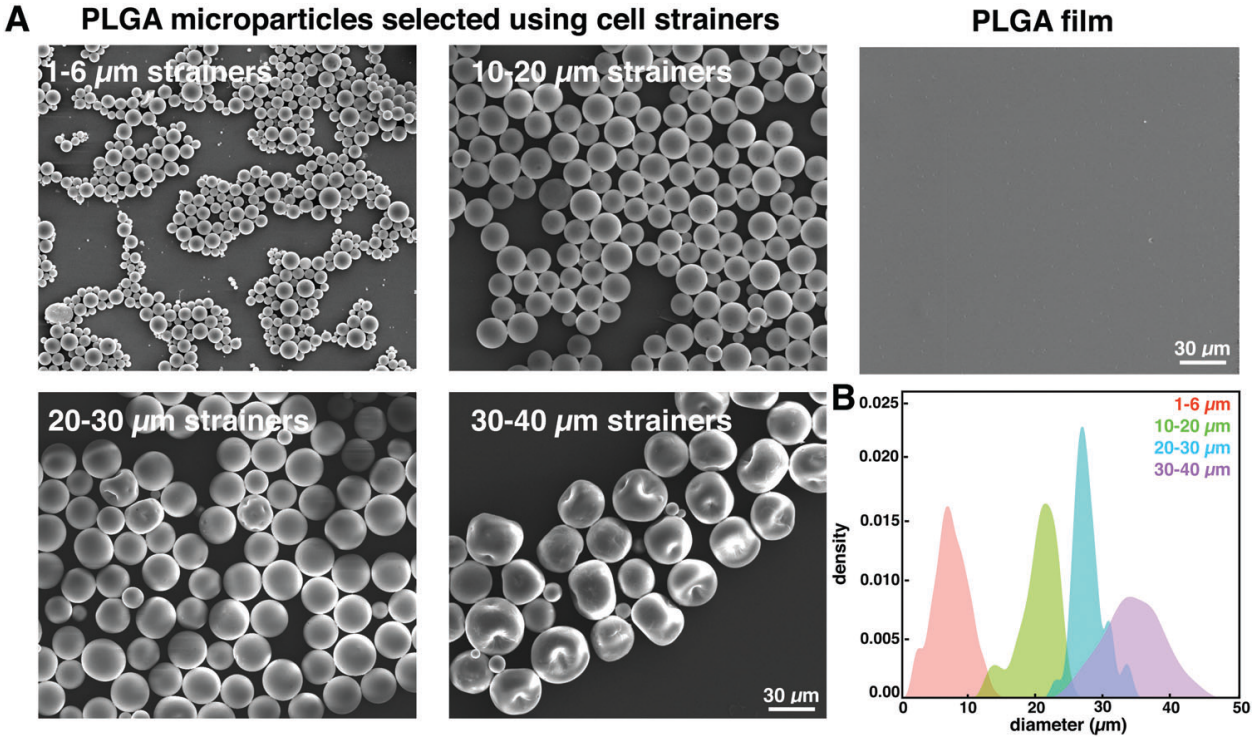

Figure 2.3 Characterization of PLGA microparticles and films. *(A) Representative scanning electron micrographs of size-selected PLGA microparticles and film. (B) Histograms depicting size distributions of PLGA microparticles after filtration using 1-6 µm, 10-20 µm, 20-30 µm, and 30-40 µm strainers.*

2.3.2 Characterization of CD200-coated PLGA

Once the particles and films were fabricated, we conjugated the biotinylated CD200 on PLGA via biotin-streptavidin interaction. First of all, we treated carboxylated PLGA with the EDC/NHS crosslinker, followed by streptavidin conjugation through an amide bond. To confirm the streptavidin conjugation, we employed PE-conjugated streptavidin. Figure 2.4 confirms streptavidin conjugation, suggested by fluorescent microscopic images. We observed higher levels of fluorescent intensity after conjugation through the amide bond when compared to non-specific absorption to PLGA particle surfaces.

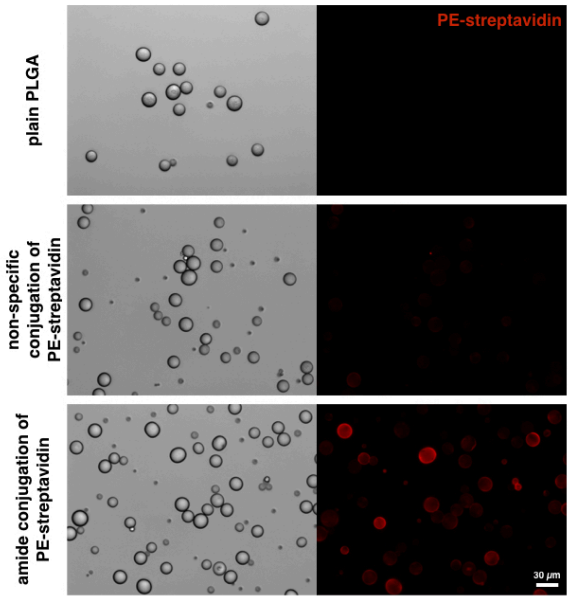

Figure 2.4 Bright field and fluorescent images of PLGA microparticles. *Plain PLGA exhibit no autofluorescence in the PE channel (top). PE-streptavidin exhibits moderate non-specific adsorption to PLGA surfaces (middle). PE-streptavidin conjugates efficiently to PLGA surfaces through covalent amide bond (bottom). Scale bar of 30 μm.*

After streptavidin was conjugated on PLGA, biotinylated CD200 was then bonded to streptavidin via biotin-streptavidin interaction. The presence of CD200 on PLGA surfaces was confirmed using PE-conjugated anti-CD200 antibodies, which detected CD200 on the modified PLGA microparticles and films, but not on the unmodified surfaces (Figure 2.5 A). Conjugation of CD200 appeared to be highly heterogeneous, and large particle-to-particle variations were observed. We

quantified the amount of CD200 on 7 μm particles by flow cytometry, which confirmed the heterogeneous levels of CD200 bound to each particle that were observed by microscopy (Figure 2.5 B). Using QuantiBRITE PE beads to calibrate the PE signal, we estimated approximately 1750 CD200 molecules on a 2-6 μm-sized particle and 7700 molecules on a 7-13 μm-sized particle, with the average density of 30 molecules/μm^2. On PLGA films, we conjugated CD200 onto surfaces at various coating concentrations and evaluated CD200 binding on the surface. Measuring the fluorescent intensity of PE-conjugated anti-CD200 antibodies indicates that the amount of bound CD200 is proportional to the coating concentration, reaching the highest levels of coating at 50 μg/well (Figure 2.5 C).

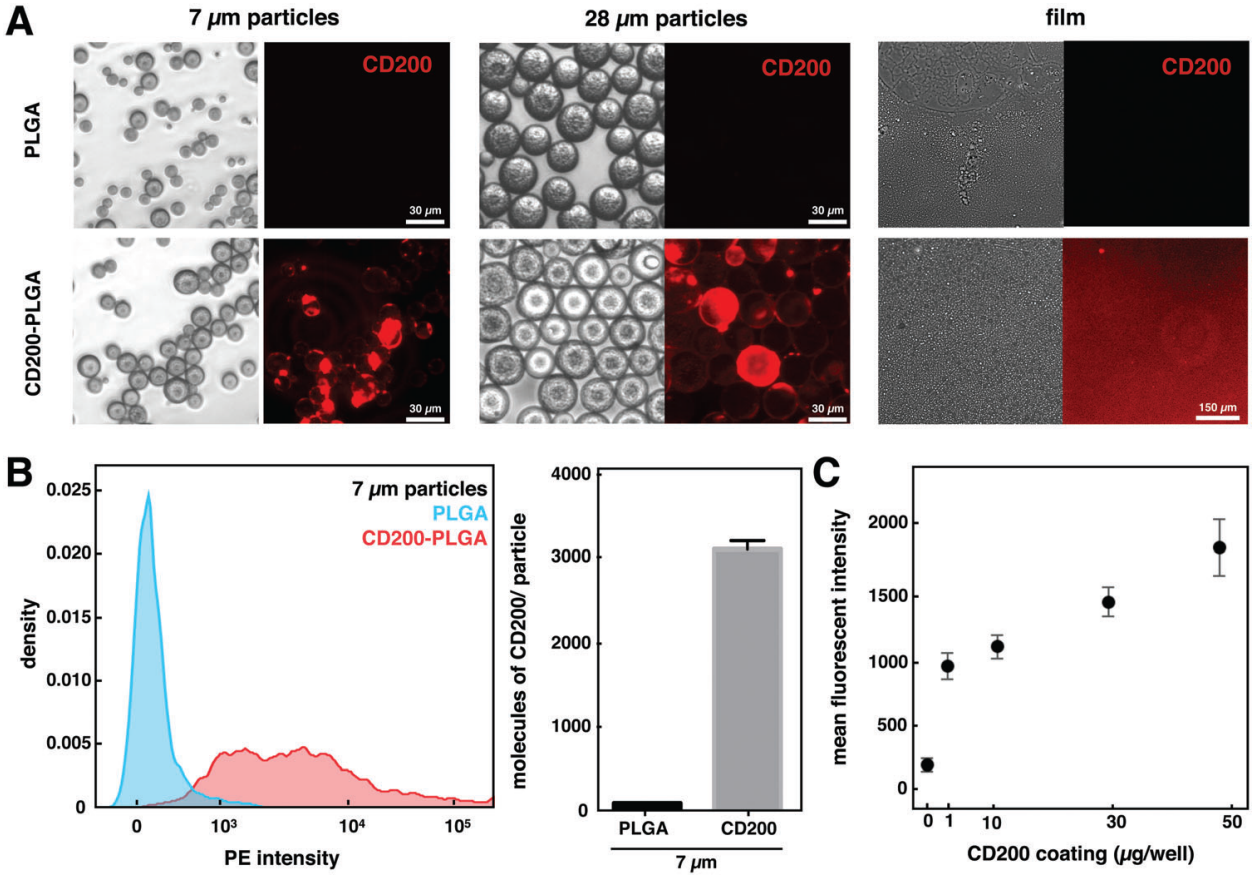

Figure 2.5 Modification of PLGA surfaces with CD200. *(A) Representative bright field (left) and fluorescent (right) images of different sized unmodified PLGA or CD200-PLGA microparticles and films. (B) Representative flow cytometry histogram of unmodified PLGA and CD200-PLGA 7 μm microparticles (left) and quantification of CD200 (right). Data represent the mean ± SEM of 10,000 particles. (C) Mean fluorescence intensity of CD200 bound on PLGA films with different coating concentration.*

2.3.3 BMDM viability

Before we investigated the influence of CD200 on cell activation, we first examined the toxicity of cytokine stimulation and PLGA microparticles by looking at cell viability. The viability of bone marrow-derived macrophages (BMDM) upon stimulation with different cytokines was measured by MTT assay. BMDM were less viable with the stimulation of LPS/IFNγ or LPS/IL-4/IL-13 when compared to cells without stimulation (Figure 2.6 A). When incubated with PLGA microparticles, increasing the amount of PLGA microparticles moderately decreased cell viability (Figure 2.6 B). Different surface modifications of PLGA microparticles did not show any effect on cell viability within the same cytokine stimulation condition (Figure 2.6 C). Interestingly, the addition of CD200-modified 28 μm PLGA particles to LPS/IFNγ treated cells somewhat enhanced their viability (Figure 2.6 D), suggesting that the ligation of CD200 protects macrophages from the toxic effects of LPS/IFNγ.

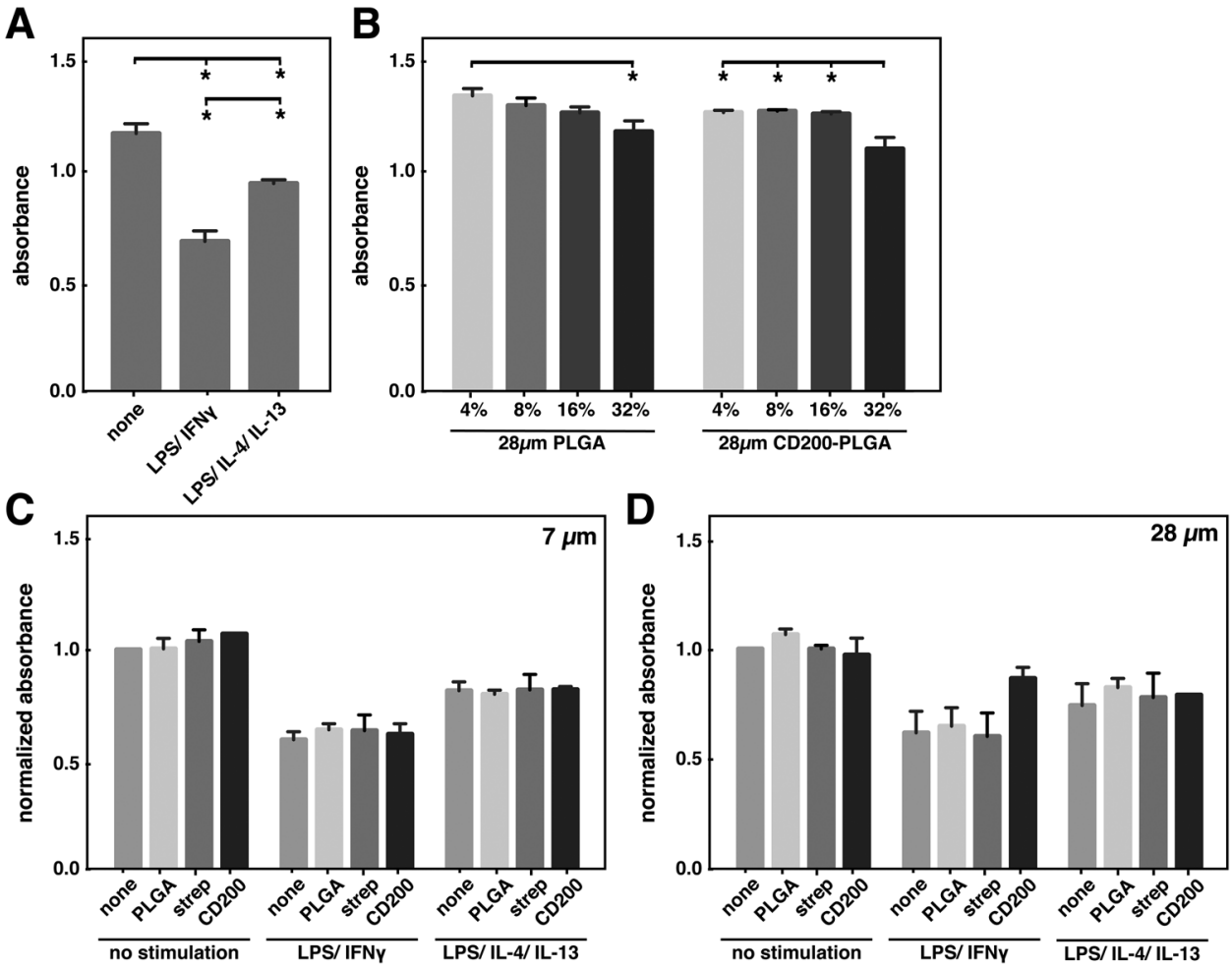

Figure 2.6 Viability of BMDM with cytokine and microparticle treatment. *(A) Viability of BMDM as measured by MTT assay upon stimulation with 0.3 ng/mL LPS and 1 ng/mL IFNγ, 0.3 ng/mL LPS, 20 ng/mL IL-4 and 20 ng/mL IL-13, or left untreated. (B) Viability of BMDM treated with different amounts (% surface coverage) of PLGA or CD200-PLGA microparticles. Viability of BMDM incubated with 7 μm (C) or 28 μm (D) PLGA microparticles with different surface modifications and stimulated with cytokines at the same concentrations described in (A). Data represent the mean ± SEM of n= 3. * denotes p< 0.05.*

2.3.4 BMDM cytokine secretion

Cytokines are proteins produced by cells, and they regulate various inflammatory responses. Here, we took cytokines as one of the indicators for BMDM activation. We examined BMDM secretion of a pro-inflammatory cytokine, TNF-alpha, and an anti-inflammatory cytokine, IL-10, upon stimuli and particle interaction. BMDM were seeded and settled on tissue-culture polystyrene. Different PLGA microparticles (unmodified PLGA, streptavidin-PLGA, or CD200-PLGA) was prepared in different stimulation media (no stimulation, LPS/IFNγ stimulation, and LPS/IL-4/IL-13 stimulation). Each stimulation media differentiated BMDM into specific phenotypes. After a 6-hr adhesion, cells were stimulated with various combinations of PLGA microparticles and stimulation media.

We first investigated how different projected surface coverage of PLGA microparticles can affect BMDM TNF-alpha secretion. Figure 2.7 suggests that the activation of BMDM was proportional to the PLGA microparticle density. The larger projected coverage of PLGA led to higher TNF-alpha secretion. Therefore, in this study, we kept the particle projected area constant across 7 μm and 28 μm microparticles in order to minimize the effects of varied surface areas on the activation of macrophages.

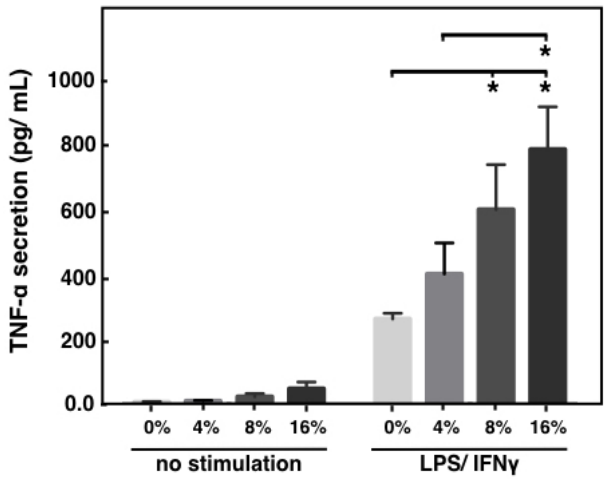

Figure 2.7 The effect of PLGA microparticles on TNF-alpha secretion by BMDM. *Levels of TNF-alpha secreted by BMDM cultured with 28 μm PLGA microparticles at the indicated surface coverage percentage and stimulated with 0.3 ng/mL LPS and 1 ng/mL IFNγ or without stimulation. Data represent the mean ± SEM of the averages of duplicate samples from n≥3 independent experiments. * denotes p<0.05.*

Next, we investigated BMDM cytokine secretion upon interaction with different surface modification of PLGA microparticles. We found that without additional cytokine stimulation, all particles had minimal effect on macrophage response and TNF-alpha and IL-10 secretion levels were undetectable. In the presence of LPS/IFNγ stimulation, macrophages cultured with unmodified PLGA particles secreted higher levels of TNF-alpha, an inflammatory cytokine, when compared to macrophages without particles (Figure 2.8 A(i) and B(i)). Modification of PLGA particles with CD200 reduced macrophage TNF-alpha secretion by approximately fifty percent, whereas coating with streptavidin alone as a control did not affect. Similar results were obtained for both 7 μm and 28 μm microparticles. When stimulated with LPS, IL-4, and IL-13, CD200 coating of 28 μm particles enhanced secretion of IL-10, an anti-inflammatory cytokine, by more than 2-fold, when compared to control microparticles (Figure 2.8 B(ii)). For 7 μm PLGA microparticles, CD200 did not significantly increase IL-10 secretion when compared to unmodified PLGA particles (Figure 2.8 A(ii)).

As for PLGA films, BMDM were allowed to adhere to PLGA films with different modification 6-hr prior to cytokine stimulation. On CD200-coated PLGA films, we observed a similar reduction of TNF-alpha and enhancement of IL-10 secretion as in the CD200-coated PLGA microparticle case. Compared to macrophages seeded on polystyrene, macrophages seeded on unmodified PLGA films secreted approximately two-fold more TNF-alpha (Figure 2.8 C(i)). Modification of PLGA surfaces with CD200 led to a decrease in TNF-alpha secretion to baseline levels and an increase in IL-10 (Figure 2.8 C(ii)).

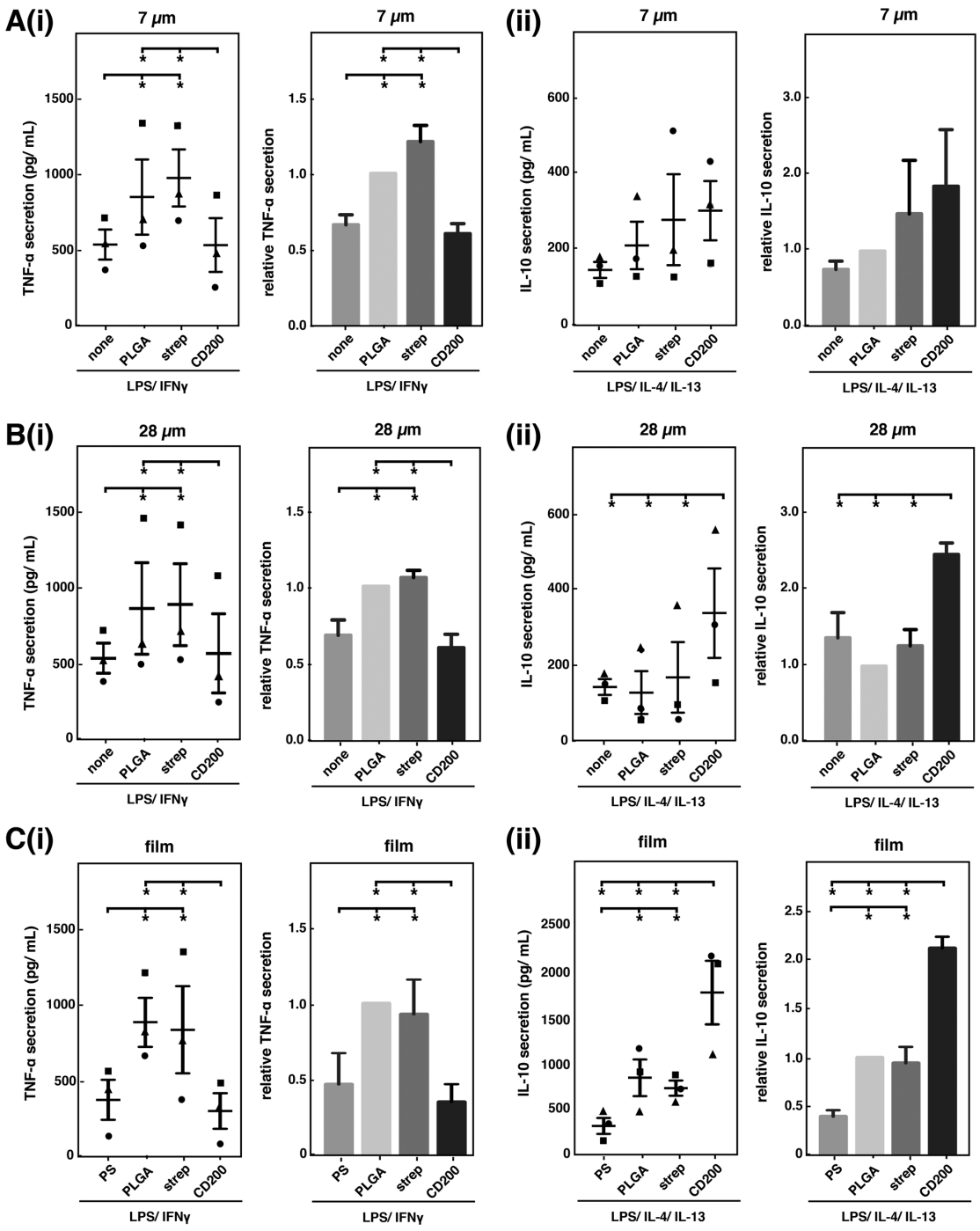

Figure 2.8 CD200 modulates macrophage cytokine secretion in response to PLGA particles and films. *Raw levels (left) and levels normalized to unmodified PLGA (right) of TNF-alpha (i) and IL-10 (ii) secretion by BMDM cultured with 7 μm (A), 28 μm (B) microparticles, or on polystyrene (PS) or PLGA films (C). For analysis of TNF-alpha secretion, cells were cultured with 0.3ng/mL LPS and 1ng/mL IFNγ. For analysis of IL-10 secretion, cells were cultured with 0.3ng/mL LPS, 20ng/mL IL-4 and 20 ng/mL IL-13. Distinct symbols (●,▲,■) represent separate biological replicates (independent experiment, each performed in duplicate). Data represent the mean ± SEM of* **n** *= 3. * denotes* $\mathbf{p} < 0.05$.

Interestingly, the effect of CD200 coating on different materials is distinct. While CD200 inhibited TNF-alpha on polystyrene by approximately two-fold similar to that seen on PLGA, no effect was observed on glass (Figure 2.9). In addition, CD200 generally inhibited the secretion of IL-10 on polystyrene and glass, in contrast to increased IL-10 when on PLGA (Figure 2.8 and 2.9). These data suggest that the biomaterial on which immunomodulatory molecules are presented may play an important role in their effect.

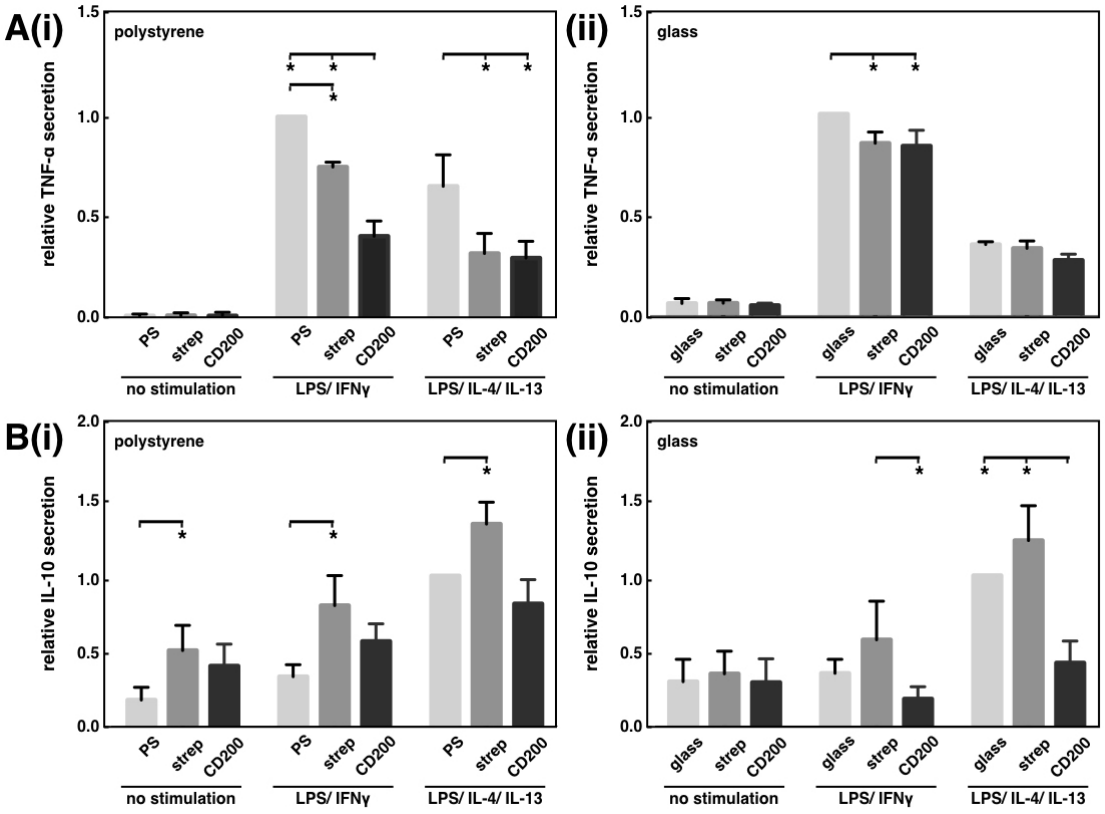

Figure 2.9. CD200 modulates macrophage cytokine secretion in response to modified polystyrene (i) and glass surfaces (ii). *BMDM were further stimulated with 0.3 ng/mL LPS and 1 ng/mL IFNγ or 0.3 ng/mL LPS, 20 ng/mL IL-4 and 20 ng/mL IL-13, or left unstimulated as a control. Relative levels of TNF-alpha (A) and IL-10 (B) secretion by BMDM are presented. Experiments were performed in duplicate. Data represent the mean ± SEM of the averages of duplicates from independent experiments n≥3. * denotes p<0.05*

Together, these data suggest that CD200 inhibits pro-inflammatory cytokine secretion in response to both PLGA microparticles and films, consistent with what we have previously observed with CD200-coated polystyrene particles and polystyrene cell culture surfaces [51]. In addition, we found that CD200 promotes IL-10 cytokine secretion by macrophages in response to PLGA particles and films, suggesting that this immunomodulatory protein may also enhance alternative activation or pro-healing macrophage function. Interestingly, upregulation of IL-10 was dependent on the biomaterial surface, as CD200-coated polystyrene or glass surfaces did not elicit this effect. These differential effects may be due to different coating densities achieved on each material. Further studies will be needed to elucidate the different responses observed in different material contexts. Nevertheless, our data suggests that CD200-coated PLGA directs macrophages toward an anti-inflammatory phenotype, and CD200 coating can potentially be used for PLGA-based devices to prevent acute inflammation and provide an anti-inflammatory signal that promotes tissue remodeling.

2.3.5 BMDM phagocytosis of PLGA microparticles

Besides secreting cytokines that help orchestrate inflammatory and wound healing processes, macrophages are also the primary phagocytes within the body capable of engulfing pathogens, small particles, cellular debris or apoptotic cells during tissue remodeling [77-79]. In this section, we further addressed the BMDM phagocytic activity of 7 μm PLGA microparticles with different surface modification and examined the potential role of CD200 on phagocytosis.

In order to detect phagocytosis of particles by microscopy or flow cytometry, fluorescein-containing PLGA microparticles were prepared, modified with CD200, and then introduced to BMDM. After 12 hours, cells were fixed and stained with phalloidin and Hoechst to visualize actin and nuclei respectively by microscopy, which showed particles internalized within cells (Figure 2.10 and 2.11 A).

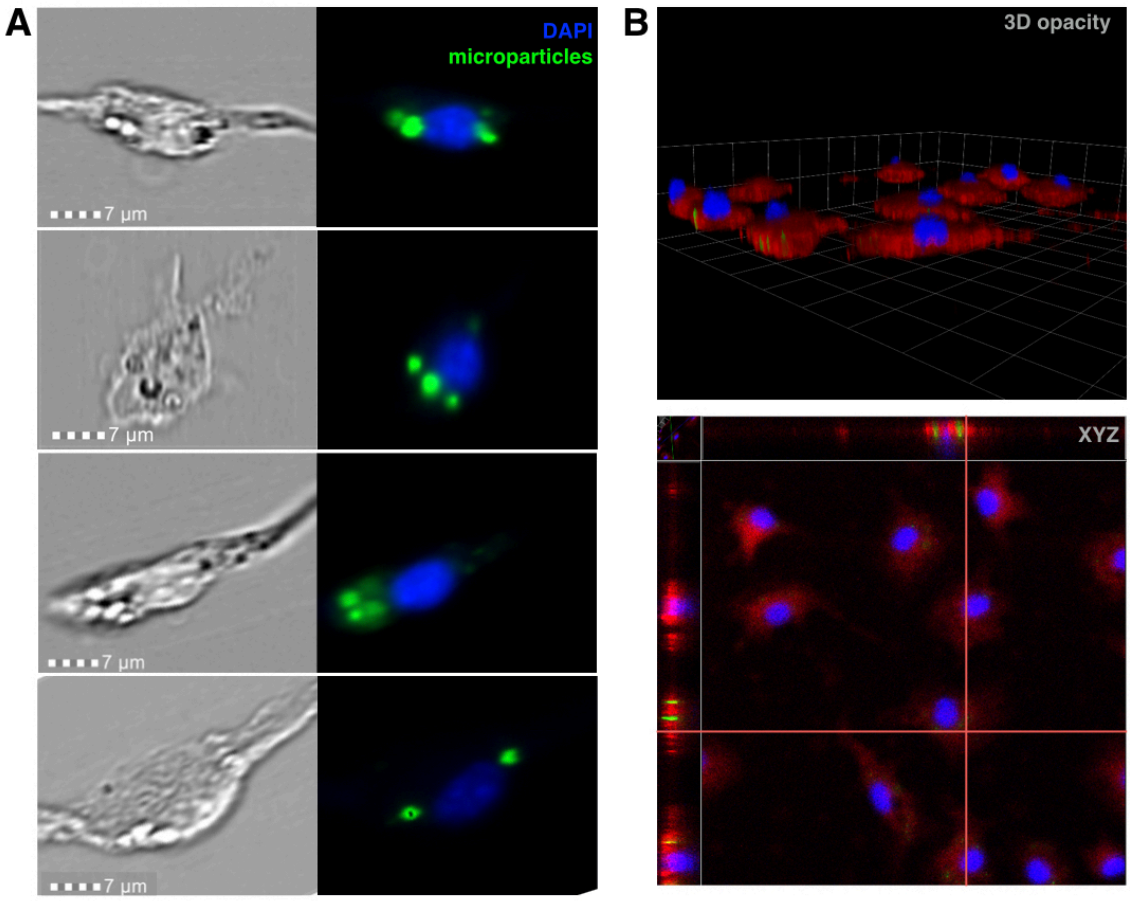

Figure 2.10 The confirmation of particles internalization. *(A) Representative bright field and fluorescent images of BMDM with phagocytosed PLGA microparticles. (B) Confocal images of phagocytic BMDM. Cells were stained with red cell tracker. Particles containing fluorescein are depicted as green, and cell nuclei stained with DAPI as blue.*

To quantify phagocytic BMDM, cells were collected for the measurement of fluorescence intensity by flow cytometry (Figure 2.11 B). We found that coating PLGA microparticles with CD200 led to a significantly higher percentage of phagocytic BMDM when compared to unmodified PLGA microparticles. While the baseline phagocytosis levels were somewhat varied (Figure 2.11 C left), likely because of natural fluctuations in primary cells isolated from individual mice, the % of cells that exhibited positive phagocytosis was approximately 1.7 times higher for cells exposed to CD200-coated particles, when compared to unmodified or streptavidin-coated particles (Figure 2.11 C right). Quantification of the median fluorescein intensity showed that BMDM treated with CD200-PLGA had nearly 3-fold higher fluorescence intensity compared to

cells treated with unmodified or streptavidin-coated particles (Figure 2.11 D). The median fluorescein intensity of the phagocytic BMDM showed no significant differences between PLGA microparticles with different surface modifications, suggesting that the number of particles taken up by phagocytic cells was likely to be similar across the different conditions (Figure 2.11E).

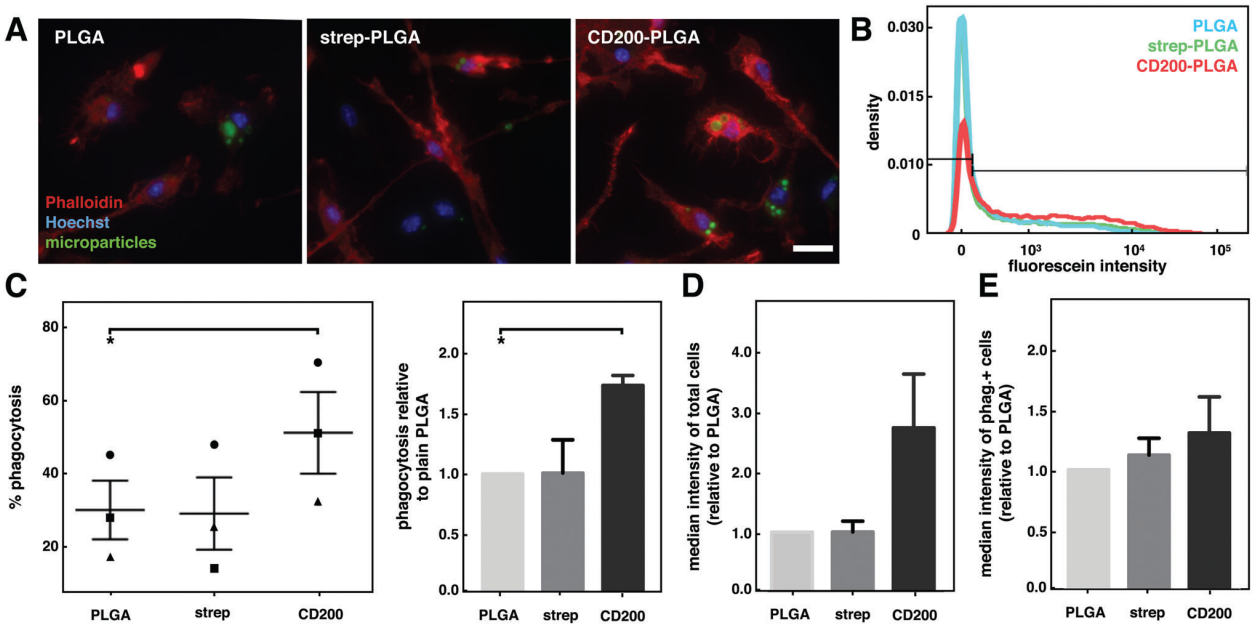

Figure 2.11 Phagocytosis of CD200-coated PLGA microparticles by BMDM. *(A) Representative fluorescence images of BMDM incubated with unmodified, streptavidin-, and CD200-PLGA microparticles (green), stained with phalloidin (red), Hoechst (blue). Scale bar is 20 µm. (B) Representative flow cytometry histogram showing fluorescein intensity of BMDM incubated with different PLGA microparticles. (C) Graph of % phagocytosis of particles by BMDM (left). Each distinct symbol (●,▲,■) represents a separate biological replicate (independent experiment, each performed in duplicate). Graph of phagocytosis of different particles, relative to unmodified PLGA particles (right). (D) Graph of median fluorescein intensity of BMDM treated with different particles, relative to unmodified PLGA. (E) Graph of median fluorescein intensity of phagocytic BMDM in different particle conditions, relative to unmodified PLGA. Data represent the mean ± SEM.* **n** *= 3.* ***p** < 0.05.*

2.3.6 Human BMDM phagocytosis of PLGA microparticles

We further explored whether the enhanced phagocytosis of microparticles by mouse CD200 translates to effects on human cells. To do so, we examined the effects of different PLGA microparticles on primary human peripheral blood monocytes. Similar to what was observed with BMDM, visualization of cells using DiI and Hoechst showed particles taken up within cells (Figure 2.12 A). Analysis by flow cytometry revealed an overall lower percentage of phagocytosis by human monocytes compared to that of BMDM, likely because they were not differentiated into macrophages (Figure 2.12 B). CD200 significantly enhanced the phagocytosis of PLGA microparticles. More than 15% of human monocytes were observed to take up CD200-PLGA microparticles, whereas only 8% of cells phagocytosed control PLGA microparticles (Figure 2.12 C). Overall, human monocytes phagocytosed 2-fold more CD200-coated PLGA microparticles when compared to other microparticles, as shown by the relative phagocytosis and median fluorescein intensity (Figure 2.12 C and E). Similar to what was observed for BMDM, individual phagocytic cells did not uptake more CD200-PLGA microparticles than other microparticles, as demonstrated by similar median intensities of phagocytosis-positive cells (Figure 2.12 E).

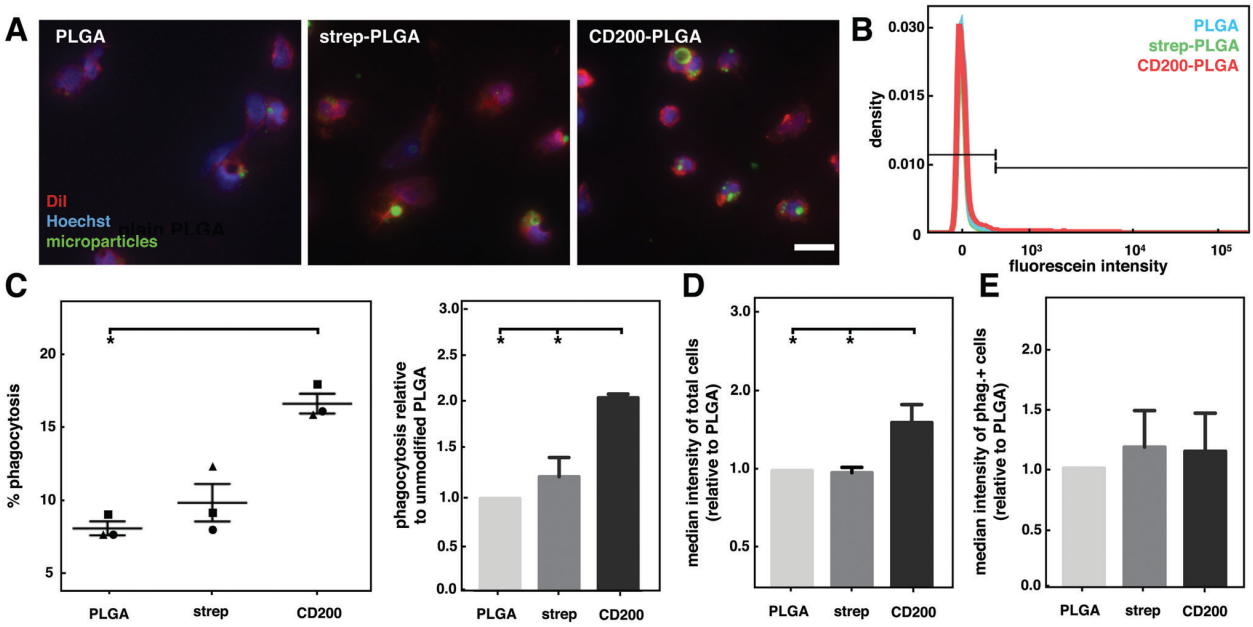

Figure 2.12 Phagocytosis of CD200-coated PLGA microparticles by human monocytes. *(A) Representative fluorescence images of human monocytes incubated with unmodified, streptavidin-, and CD200-PLGA microparticles (green), stained with DiI (red), and Hoechst (blue). Scale bar is 20 μm. (B) Representative flow cytometry histogram showing fluorescein intensity of human monocytes incubated with different PLGA microparticles. (C) Graph of % phagocytosis of particles by human monocytes (left). Each distinct symbol (●,▲,■) represents a separate biological replicate (independent experiment, each performed in duplicate). Graph of monocyte phagocytosis of different particles, relative to unmodified PLGA condition (right). (D) Graph of median fluorescein intensity of human monocytes treated with different particles, relative to unmodified PLGA. (E) Graph of median fluorescein intensity of phagocytosis + human monocytes treated with different particle conditions, relative to unmodified PLGA. Data represent the mean ± SEM.* **n** *= 3.* ***p** < 0.05.*

2.3.7 Human monocyte and macrophage phagocytosis of opsonized targets

Now that we've evaluated macrophage phagocytosis of CD200-modified microparticles, we further examined the phagocytosis of opsonized targets by human phagocytes pre-tuned with a CD200-coated surface. Herein, primary human peripheral blood monocytes or monocyte-derived macrophages were seeded on surfaces coated with different concentrations of CD200, followed by the introduction of opsonized sheep erythrocytes. We found that human monocytes and macrophages cultured on CD200-coated surfaces were significantly more phagocytic than cells on unmodified surfaces, as demonstrated by the increased percentage of cells engulfing erythrocytes

(Figure 2.13 A(i) and B(i)). The effect of CD200 on human monocyte phagocytosis was concentration-dependent, with increasing phagocytic activity observed in response to higher CD200 coating concentrations. Besides, the phagocytic index, or the number of targets ingested per monocyte, was also enhanced by CD200 coating (Figure 2.13 A(ii)). Although CD200 enhanced the phagocytic capacity of individual human monocyte, it only had a moderate effect on human macrophages (Figure 2.13 B (ii)), perhaps because the phagocytic activity of these cells is already high. Nevertheless, our data showed not only that CD200 enhances the phagocytosis of particles, but also that adhesion of monocyte/macrophages to CD200 surfaces enhances their phagocytosis of opsonized targets. This effect has also been observed with surfaces modified with C1q, a complement protein [80], that enhances the phagocytosis of pathogens, cellular debris, and apoptotic cells [81, 82] and these surfaces promote anti-inflammatory cytokine secretion [83].

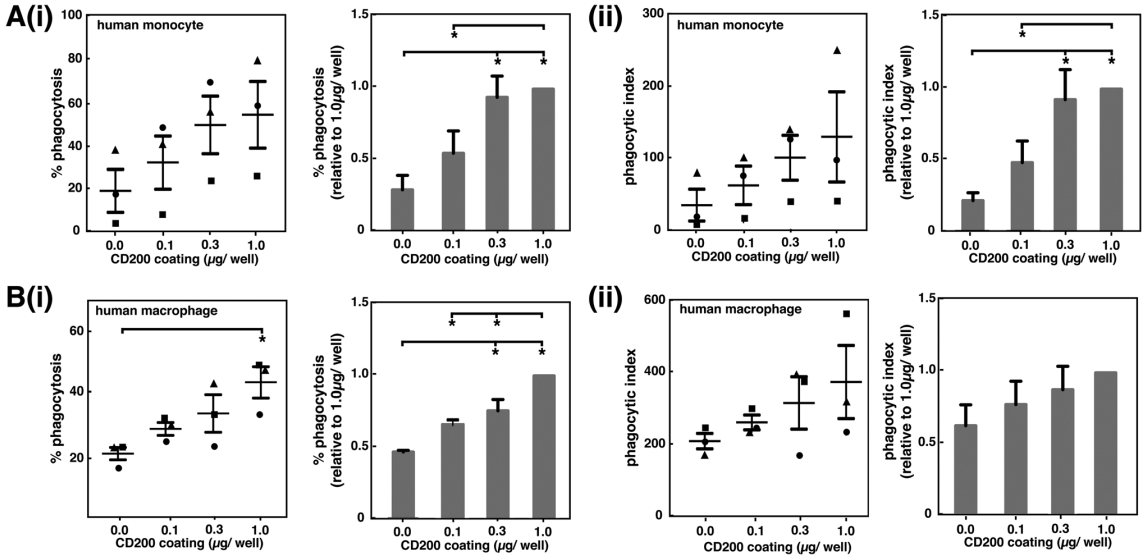

Figure 2.13 Modulation of human phagocytic activity by CD200. *Graphs of % phagocytosis, or the percentage of human monocytes A(i) or macrophages B(i) ingesting at least one target when cultured on surfaces coated with different concentrations of CD200 and incubated with suboptimally IgG-opsonized sheep erythrocytes. The graph on the left of each panel shows the raw data from three independent experiments and the graph on the right shows the value relative to 1.0 μg per well coating condition. Phagocytic index or the number of ingested targets per 100 cells of human monocytes A(ii) or macrophages B(ii) ingesting at least one target when cultured on surfaces coated with different concentrations of CD200 and incubated with suboptimally opsonized sheep erythrocytes. Data represent the mean ± SEM.* **n** *= 3.* ***p** < 0.05.*

2.4 Summary

In this chapter, we demonstrated the effect of the immunomodulatory protein, CD200, on the macrophage responses to PLGA microparticles and films. We investigated particles and films, geometries-associated with different potential clinical applications, including drug delivery and implanted devices, respectively. We found that regardless of geometry, CD200 reduced the secretion of the pro-inflammatory cytokine TNF-alpha. For large particles or surfaces, CD200 enhanced the secretion of the anti-inflammatory cytokine IL-10. Interestingly, although TNF-alpha was consistently downregulated in the presence of CD200, the increase in IL-10 secretion appeared to be somewhat dependent on the geometry, and the effect was only moderate with smaller particles. It is possible that this observation is limited to the time point of evaluation (24 h of culture) or the stimulation conditions used (LPS, IL-4, and IL-13), and further studies exploring additional time points or cytokines of interest would help provide a deeper understanding of the effect of CD200 on macrophage activation.

In addition to the modulation of cytokine secretion, CD200 enhanced the monocyte and macrophage phagocytosis of PLGA particles and opsonized targets. When particles were coated with CD200, a higher percentage of BMDM engulfed at least one particle, although the phagocytic capacity of individual cells was similar. The same trend was observed in human monocytes incubated with CD200-PLGA microparticles. Moreover, human monocyte and macrophage phagocytosis of opsonized erythrocytes were also enhanced in the presence of CD200. Together, these data suggest that CD200 promotes phagocytosis without triggering pro-inflammatory activation.

The immunomodulatory activity of CD200, specifically eliciting a decrease in TNF-alpha and an increase in IL-10, suggests that it may be used to mitigate inflammation and promote wound healing in response to implanted biomaterials. In addition, the “eat me” signal may potentially be

leveraged as a strategy to improve the delivery of therapeutic microparticles into macrophages. While biomaterials have been tremendously beneficial in the controlled delivery of drugs or genes, delivery of anti-inflammatory agents has been challenging, given the inflammatory response to the biomaterials themselves. Our findings suggest that CD200-coated PLGA microparticles may be used to enhance the delivery of anti-inflammatory agents. They may also be used to treat diseases including atherosclerosis or arthritis, where the phagocytic activity of macrophages to clear cellular debris may be desirable, but inhibition of an inflammatory response and preventing the induction of an adaptive response to self -proteins is desirable.

Chapter 3: CD200-coated PLGA nanoparticles and their immunomodulatory effects

3.1 Introduction

In chapter 2, we demonstrated the immunomodulatory effects of CD200 on PLGA microparticles and PLGA films, and we found that the effects are geometry dependent. In order to landscape the potential applications of CD200 coating, we investigated how CD200 coating on nanoparticles influence macrophage behaviors *in vitro* and *in vivo*.

In the past decades, there has been an increased amount of studies developing stealth nanoparticles as drug delivery systems to improve delivery efficiency [84]. Poly(ethylene glycol) (PEG) is a hydrophilic, and non-ionic polymer that has been used as a surface modification of nanoparticles to prolong circulation and provide a stable nanoparticles in biological fluids [85, 86]. To compare the effects of PEGylation and CD200-coating on macrophage behaviors, we fabricated plain PLGA and PEGylated PLGA nanoparticles and further conjugated CD200 on both groups. Four groups of nanoparticles: PLGA, PLGA-CD200, PLGA-PEG, and PLGA-PEG-CD200, were characterized with size distribution, zeta potential, CD200 conjugation, and CD200 release profile. Next, we investigated the activities of bone marrow-derived macrophages (BMDM) including cell viability, phagocytosis, and cytokine secretion. To confirm that the immunomodulatory effects were CD200-mediated, we knocked down CD200R expression on BMDM and explored the phagocytosis behavior of BMDM. In addition to *in vitro* studies, the *in vivo* effects of CD200 coating were examined in the intraperitoneal (IP) injection study.

We hypothesize that CD200-coated PLGA nanoparticles exhibit immunomodulatory effects and CD200-coated PLGA-PEG nanoparticles potentially supplement the biomedical applications of PEGylated nanoparticles in drug delivery.

3.2 Experimental Design

3.2.1 Production of CD200

Production of recombinant CD200 was described in chapter 2.2. Briefly, we constructed the extracellular domain of mouse CD200, a 15-amino acid stiff linker, an AviTag amino acid sequence, and a 6x His sequence in an expression vector for protein expression in a mammalian cell line, CHO-K1. CHO-K1 cells were transfected with the CD200 vector using lipofectamine according to the manufacturer's instructions (Invitrogen) and cultured in complete DMDM media. Transfected cells were selected using L-methionine sulfoximine (MSX) and protein expression was determined by Western blotting. For protein production, transfected CHO-K1 cells were cultured in protein-free chemically-defined media, Pro CHO-AT containing 1% HT supplement, 50U/mL penicillin, and 50 µg/mL streptomycin. The supernatant containing CD200 protein was collected and condensed using a Pellicon XL Device with the Labscale Tangential Flow Filtration system. Concentrated protein was then purified using a HisSpin Ni Column following the manufacturer's manual and the final concentration of the protein was determined using µBCA Protein Assay Kit. Endotoxin level was determined by the *Limulus* Amebocyte Lysate Gel Clot Endotoxin Assay Kit.

3.2.2 Fabrication of PLGA and PEGylated PLGA nanoparticles

3.2.2.1 Synthesis of PLGA-PEG copolymer

In this study, we used Resomer RG 504 H, Poly(D,L-lactide-co-glycolide), acid-terminated, Mw 38,000-54,000 (Sigma). 100 mg of PLGA was dissolved in 1 mL dichloromethane (DCM) (Fisher Scientific). 4mg of EDC (1-ethyl-3-(e-dimethylaminopropyl)carbodiimide hydrochloride) in 0.5 mL DCM was further added to the PLGA solution and reaction was stirred for 10 min. 10 mg of sulfo-NHS (N-hydroxysulfosuccinimide) in 0.5 mL DCM was then added to the reaction. The reaction was incubated at room temperature (RT) on the rotator for 1hr. For precipitation, the

reacting solution was then added dropwise into 50 mL MeOH, followed by centrifugation and pellet collection. The resultant pellet was dissolved in 1 mL DCM and the precipitation was repeated twice. The pellet was allowed to dry under vacuum for 90 min. For PEGylation, the NHS-activated PLGA pellet was dissolved in 1mL chloroform ($CHCl_3$) (Fisher Scientific). To the NHS-activated PLGA solution, 50 mg NH_2-PEG20K-COOH (Sigma) in 1 mL $CHCl_3$ was added, followed by the addition of 4.99 μL N,N-Diisopropylethylamine (DIEA) (Fisher Scientific). The reaction was incubated at RT for 12hr on a rotator. The copolymer solution was dropwise added into cold diethylether/methanol (30 mL:70 mL) (Fisher Scientific) for precipitation. After centrifugation at 4000g for 10min, the supernatant was discarded, and the pellet was dissolved in 1 mL CHCl3. The precipitation was repeated twice before drying the pellet under vacuum. The final copolymer product was characterized using ^{1}H-NMR.

3.2.2.2 Fabrication of PLGA nanoparticles

We fabricated PLGA nanoparticles using single emulsion evaporation techniques. All the reagent was sterile filtered using a 0.22 μm syringe filter unit. For nanoparticle synthesis, 1 mL of 1%w/v PLGA (or PLGA-PEG), together with 2% BODIPY dye (ThermoFisher), was dissolved in dichloromethane (DCM) (Fisher Scientific), and then pipetted into 50 mL 0.5% polyvinyl alcohol (PVA) under homogenization. Once the PLGA droplets were formed, the solvent was allowed to evaporate under continuous stirring for an additional 5min. Solid PLGA particles formed when the solvent evaporated completely. We further size-selected PLGA nanoparticles using 1 μm cell strainers. PLGA particles were washed with sterile PBS 3 times followed by centrifugation. Particle size and morphology were determined by SEM imaging and analysis. PLGA nanoparticles were further characterized using a Malvern Zetasizer Nano ZS.

3.2.3 Conjugation of CD200 on PLGA nanoparticles

Carboxylic acid-terminated PLGA was treated with EDC/NHS crosslinkers as mentioned in chapter 2. Immediately after washing with MES buffer, 10 μg of CD200 in 500 μL PBS solution was used to resuspend EDC/NHS-reacted nanoparticles. The reaction was incubated at RT for 4hr on a rotator. The conjugation of CD200 was also confirmed by PE-conjugated anti-CD200 antibody using microscopic techniques. PLGA nanoparticles with different surface modifications were characterized using a Malvern Zetasizer Nano ZS to determine surface charge and size distribution. CD200 release from nanoparticles was examined by μBCA assay.

3.2.4 BMDM culture

All protocols involving animals were approved by the Institutional Animal Care and Use Committee at the University of California Irvine prior to initiation of the study. Bone marrow-derived macrophages (BMDM) were harvested following the protocol described in chapter 2. For cell viability after uptake of nanoparticles, BMDM were seeded on tissue culture plates at 100,000 cells/cm^2. At 6hr after cell seeding, the culture media was replaced with D-10 media containing different combinations of the following stimuli: 0.3 ng/mL Lipopolysaccharide (LPS), 1.0 ng/mL interferon-gamma (IFNγ), 20 ng/mL interleukin-4 (IL-4), and 20 ng/mL interleukin-13 (IL-13). PLGA nanoparticles with different surface modifications were introduced to the cells together with culture media containing different stimuli. After 12hr or 48hr of incubation, the viability of BMDM was analyzed by MTT cell proliferation assay kit (ThermoFisher) following the manufacturer's protocol and reading absorbance at 570 nm.

3.2.5 BMDM phagocytosis assay

BMDM were seeded in 12-well plate at 100,000 cells/cm^2. After 2hr adhesion, cells were pre-stimulated with stimuli (concentration listed above) to differentiate into different phenotypes for 12hr. After which, 100 μg of fluorescent PLGA nanoparticles of different surface modifications

were introduced to the cells, followed by a 1hr phagocytosis period. After 1hr, the un-phagocytosed particles were washed out with PBS. The cells were then collected using a cell scraper and suspended in PBS. Phagocytosed cell acquisition and analysis were performed using a BD LSR II flow cytometer and FlowJo software.

3.2.6 BMDM cytokine secretion

For cytokine secretion assay, BMDM were seeded on the tissue culture plates at a cell density of 100,000 cells/cm^2. At 6hr after cell seeding, the culture media was replaced with D-10 media containing different combinations of stimuli together with 100 μg of PLGA nanoparticles different surface modifications. After 12hr or 48hr of incubation, the supernatants were collected and analyzed for TNF-alpha and IL-10 secretion by enzyme-linked immunosorbent assay (ELISA) following the manufacturer's instructions (BioLegend).

3.2.7 CD200R1 siRNA knock-down

siGENOME Mouse CD200R1 siRNA (#57781, Dharmacon) and control nontargeting siRNA (Dharmacon) were used for BMDM transfection. The knock-down was performed using P3 Primary Cell 4D-Nucleofector kit (Lonza) with 4D-Nucleofector Unit (Lonza) following the manufacturer's protocol. Briefly, for a single reaction, 16.4 μL of Nucleofector solution was pre-mixed with 3.6 μL Supplement. BMDM were harvested, counted, and further centrifugated at the required amount (total of 500,000 cells). The cell pellet was carefully resuspended in 20 μL Nucleofector solution. 300 nM siRNA was then added to the cell suspension, and the reaction was transferred into the Nuclecuvette vessels. The vessel was then placed into the retainer of 4D-Nucleofector Unit. After run completion, transfected cells were resuspended and plated on 12 mm coverslips in a 24-well plate. Cells were cultured for 48hr before studies. The CD200R knock-down was confirmed by Western blot and flow cytometry.

After the phagocytosis study, BMDM were fixed with 4% paraformaldehyde (Electron Microscopy Sciences) for 5 min, and washed carefully with PBS. Cells were then stained with PE-conjugated anti-CD200R antibody (BioLegend) and Hoechst 33342 dye (Invitrogen) for 1hr, followed by thorough washes with PBS. Finally, the coverslips were mounted on glass slides using Fluoromount-G (Southern Biotech). Fluorescence images were obtained using an Olympus confocal laser scanning microscope. CD200R expression and phagocytic cell acquisition and analysis were performed using ImageJ software.

3.2.8 Intraperitoneal (IP) injection of PLGA nanoparticles

All protocols involving animals were approved by the Institutional Animal Care and Use Committee at the University of California Irvine prior to initiation of the study. 12-week-old C57BL/6 mice (Jackson Laboratories) were used in this study. Plain PLGA, CD200-coated PLGA, PEGylated PLGA, and CD200-coated PEGylated PLGA nanoparticles were administrated by intraperitoneal (IP) injection. Each injection contained 500 μL of 0.2% (w/v) particle suspension in PBS. 60 min after administration, mice were euthanized, and 5 mL of PBS was injected into the peritoneal cavity. We gently massaged the peritoneum to dislodge any attached cells into the PBS solution. The peritoneal cells were collected and fixed with 10% formalin. In order to elucidate the types of peritoneum cells, cells were stained with fluorescent antibodies: F4/80 (PE or APC, BioLegend, #123110 or #123116), CD11b (PerCp/Cy5.5, BioLegend, #101228), and CD200R (PE, BioLegend, #128908). Stained samples were analyzed by flow cytometry to determine biomarkers and phagocytosis. Phagocytic cell acquisition and analysis were performed using a BD LSR II flow cytometer and FlowJo software.

3.2.9 Statistical analysis

Statistical analysis was performed using student's *t*-test and $p<0.05$ was considered statistically significant.

3.3 Results and Discussions

3.3.1 Characterization of PLGA-PEG copolymer

PEGylation of PLGA nanoparticles has been found to prolong circulation and improved drug delivery in many studies [86-89]. In this study, we investigated the immunomodulatory effects of both plain PLGA and PEGylated PLGA nanoparticles. First, we synthesized PLGA-PEG copolymer following published literature [90]. Carboxyl-terminated PLGA was PEGylated via the reaction between the -COOH group (on PLGA) and the $-NH_2$ group (on PEG) using EDC/NHS crosslinker. The reaction and structure of the copolymer are illustrated in Figure 3.1 A. The product of PLGA-PEG copolymer synthesis was characterized by ^1H NMR. The ^1H NHR spectrums of plain PLGA and PLGA-PEG copolymer are shown in Figure 3.1 B (courtesy of Andrew T. Rowley). The characteristics signals appear at 5.26, 4.86, 3.68, 1.63 ppm are assigned to the methane hydrogen of lactide units (-CH) (a), methylene hydrogen of the glycolide units ($-CH_2$) (b), the methylene hydrogen of the PEG ($-CH_2$) (d) and the methyl hydrogen of the lactide units ($-CH_3$) (c), respectively. After copolymer synthesis, the methylene hydrogen of the PEG ($-CH_2$) shifted into three peaks (e-g) confirming successful conjugation.

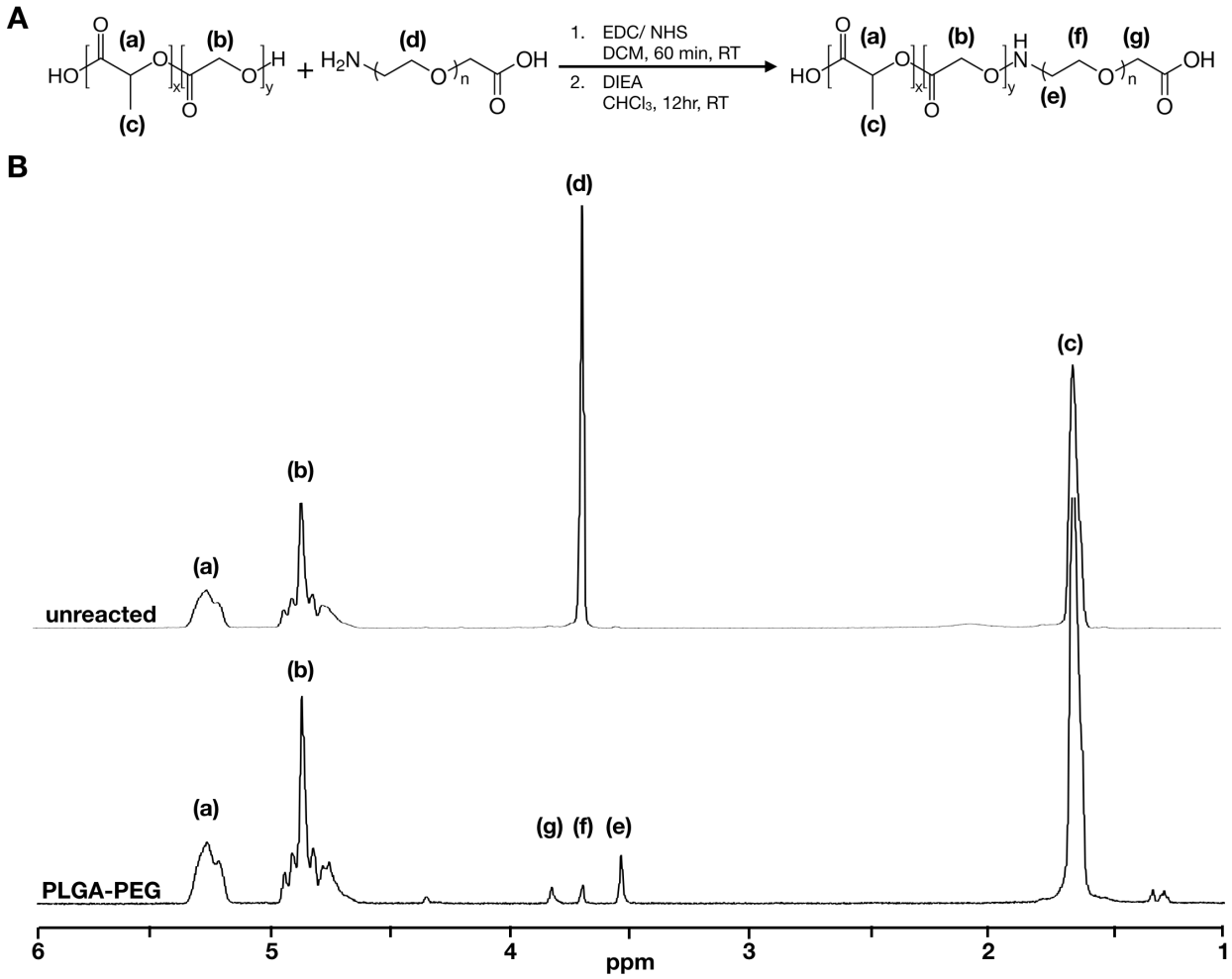

Figure 3.1 Characterization of PLGA-PEG copolymer. *(A) Conjugation of PLGA and PEG molecules. (B) ^{1}H NMR spectrum of unreacted PLGA and PEG (top), and PLGA-PEG copolymer (bottom). ^{1}H NMR result is by courtesy of Andrew T. Rowley.*

3.3.2 Characterization of PLGA and PLGA-PEG nanoparticles

After copolymer synthesis, we fabricated two groups of nanoparticles, PLGA and PLGA-PEG. Single emulsion technique was used for nanoparticle fabrication. Plain PLGA or PLGA-PEG copolymer was dissolved in dichloromethane (DCM) at 1%(w/v), followed by homogenization in 0.5% poly(vinyl alcohol) (PVA) solution. Nanoparticles were further selected using 1 μm cell strainer. The morphology of the nanoparticles was determined by scanning electron microscopy (SEM) imaging, and the size distribution was further evaluated. PLGA nanoparticle

production yielded round and smooth nanoparticles with a medium diameter of 623nm, while PLGA-PEG nanoparticle fabrication led to broader distribution with a medium diameter of 887nm.

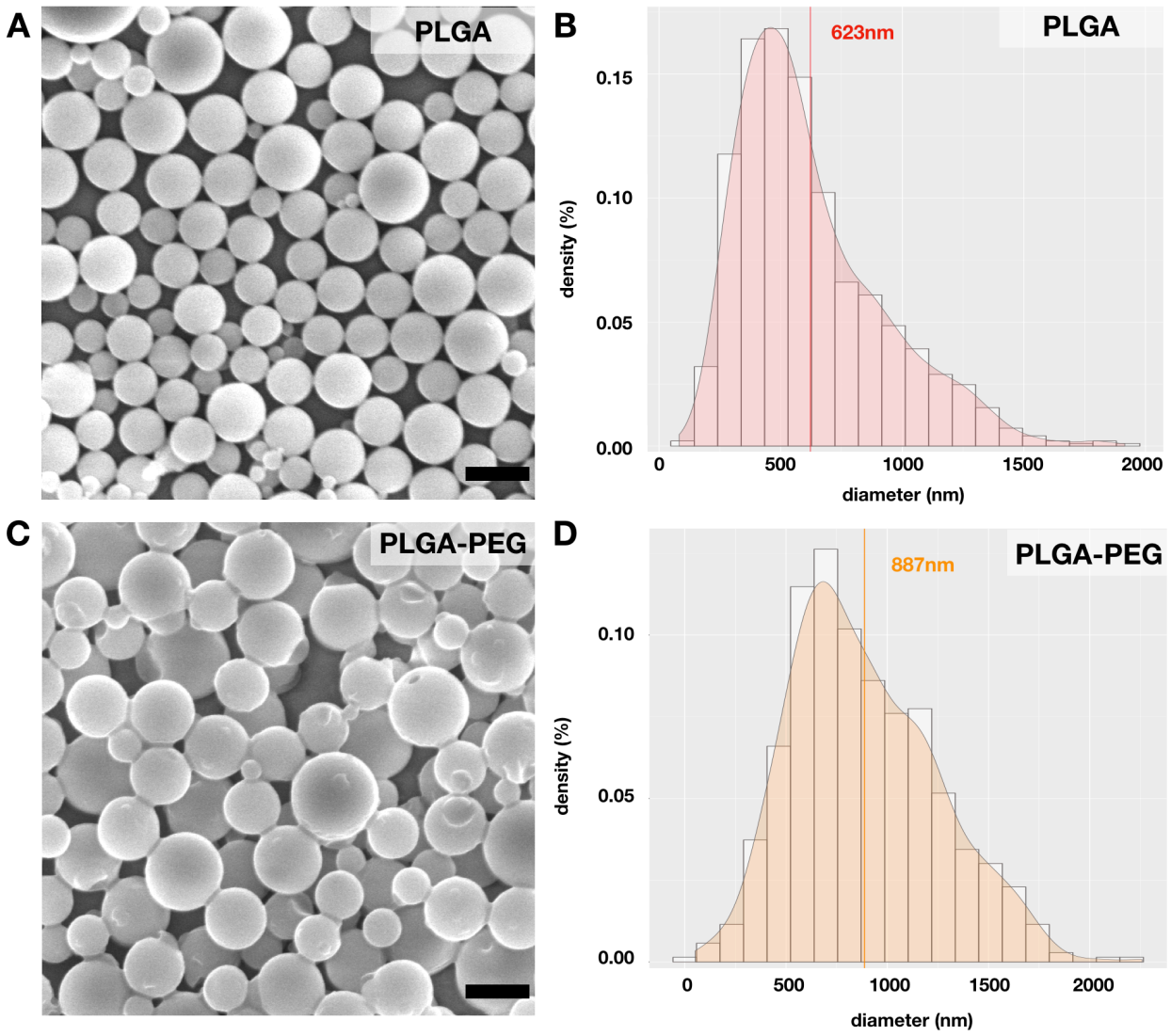

Figure 3.2 Characterization of PLGA and PLGA-PEG nanoparticles. *(A) SEM image of PLGA nanoparticles (B) Size distribution of PLGA nanoparticle (C) SEM image of PLGA-PEG nanoparticles (D) Size distribution of PLGA-PEG nanoparticles. Scale bar of 1μm.*

3.3.3 Characterization of CD200-coated PLGA nanoparticles

We further conjugated CD200 on PLGA and PLGA-PEG nanoparticles. There were four groups of nanoparticles carried out in this study, including plain PGLA nanoparticles, PLGA-CD200 nanoparticles, PLGA-PEG nanoparticles, and PLGA-PEG-CD200 nanoparticles. The zeta potential of nanoparticles was determined using a Malvern DLS NanoSizer. All groups of particles exhibited a net negative charge with zeta potential values ranging from -9.887 mV to -0.861 mV (Figure 3.3 A). PLGA nanoparticles had a negative surface charge of -9.887 mV, and CD200 coating neutralized the charge to be -0.931 mV. PEGylation brought the baseline of nanoparticles to be around -3.893 mV. Again, CD200 on PEG neutralized surface zeta potential to be -0.861 mV. The CD200 conjugation on nanoparticles was confirmed by PE-conjugated anti-CD200 antibody (Figure 3.3 C). The *in vitro* release behavior of CD200 from PLGA surface was performed using the μBCA kit to detect released CD200 in the PBS solution. The release showed a fast initial release, followed by slower and continuous release afterward (Figure 3.3 B). Less than 60% of CD200 remained on PLGA-PEG-CD200 nanoparticles after day 1, while there is 80% remaining on PLGA-CD200 nanoparticles.

A

particle	zeta potential (mV)
PLGA	-9.877 ± 0.381
PLGA-CD200	- 0.931 ± 0.030
PLGA-PEG	- 3.893 ± 0.102
PLGA-PEG-CD200	- 0.861 ± 0.010

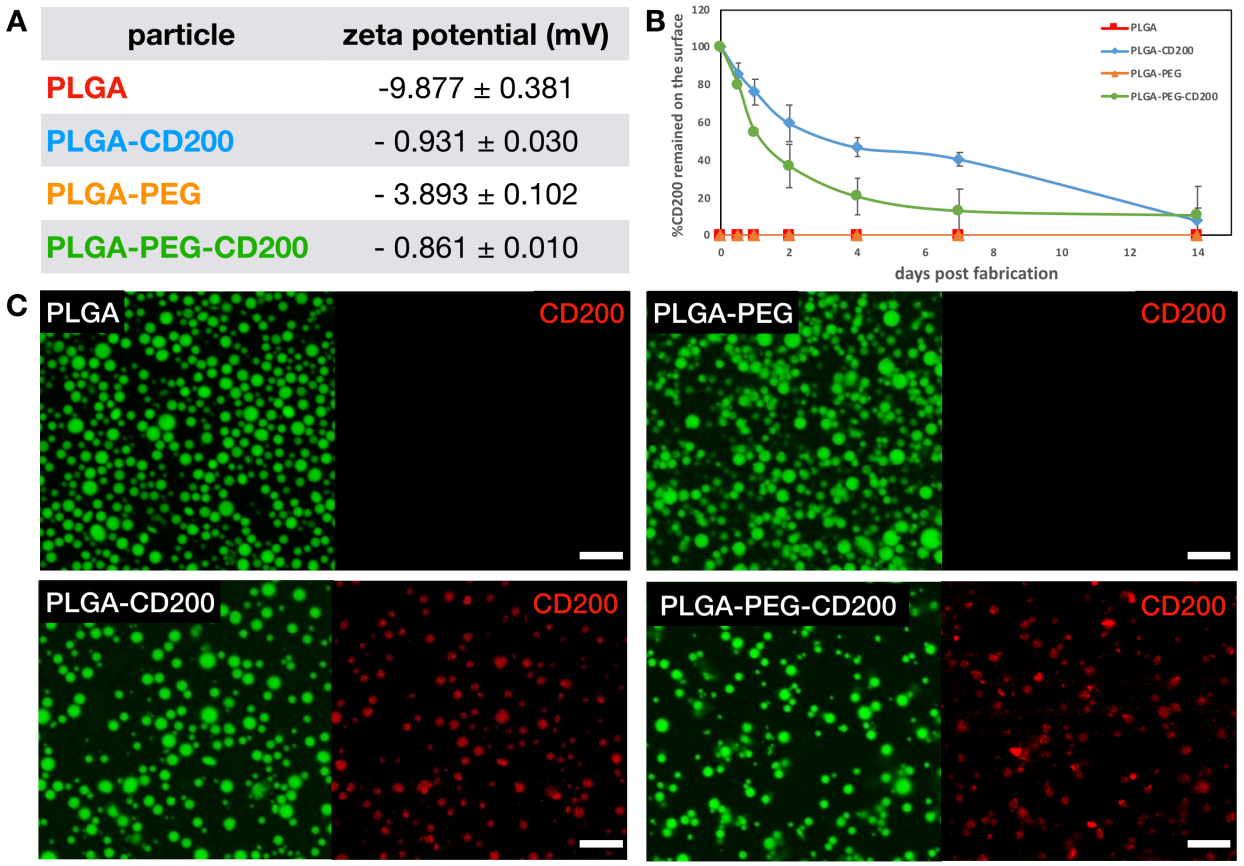

Figure 3.3 Characterization of PLGA nanoparticles with different modifications. *(A) PLGA nanoparticle parameters determined by dynamic light scattering (DLS). (B) Percentage of CD200 remained on the particle surface. Data represent the mean ± SD. (C) Fluorescent images of CD200-coated nanoparticles detected by PE-conjugated anti-CD200 antibodies. Scale bar of 5μm.*

3.3.4 BMDM viability with PLGA nanoparticles

The cytotoxic activity of different groups of PLGA nanoparticles was evaluated by MTT assay assessing BMDM metabolism. BMDM were incubated with different groups of PLGA nanoparticles and cytokine stimulating media for 12hr or 48hr. The data suggest no BMDM metabolic difference between different stimulations nor different nanoparticles (Figure 3.4). The overall metabolism level was observed higher in 48hr post seeding than in 12hr post seeding.

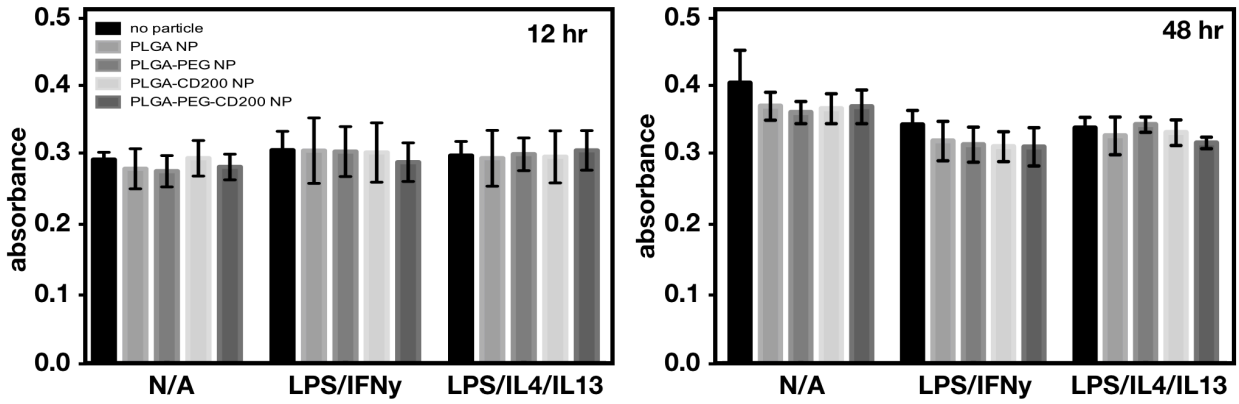

Figure 3.4 Viability of BMDM cells incubated with PLGA nanoparticles of different modifications. *Cells were seeded into 96-well plates and incubated with particles with different stimulation media for 12hr or 48hr and examined by MTT assay. Data represent the mean ± SEM of n=3.*

3.3.5 CD200R expression of BMDM

We further investigated the expression level of CD200 receptor, CD200R, on different BMDM phenotypes. BMDM were pre-stimulated with no stimulation, LPS/IFNγ, or IL-4/IL-13 for 12hr before collected for flow cytometry. CD200R expressed on the cell surface was detected using PE-conjugation anti-CD200R antibodies. We found that IL-4/IL-13-stimulated (M2) BMDM, which is the anti-inflammatory phenotype, expressed higher CD200R than non-stimulated or LPS/IFNγ-stimulated (M1) BMDM (Figure 3.5 A). Only 15% of LPS/IFNγ-stimulated BMDM were found to be CD200R positive, while non-stimulated BMDM had 48% CD200R positive and 88% IL-4/IL-13-stimulated BMDM were expressing CD200R (Figure 3.5 B). Not only were more cells expressing CD200R, but this anti-inflammatory BMDM also expressed higher CD200R as suggested in the intensity quantification (Figure 3.5C). We hypothesized that the immunomodulatory effect of CD200 would be more pronounced in the anti-inflammatory phenotype (IL-4/IL-13-stimulated BMDM) than the other two phenotypes due to the higher expression of its receptor, CD200R.

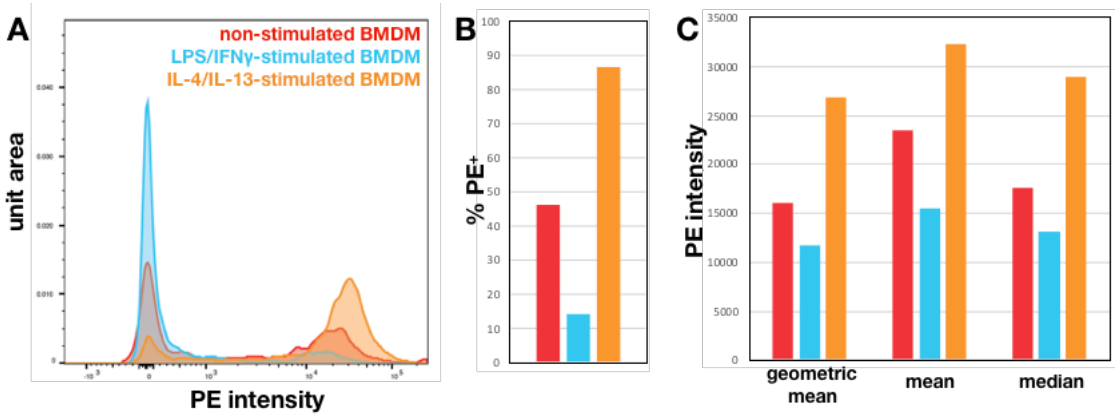

Figure 3.5 CD200R expression of different BMDM phenotypes. *(A) Flow cytometry histogram of CD200R expression of different BMDM phenotypes. (B) Graph of % CD200R positive. (C) Graph of PE intensity in geometric mean, mean, or median. CD200R was detected using PE-conjugated anti-CD200R antibody.*

3.3.6 BMDM phagocytosis of PLGA nanoparticles

After characterization of different nanoparticles and CD200R expression on BMDM, we first examined the effect of CD200 on BMDM phagocytosis. To investigate the phagocytic behavior of BMDM with different phenotypes, we pre-stimulated BMDM with cytokines (no stimulation, LPS/IFNγ, or IL-4/IL-13. After 12hr stimulation, fluorescent PLGA nanoparticles with different surface modifications were seeded on top of BMDM, followed by a 1hr phagocytosis assay. Phagocytic behavior was examined by flow cytometry. LPS/IFNγ-stimulated BMDM exhibited a higher frequency of phagocytic events than non-stimulated BMDM and IL-4/IL-13-stimulated BMDM (Figure 3.6 A). In addition, all different BMDM phenotypes phagocytosed more PLGA-PEG copolymer nanoparticles than plain PLGA nanoparticles. In non-stimulated BMDM, CD200 coating (PLGA-CD200 or PLGA-PEG-CD200) decreased phagocytic events compared to their control particle groups (PLGA or PLGA-PEG, respectively) (Figure 3.6 B). The CD200-mediated inhibition of phagocytosis was more dramatic in IL-4/IL-13-stimulated BMDM. Interestingly, CD200 conjugation does not have an influence on the phagocytosis of LPS/IFNγ-stimulated BMDM due to their low expression on CD200R.

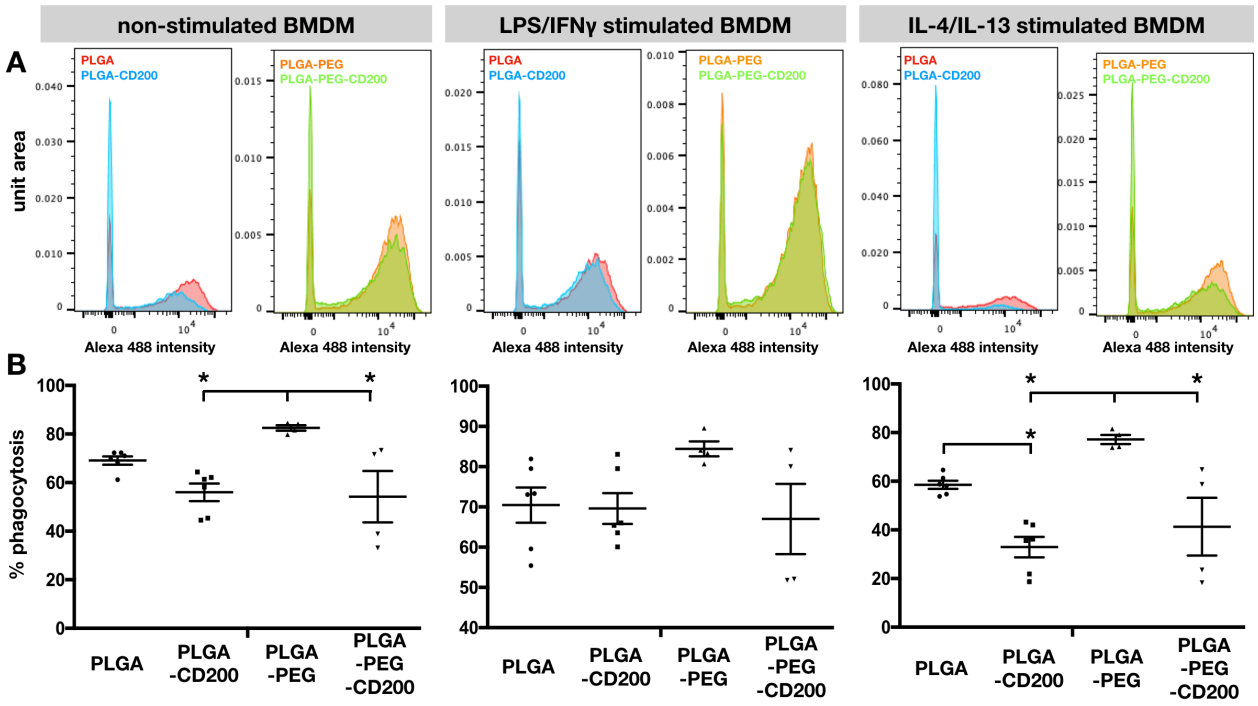

Figure 3.6 BMDM Phagocytosis of PLGA nanoparticles. *BMDM were pre-stimulated with cytokines: no stimulation, LPS/IFNγ stimulation, or IL-4/IL-13 stimulation. (A) Representative flow cytometry histograms showing the fluorescent intensity of BMDM incubated with different groups of PLGA nanoparticles (Alexa 488) for 1hr. (B) Graphs of % phagocytosis of particles by BMDM. Data represent the mean ± SEM of n>4. * denotes* $p < 0.05$.

3.3.7 BMDM cytokine secretion

Macrophages not only phagocytose foreign particles but also secrete cytokines in response to invaders. We further examined BMDM cytokine secretions in response to different modifications of PLGA nanoparticles. In this study, BMDM were incubated with different cytokine stimulations (LPS/IFNγ or LPS /IL-4/IL-13) and PLGA nanoparticles (PLGA, PLGA-CD200, PLGA-PEG, or PLGA-PEG-CD200) for 12hr or 48hr before collection for ELISA. In chapter 2, we found that PLGA microparticles stimulated TNF-alpha secretion compared to the no-particle case. Herein, the addition of PLGA nanoparticles did not further enhance TNF-alpha secretion (Figure 3.7). After 12hr-stimulation, there is no significant difference observed in either TNF-alpha or IL-10 secretion across different PLGA nanoparticles. However, PLGA-CD200 and PLGA-PEG both exhibited lower TNF-alpha secretion when compared to the PLGA nanoparticle case after 48hr-stimulation. CD200-coated nanoparticles did not augment IL-10 secretion as CD200-coated microparticles did. This data combined suggested a geometry-dependent effect of CD200 on macrophage behaviors.

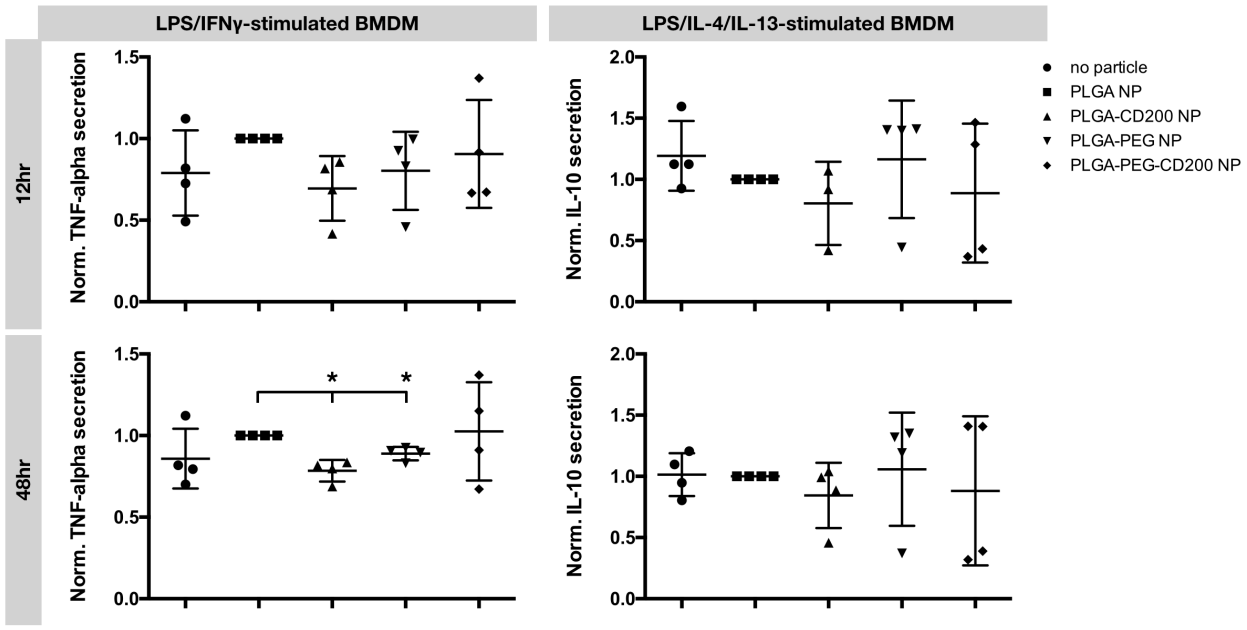

Figure 3.7 BMDM TNF-alpha and IL-10 secretions after incubation with cytokines and nanoparticles. *BMDM were stimulated with either LPS/IFNγ or LPS/IL-4/IL-13 for TNF-alpha or IL-10 secretion respectively. Data were normalized to PLGA nanoparticle case in each biological replicate. Data represent the mean ± SEM of* $n = 3$. **denotes* $p < 0.05$.

3.3.8 CD200R1 siRNA knock-down

To confirm the CD200-mediated effect on phagocytosis, we performed CD200R1 siRNA knock-down. BMDM were transfected with CD200R1 SmartPool siRNA using Lonza Nucleofector unit and kit. Cells were cultured for 48hr before analysis for CD200R expression. The CD200R protein expression was evaluated by Western blotting, showing successful knock-down compared to the non-target (NT) case (Figure 3.8 A). CD200R surface expression was further evaluated by immunofluorescent staining using PE-conjugated anti-CD200R antibodies (Figure 3.8 B). IL-4/IL-13-stimulated BMDM expressed higher CD200R than the other two phenotypes, which is consistent with the flow cytometry data in section 3.3.5. Quantitative data from image analysis confirmed that there is a 95% knock-down.

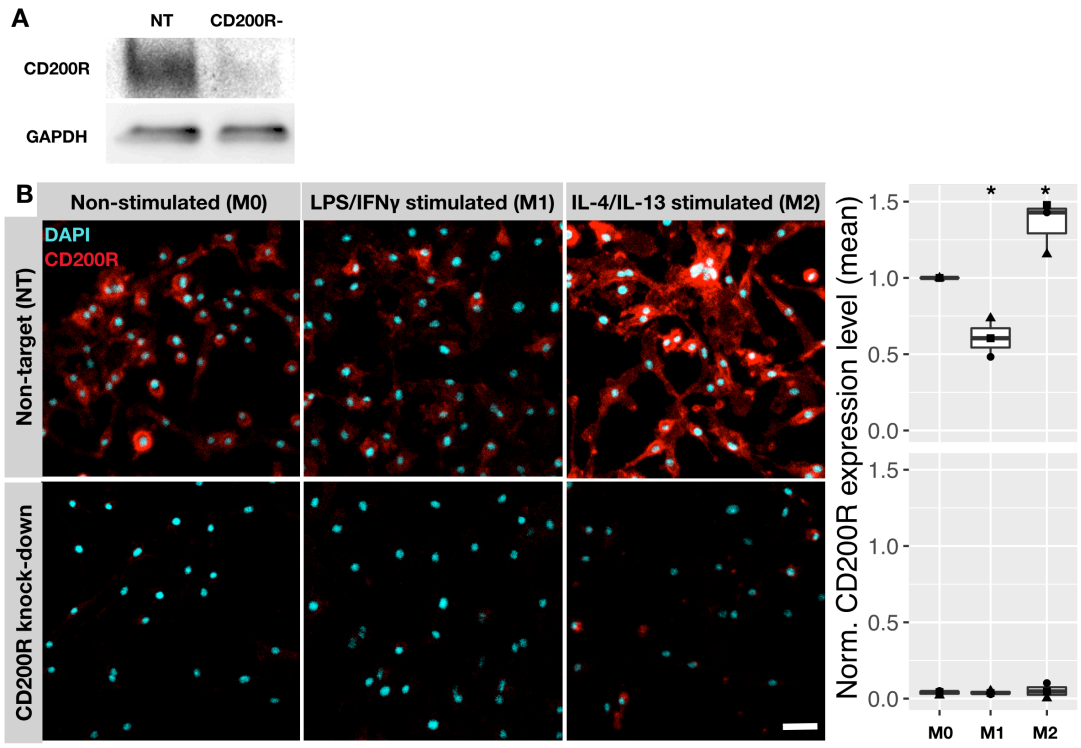

Figure 3.8 CD200R expression after CD200R siRNA transfection*. (A) Western blots of CD200R protein expression of non-target (NT) and CD200R knock-down BMDM. GAPDH was used as a housekeeping protein. (B) Immunofluorescent images of BMDM stained with CD200R (PE-conjugated antibody) and quantitative analysis on normalized PE mean intensity. Scale bar= 20μm. Data were normalized to the non-stimulated case in each biological replicate. Data represent the mean ± SD of* n = *3.*

3.3.9 The effect of CD200-coated nanoparticles on CD200R knock-down BMDM

We further investigated the effect of CD200 on the phagocytic behavior of CD200R knock-down BMDM. 48hr after siRNA transfection, cells were stimulated with either no-stimulation, LPS/IFNγ or IL-4/IL-13 for 12hr. PLGA nanoparticles with different modifications were then introduced to BMDM, followed by a 1hr phagocytosis assay. Non-phagocytosed particles were washed away with PBS, and the cells were fixed and stained with PE-conjugated anti-CD200R antibodies. The immunofluorescent images in Figure 3.9 shows that non-target BMDM expressed high levels of CD200R, while CD200R knock-down BMDM did not present CD200R. In the non-target case, there are less BMDM phagocytosing PLGA-CD200 or PLGA-PEG-CD200 when compared to PLGA or PLGA-PEG respectively. However, after CD200R knock-down, the phagocytic activity of BMDM was independent of PLGA modifications.

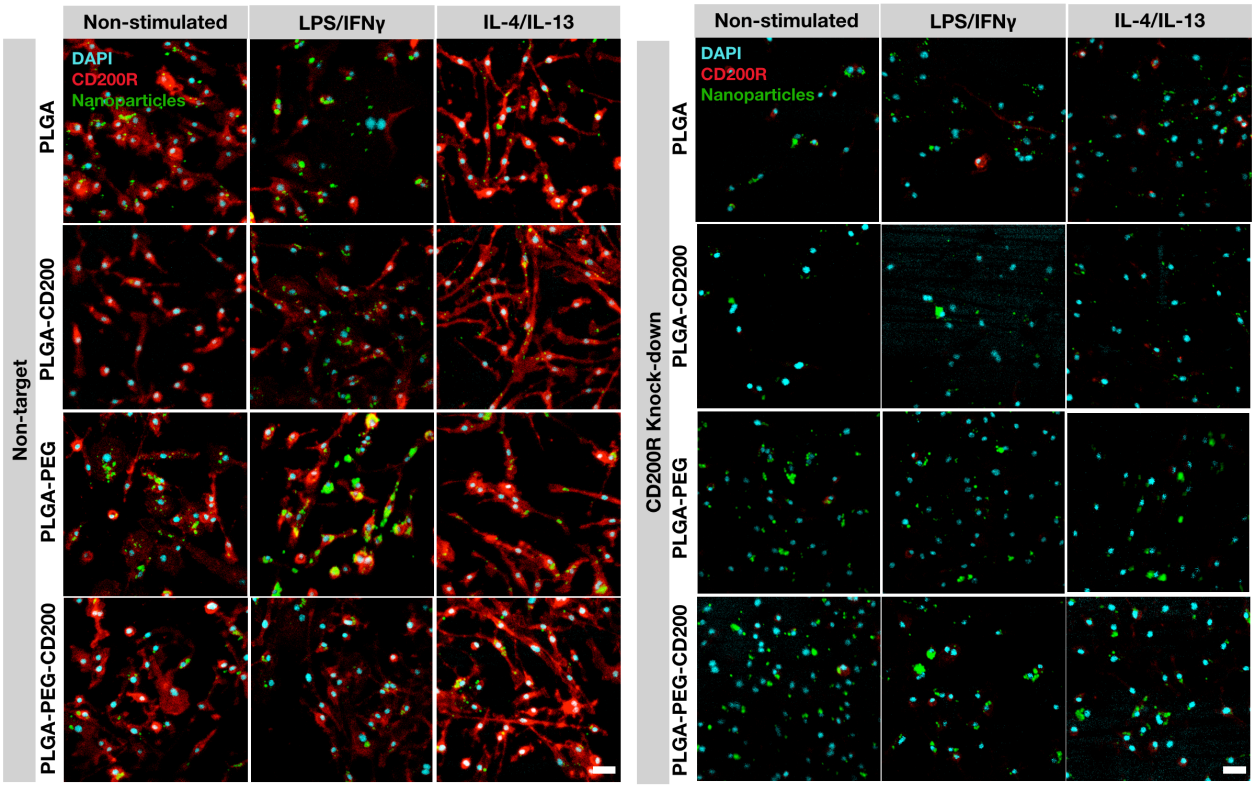

Figure 3.9 Representative immunofluorescent images of BMDM phagocytosing PLGA nanoparticles. *BMDM were knock-down with non-target siRNA (left) or CD200R siRNA (right), and further stimulated with cytokines of no-stimulation, LPS/IFNγ or IL-4/IL-13. Different groups of PLGA nanoparticles (PLGA, PLGA-CD200, PLGA-PEG, or PLGA-PEG-CD200) were then incubated with the cells for 1hr. Cells were fixed and stained with DAPI and PE-conjugated anti-CD200R antibodies followed by confocal microscopy imaging. Scale bar=20μm.*

Additionally, we quantified CD200R expression (Figure 3.10 A), percentage phagocytosis (Figure 3.10 B), particle fluorescent intensity of all cells (Figure 3.10 C), and fluorescent particle intensity of phagocytic cells (Figure 3.10 D). M2 (IL-4/IL-13-stimulated) BMDM exhibited higher CD200R independent of phagocytosing particles compared to the other two phenotypes (Figure 3.10 A). M1 (LPS/IFNγ-stimulated) BMDM expressed 40% lower CD200R in comparison to M0 BMDM. siRNA knock-down resulted in 95% lower CD200R expression as shown in Figure 3.10 A. We next determined the percentage phagocytosis of BMDM by setting a threshold to particle fluorescent intensity histogram. Data in Figure 3.10 B was normalized to the PLGA case of each biological replication. PLGA-CD200 and PLGA-PEG-CD200 cases exhibited lower phagocytosis percentage in M0 and M2 BMDM, but no difference in M1 BMDM. Interestingly, BMDM phagocytosed more PLGA-PEG nanoparticles than PLGA nanoparticles as suggested by fluorescent particle intensity (Figure 3.10 C). The fluorescent intensity for phagocytic cells indicates the phagocytic capacity of an individual cell. As Figure 3.10 D shows, there were not only fewer phagocytic BMDM, but individual phagocytes also engulfed less CD200-coated nanoparticles.

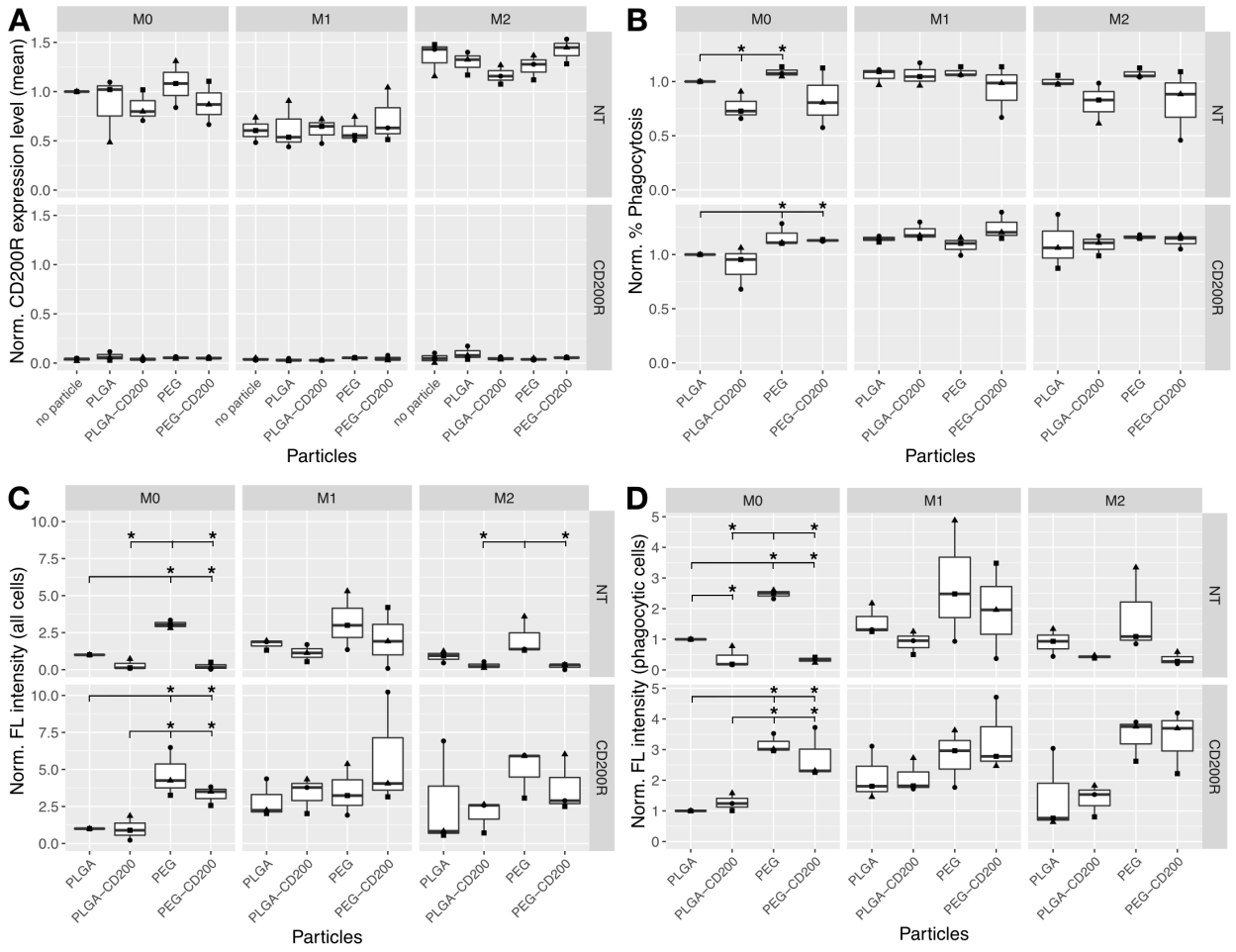

Figure 3.10 Quantification of CD200R knock-down study*. (A) CD200R expression (B) Percentage phagocytosis (C) Fluorescent intensity of all cells and (D) Fluorescent intensity of phagocytic cells. CD200R expression levels were normalized to no particle case in each biological replicate. Data in (B) (C) (D) was normalized to PLGA case in each biological replicate. Data represent the mean ± SD of* n = *3.*

3.3.10 Intraperitoneal (IP) injection of PLGA nanoparticles

To investigate PLGA nanoparticles *in vivo* responses, we performed intraperitoneal injection in C57BL/6 mice and collected peritoneum cells to study population and phagocytosis. Different groups of PLGA nanoparticles were prepared in PBS solution at 0.2%(w/v). Each mouse was administrated with 1 mg nanoparticles (in 500 μL PBS). 1hr after injection, peritoneal cavity cells were collected and stained for phenotypic analysis and phagocytosis behavior by flow cytometry. We then examined cell population highly expressing F4/80 and CD11b, as well as the population highly expressing F4/80 and CD200R.

Cells were stained with anti-F4/80 antibodies (PE) and anti-CD11b antibodies (PerCp/Cy5.5) to identify peritoneum macrophages. Percentage of $F4/80^+$ and $CD11b^+$ population was determined by flow cytometry (Figure 3.11 A). Quantitative data suggested that particle injections led to the recruitment of non-F4/80-CD11b cell types and exhibited lower % of $F4/80^+$ and $CD11b^+$ cells when compared with PBS-only injection (Figure 3.11 B). Interestingly, PLGA-CD200-injection resulted in the lowest percentage of cells with F4/80 and CD11b expressions. We further looked into the phagocytic behavior of $F4/80^+$ and $CD11b^+$ cells. Flow cytometric histogram of nanoparticle fluorescent intensity suggested lower phagocytes in CD200 cases when compared with control cases (Figure 3.11 C). PEGylation of PLGA nanoparticles reduced *in vivo* phagocytosis, and addition of CD200 potentially diminished phagocytosis further (Figure 3.11 D). The geometric mean of phagocytic cells was evaluated for the phagocytic capacity of individual cells (Figure 3.11 E). $F4/80^+$ and $CD11b^+$ phagocytes exhibited lower PLGA-CD200 nanoparticle uptake when compared with plain PLGA, and so did PEGylated nanoparticle cases (Figure 3.11 F).

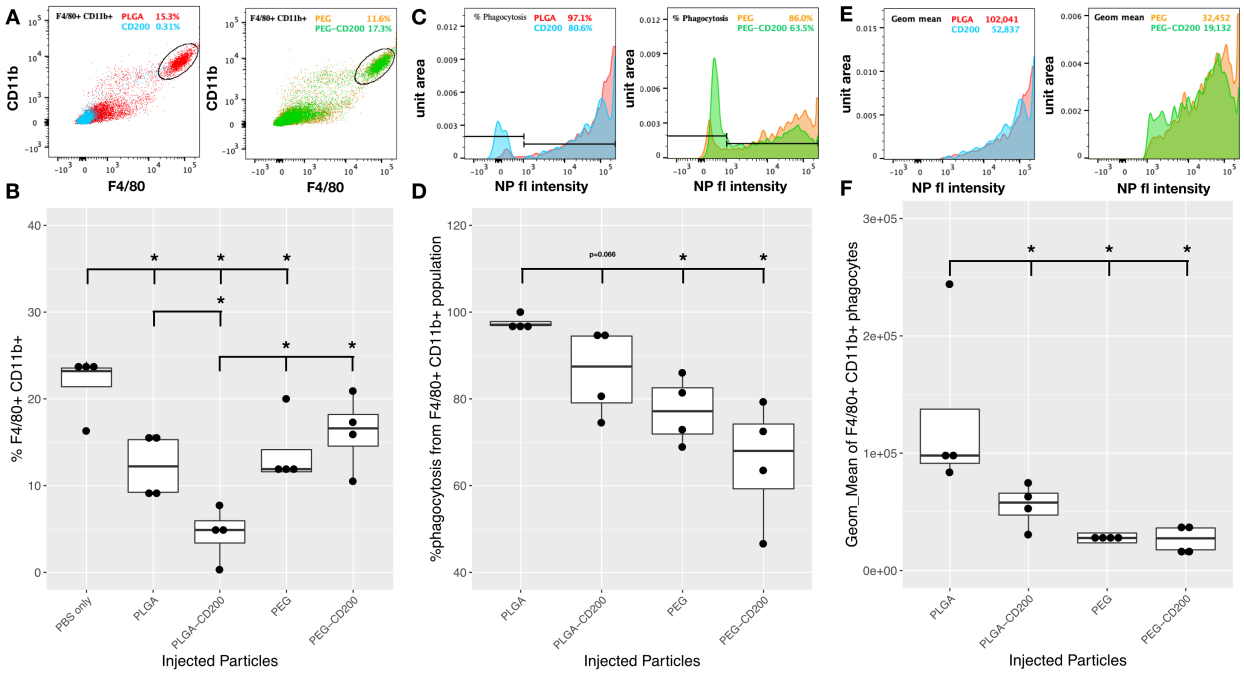

Figure 3.11 F4/80 and CD11b population of peritoneum cavity cells. *(A) Representative flow cytometric histograms of cells expressing F4/80 and CD11b. (B) Quantitative analysis of the percentage of cells with F4/80 and CD11b expressions. (C) Representative flow cytometric histograms of the percentage of phagocytosis in F4/80⁺ and CD11b⁺ population. (D) Graph of % phagocytosis of F4/80⁺ and CD11b⁺ population. (E) Representative flow cytometric histograms with a geometric mean intensity of nanoparticles in the F4/80⁺ and CD11b⁺ phagocytes. (F) Graph of geometric mean intensity of nanoparticles from the F4/80⁺ and CD11b⁺ phagocytes. Data represent the mean ± SD of* n = *4. *p<0.05.*

In addition to F4/80 and CD11b macrophage population, we also investigated F4/80 and CD200R expressing cells. Flow cytometric histograms showed a population of cells expressing both F4/80 and CD200R, and another population with CD200R expression only (Figure 3.12 A). The quantitative result suggested that 28% of cells were expressing both F4/80 and CD200R in the peritoneum cavity after PBS injection, while nanoparticle injections reduced the population, especially in the PLGA-CD200 case (Figure 3.12 B). The nanoparticle fluorescent intensity histograms proposed that CD200 coating reduced the number of phagocytes in comparison to the control cases (Figure 3.12 C). Indeed, the graph of percentage phagocytosis (Figure 3.12 D) demonstrated lower phagocytosis in PLGA-CD200, PLGA-PEG, and PLGA-PEG-CD200

injections. Interestingly, the geometric mean of fluorescent particle intensity indicated higher uptake of PLGA nanoparticles, when compared with CD200-coated PLGA and PEGylated PLGA (Figure 3.12 E and F). Among the four groups of nanoparticles, PLGA-PEG exhibited the lowest geometric mean.

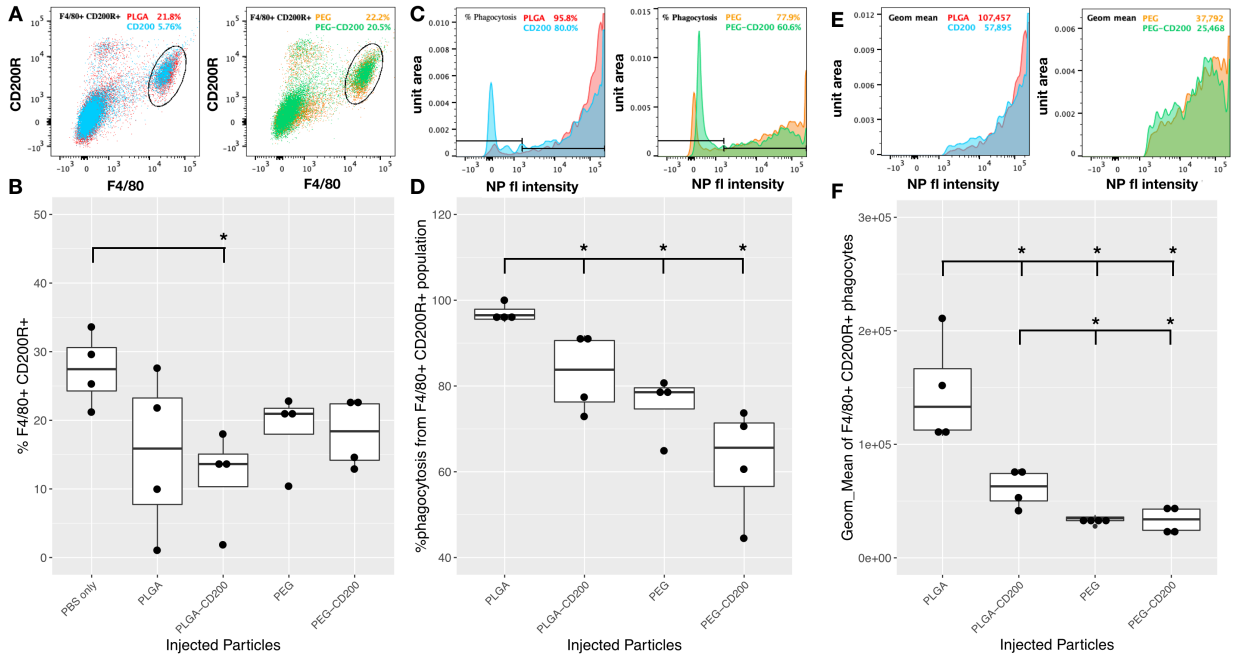

Figure 3.12 F4/80 and CD200R population of peritoneum cavity cells. *(A) Representative flow cytometric histograms of cells expressing F4/80 and CD200R. (B) Quantitative analysis of the percentage of cells with F4/80 and CD200R expressions. (C) Representative flow cytometric histograms of the percentage of phagocytosis in F4/80⁺ and CD200R⁺ population. (D) Graph of % phagocytosis of F4/80⁺ and CD200R⁺ population. (E) Representative flow cytometric histograms with a geometric mean intensity of nanoparticles in the F4/80⁺ and CD200R⁺ phagocytes. (F) Graph of geometric mean intensity of nanoparticles from the F4/80⁺ and CD200R⁺ phagocytes. Data represent the mean ± SD of* n = *4. *p<0.05.*

3.4 Summary

In this chapter, we investigated the immunomodulatory effects of CD200-coated PLGA nanoparticles. We included PLGA-PEG copolymer since the PEGylation of PLGA nanoparticles has been widely studied for its higher stability and improvement in drug delivery. We started with PLGA-PEG copolymer synthesis, followed by nanoparticle fabrications of both PLGA and PLGA-PEG. CD200 was then conjugated on the surface of nanoparticles through carboxyl/amine reactivity with EDC/NHS crosslinker. PEGylated PLGA yielded wider nanoparticle size distribution and larger particles after single emulsion fabrication because of its hydrophilic property. Additionally, hydrophilic PLGA-PEG led to faster degradation of nanoparticles resulting in rapid release of CD200 from the surface. To evaluate the cytotoxicity of different groups of nanoparticles, we performed MTT assay. The results suggested no difference in macrophage metabolic activity upon different nanoparticle uptakes, and the metabolic levels did not decrease 48hr after phagocytosis.

Macrophages are one of the major phagocytes that protect the body by engulfing foreign particles, bacteria, pathogens and clearing dead cells. To look at the immunomodulatory effects of PLGA nanoparticles, we first examined macrophage phagocytosis of different PLGA nanoparticles. Bone marrow-derived macrophages (BMDM) were pre-stimulated with cytokines to differentiate into phenotypes such as non-stimulated (M0), pro-inflammatory (M1), and anti-inflammatory (M2) BMDM. Moreover, due to the diverse functionality of different BMDM phenotypes, we observed the phenotype-dependent effect of CD200-coated nanoparticles. M2 BMDM, which we found to express high CD200R, exhibited the inhibitory effect of CD200 on phagocytosis. This anti-inflammatory BMDM engulfed fewer PLGA-CD200 and PLGA-PEG-CD200 nanoparticles when compared with PLGA and PLGA-PEG respectively. On the contrary, M1 BMDM, a pro-inflammatory phenotype who expresses low CD200, did not uptake CD200-

coated or non-coated nanoparticles differently. In addition to the ability to phagocytose objectives, macrophages also secrete cytokines to initiate communications between different cells. We further examined the cytokine secretions of BMDM in response to different PLGA nanoparticles. Interestingly, CD200 not only performed the immunomodulatory effect on phagocytosis but it also inhibited TNF-alpha secretion, in spite of the fact that there is no difference in IL-10 secretion.

To confirm that the effect on phagocytosis is CD200-mediated, we knocked down CD200R expression and performed phagocytosis assay. In the non-targeted knock-down control BMDM case, the inhibitory effect of CD200 coating on phagocytosis was pronounced, especially in M0 and M2 macrophages. However, CD200R knock-down BMDM phagocytosed similar amounts of nanoparticles independent of their surface modifications, confirming that the inhibitory phagocytic behavior is mediated by CD200-CD200R interaction.

Furthermore, we explored the immunomodulatory effects of CD200-coated nanoparticles *in vivo*. Herein, we conducted intraperitoneal administration of different groups of nanoparticles and examined peritoneal macrophage phagocytosis behavior. The peritoneal macrophage population ($F4/80^+$ and $CD11b^+$) displayed lower uptake of PLGA-CD200, PLGA-PEG, and PLGA-PEG-CD200 in comparison to PLGA nanoparticles. The $F4/80^+$ and $CD200R^+$ population also reveal similar results. Together these data suggest that CD200-coated PLGA nanoparticles can be used as a drug delivery system that inhibits macrophage clearance of foreign particles. Also, CD200-coating on PEGylated PLGA demonstrated more additional inhibitory effects comparing to PEGylated PLGA.

Chapter 4. Conclusions and Future Directions

Material-induced host immune response is one of the current challenges in developing biomedical implants such as biosensor, tissue scaffolds, or drug delivery system [2, 91, 92]. Since the foreign body response usually initiates with protein adsorption on material surfaces, many studies have focused on providing a hydrophilic poly(ethylene glycol) (PEG) surface to prevent serum protein attachment [93-95]. However, numerous studies have recently demonstrated the drawbacks of PEGylated biomaterials [96] such as lower uptake by targeted cells. Therefore, a biological approach to alleviating immune cell activation is essential.

In this Ph.D. study, we modified surfaces of the biomaterial (PLGA) with the extracellular domain of an endogenously expressed protein, CD200. Commercially available PLGA products for medical applications come in various form: mesh, suture, scaffold, microparticles, etc. In order to investigate the immunomodulatory effect of CD200 coating on different geometries, we fabricated CD200-coated PLGA in microparticles (Chapter 2), films (Chapter 2), and nanoparticles (Chapter 3), and examined macrophage activities including cytokine secretions and phagocytosis behavior.

Even though PLGA is relatively biocompatible, bone marrow-derived macrophages exhibited decreased viability with an increased feeding amount of PLGA microparticles (28 μm). CD200-coated PLGA microparticles demonstrated a protective effect on cell viability up to the bead-to-cell ratio of 1-to-2. For cytokine secretion, CD200 diminished TNF-alpha secretion-induced by PLGA, and the inhibitory effect was identical in PLGA film, large microparticles (28 μm) and small microparticles (7 μm). The anti-inflammatory cytokine (IL-10) secretion, on the other hand, is geometry-dependent. CD200-coated PLGA films and 28 μm microparticles enhanced IL-10 secretion significantly, while CD200-coated 7 μm PLGA did not secrete more IL-10 than the control particle case. Interestingly, these 7 μm CD200-coated PLGA microparticles

augmented macrophage phagocytosis. The rationale behind it might be that CD200 initiated a self-clearance process of macrophages without promoting pro-inflammatory activity as suggested by reduced TNF-alpha secretion. Indeed, CD200 expression was found to increase during cell apoptosis [97]. The influence of CD200 on phagocytosis was further carried out on human monocytes and human macrophages. Similarly, human monocytes phagocytosed more CD200-coated PLGA microparticles. In addition, CD200-coated surfaces promoted uptake of opsonized red blood cells by human monocytes and macrophages. In conclusion, CD200-coated PLGA microparticles and films suggested a biomaterial system with an anti-inflammatory property for tissue engineering purposes.

To examine the potential of CD200 on drug delivery applications, we synthesized CD200-coated PLGA nanoparticles and included PEGylated PLGA nanoparticles in the macrophage response studies. Different from what we observed in the microparticle and film geometries, the effect of CD200 on cytokine secretions indicated minimum inhibition of TNF-alpha, and similar levels of IL-10 secretion by BMDM in contacted with CD200-coated nanoparticles. Nevertheless, CD200-coated PLGA nanoparticles downregulated macrophage phagocytosis significantly. The inhibitory phagocytosis was also observed in CD200-coated PEGylated PLGA nanoparticles compared to PEGylated PLGA nanoparticles. The effect was pronounced in both M0 and M2 macrophages, while M1 macrophages displayed high uptake independent of different particle modifications. This inhibitory effect of CD200 coating on phagocytosis was further confirmed with CD200R knock-down study. To evaluate the translational potential of CD200-coated nanoparticles, we administrated nanoparticles intraperitoneally in the mouse model and studied peritoneal macrophage phagocytosis of the nanoparticles. $F4/80^{+}/CD11b^{+}$ population (peritoneal macrophages) was found to phagocytosed fewer CD200-modified nanoparticles, which is

consistent with what we observed in the *in vitro* studies. This data suggested a novel drug delivery system that potentially prolongs circulation.

In this study, we looked at TNF-alpha and IL-10 secretion as representatives of pro-inflammatory and anti-inflammatory cytokine. To understand the complete profile of BMDM functionally, more complex analysis can be performed just as multiplex ELISA to examine broader cytokine secretions. Additionally, inflammatory gene and protein markers (ex. TLR-4, NFkB, iNOS, CD68, and Arginase) can be identified to distinguish CD200-mediated macrophage phenotypes better. We observed geometric dependency of CD200's immunomodulatory effects on both cytokine secretions and phagocytosis. For example, the cytokine inhibitory effect of CD200 diminished with smaller geometries, such as small microparticles and nanoparticles. And CD200-coated microparticles enhanced phagocytosis, while CD200-coated nanoparticles decreased uptake. The mechanism behind the integrated effects of size and CD200 still need to be further investigated. Even though we observed no metabolic level difference between different nanoparticles, it is valuable to understand the internal trafficking after nanoparticle uptakes, such as lysosome localization (LAMP-1 and particle localization), cell autophagy (LC3B expression), and cell apoptosis (BCL-2 expression). In additional to mouse macrophages, we also examined the translational potential toward different species such as human monocytes and macrophages. Cross-species functionality of CD200 can also be explored to expand its potential applications. Furthermore, in-depth *in vivo* studies should also be performed to evaluate clinical potentials. For instance, biodistribution study could bring a detailed understanding of CD200-coated nanoparticles as systematic drug delivery vehicles.

With the proven anti-inflammatory property of CD200-coated biomaterial, we hypothesize that this unique system can be used as a potential treatment for inflammatory diseases, such as osteoarthritis (OA). OA is a complex joint disease rising various degrees of inflammation in the

synovium (Figure 4.1). Although the mechanisms behind OA are not fully understood, a severe problem is the continuous regression of inflammation and cartilage degradation, making OA not treatable with a single therapy. Controlling inflammation is crucial to facilitate the regenerative environment in OA patients, and this is where the anti-inflammatory property of CD200 can take place. One hypothesis is that delivery of CD200 to synovial macrophages will inhibit pro-inflammatory activity in the synovium and promote a pro-healing environment to assist OA joint regeneration. The study may include the examination of the functionality of the mouse CD200 on the arthritis animal model to ensure species-reactivity, the survey on synovial macrophage activities and the investigation of CD200-coated microparticles in the arthritis model.

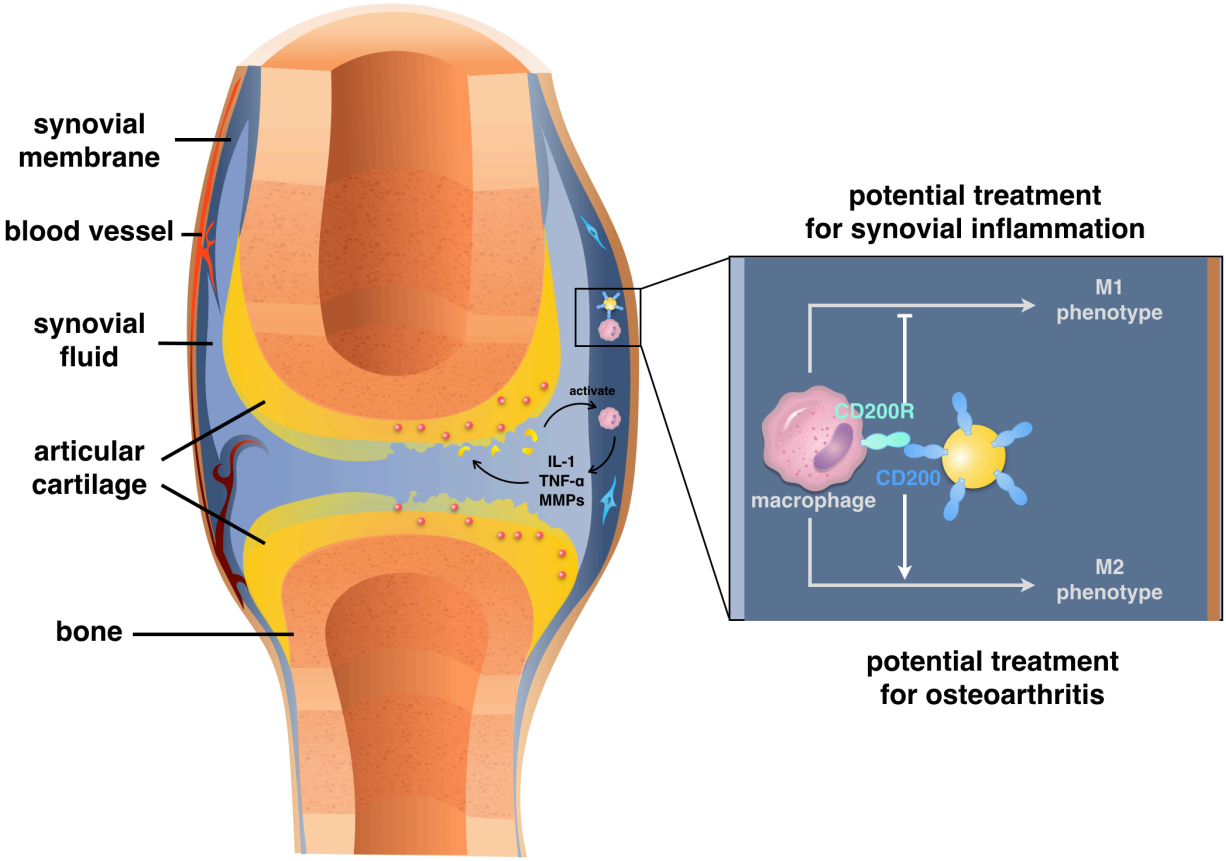

Figure 4.1 Illustration of osteoarthritis (OA) and proposal of using CD200-coated microparticles for synovial inflammation treatment.

REFERENCE

1. Hubbell, J.A., *Biomaterials in tissue engineering.* Bio/technology (Nature Publishing Company), 1995. **13**(6): p. 565-576.
2. Anderson, J.M., A. Rodriguez, and D.T. Chang, *Foreign body reaction to biomaterials.* Semin Immunol, 2008. **20**(2): p. 86-100.
3. Wilson, C.J., et al., *Mediation of biomaterial-cell interactions by adsorbed proteins: a review.* Tissue engineering, 2005. **11**(1-2): p. 1-18.
4. Luttikhuizen, D.T., M.C. Harmsen, and M.J.V. Luyn, *Cellular and molecular dynamics in the foreign body reaction.* Tissue engineering, 2006. **12**(7): p. 1955-1970.
5. DiPietro, L.A., *Wound healing: the role of the macrophage and other immune cells.* Shock, 1995. **4**(4): p. 233-240.
6. Hoek, R.M., et al., *Down-regulation of the macrophage lineage through interaction with OX2 (CD200).* Science, 2000. **290**(5497): p. 1768-71.
7. Oldenborg, P.-A., et al., *Role of CD47 as a marker of self on red blood cells.* Science, 2000. **288**(5473): p. 2051-2054.
8. Sarrazin, S., W.C. Lamanna, and J.D. Esko, *Heparan sulfate proteoglycans.* Cold Spring Harbor perspectives in biology, 2011. **3**(7): p. a004952.
9. Chen, E.Y., et al., *Understanding and utilizing the biomolecule/nanosystems interface*, in *Nanotechnologies in Preventive and Regenerative Medicine*. 2018, Elsevier. p. 207-297.
10. Kim, Y.K., E.Y. Chen, and W.F. Liu, *Biomolecular strategies to modulate the macrophage response to implanted materials.* J. Mater. Chem. B, 2016. **4**(9): p. 1600-1609.
11. Ward, W.K., *A review of the foreign-body response to subcutaneously-implanted devices: the role of macrophages and cytokines in biofouling and fibrosis.* Journal of diabetes science and technology, 2008. **2**(5): p. 768-777.
12. Badylak, S.F., et al., *Macrophage phenotype as a determinant of biologic scaffold remodeling.* Tissue Eng Part A, 2008. **14**(11): p. 1835-42.
13. McBride, W.H., *Phenotype and functions of intratumoral macrophages.* Biochimica et Biophysica Acta (BBA) - Reviews on Cancer, 1986. **865**(1): p. 27-41.
14. Mantovani, A., et al., *Macrophage plasticity and polarization in tissue repair and remodelling.* J Pathol, 2013. **229**(2): p. 176-85.
15. Gordon, S. and F.O. Martinez, *Alternative Activation of Macrophages: Mechanism and Functions.* Immunity, 2010. **32**(5): p. 593-604.
16. Mantovani, A., et al., *The chemokine system in diverse forms of macrophage activation and polarization.* Trends in immunology, 2004. **25**(12): p. 677-686.
17. Mosser, D.M. and J.P. Edwards, *Exploring the full spectrum of macrophage activation.* Nat Rev Immunol, 2008. **8**(12): p. 958-69.
18. Galli, S.J., N. Borregaard, and T.A. Wynn, *Phenotypic and functional plasticity of cells of innate immunity: macrophages, mast cells and neutrophils.* Nature immunology, 2011. **12**(11): p. 1035-1044.
19. Smith, T.D., et al., *Harnessing macrophage plasticity for tissue regeneration.* 2017. **114**: p. 193-205.

20. Morais, J.M., F. Papadimitrakopoulos, and D.J. Burgess, *Biomaterials/tissue interactions: possible solutions to overcome foreign body response.* The AAPS journal, 2010. **12**(2): p. 188-196.
21. Ward, W.K., et al., *The effect of microgeometry, implant thickness and polyurethane chemistry on the foreign body response to subcutaneous implants.* Biomaterials, 2002. **23**(21): p. 4185-4192.
22. Hotchkiss, K.M., et al., *Titanium surface characteristics, including topography and wettability, alter macrophage activation.* Acta Biomaterialia, 2016. **31**: p. 425-434.
23. Blakney, A.K., M.D. Swartzlander, and S.J. Bryant, *The effects of substrate stiffness on the in vitro activation of macrophages and in vivo host response to poly(ethylene glycol)-based hydrogels.* Journal of Biomedical Materials Research Part A, 2012. **100A**(6): p. 1375-1386.
24. Hezi-Yamit, A., et al., *Impact of polymer hydrophilicity on biocompatibility: implication for DES polymer design.* J Biomed Mater Res A, 2009. **90**(1): p. 133-41.
25. Lynn, A.D. and S.J. Bryant, *Phenotypic changes in bone marrow-derived murine macrophages cultured on PEG-based hydrogels activated or not by lipopolysaccharide.* Acta Biomater, 2011. **7**(1): p. 123-32.
26. Thevenot, P., W. Hu, and L. Tang, *Surface chemistry influences implant biocompatibility.* Curr Top Med Chem, 2008. **8**(4): p. 270-80.
27. Kim, Y.K., et al., *Modification of biomaterials with a self-protein inhibits the macrophage response.* Adv Healthc Mater, 2014. **3**(7): p. 989-94.
28. Zaveri, T.D., et al., *Integrin-directed modulation of macrophage responses to biomaterials.* Biomaterials, 2014. **35**(11): p. 3504-15.
29. Lynn, A.D., et al., *Temporal progression of the host response to implanted poly(ethylene glycol)-based hydrogels.* J Biomed Mater Res A, 2011. **96**(4): p. 621-31.
30. Lynn, A.D., T.R. Kyriakides, and S.J. Bryant, *Characterization of the in vitro macrophage response and in vivo host response to poly(ethylene glycol)-based hydrogels.* J Biomed Mater Res A, 2010. **93**(3): p. 941-53.
31. Zaveri, T.D., et al., *Macrophage integrins modulate response to ultra-high molecular weight polyethylene particles and direct particle-induced osteolysis.* Biomaterials, 2017. **115**: p. 128-140.
32. Blakney, A.K., M.D. Swartzlander, and S.J. Bryant, *The effects of substrate stiffness on the in vitro activation of macrophages and in vivo host response to poly(ethylene glycol)-based hydrogels.* J Biomed Mater Res A, 2012. **100**(6): p. 1375-86.
33. Mokarram, N., et al., *Effect of modulating macrophage phenotype on peripheral nerve repair.* Biomaterials, 2012. **33**(34): p. 8793-8801.
34. Spiller, K.L., et al., *Sequential delivery of immunomodulatory cytokines to facilitate the M1-to-M2 transition of macrophages and enhance vascularization of bone scaffolds.* Biomaterials, 2015. **37**: p. 194-207.
35. Oldenborg, P.A., et al., *Role of CD47 as a marker of self on red blood cells.* Science, 2000. **288**(5473): p. 2051-4.
36. Rodriguez, P.L., et al., *Minimal "Self" peptides that inhibit phagocytic clearance and enhance delivery of nanoparticles.* Science, 2013. **339**(6122): p. 971-5.

37. Finley, M.J., et al., *Diminished adhesion and activation of platelets and neutrophils with CD47 functionalized blood contacting surfaces.* Biomaterials, 2012. **33**(24): p. 5803-11.
38. Slee, J.B., et al., *Enhanced biocompatibility of CD47-functionalized vascular stents.* Biomaterials, 2016. **87**: p. 82-92.
39. Koning, N., et al., *Expression of the Inhibitory CD200 Receptor Is Associated with Alternative Macrophage Activation.* Journal of Innate Immunity, 2010. **2**(2): p. 195-200.
40. Holmannová, D., et al., *CD200/CD200R paired potent inhibitory molecules regulating immune and inflammatory responses; Part I: CD200/CD200R structure, activation, and function.* acta Medica (hradec Králové), 2012. **55**(1): p. 12-17.
41. Zhang, S., et al., *Molecular Mechanisms of CD200 Inhibition of Mast Cell Activation.* The Journal of Immunology, 2004. **173**(11): p. 6786-6793.
42. Mihrshahi, R. and M.H. Brown, *Downstream of Tyrosine Kinase 1 and 2 Play Opposing Roles in CD200 Receptor Signaling.* The Journal of Immunology, 2010. **185**(12): p. 7216-7222.
43. Jenmalm, M.C., et al., *Regulation of Myeloid Cell Function through the CD200 Receptor.* The Journal of Immunology, 2006. **176**(1): p. 191-199.
44. Rygiel, T.P. and L. Meyaard, *CD200R signaling in tumor tolerance and inflammation: A tricky balance.* Current opinion in immunology, 2012. **24**(2): p. 233-238.
45. Hoek, R.M., et al., *Down-regulation of the macrophage lineage through interaction with OX2 (CD200).* Science, 2000. **290**(5497): p. 1768-1771.
46. Wright, G.J., et al., *Lymphoid/neuronal cell surface OX2 glycoprotein recognizes a novel receptor on macrophages implicated in the control of their function.* Immunity, 2000. **13**(2): p. 233-42.
47. Chakera, A., et al., *The phenotype of circulating follicular-helper T cells in patients with rheumatoid arthritis defines CD200 as a potential therapeutic target.* 2012. **2012**.
48. Gorczynski, R.M., et al., *CD200 immunoadhesin suppresses collagen-induced arthritis in mice.* 2001. **101**(3): p. 328-334.
49. Walker, D.G. and L.-F. Lue, *Understanding the neurobiology of CD200 and the CD200 receptor: a therapeutic target for controlling inflammation in human brains?* Future neurology, 2013. **8**(3): p. 321-332.
50. Snelgrove, R.J., et al., *A critical function for CD200 in lung immune homeostasis and the severity of influenza infection.* 2008. **9**(9): p. 1074.
51. Kim, Y.K., et al., *Modification of Biomaterials with a Self-Protein Inhibits the Macrophage Response.* Advanced Healthcare Materials, 2014. **3**(7): p. 989-994.
52. Lee, S.C., et al., *Healing of large segmental defects in rat femurs is aided by RhBMP‐2 in PLGA matrix.* Journal of biomedical materials research, 1994. **28**(10): p. 1149-1156.
53. Tai, I.c., et al., *Local delivery of controlled-release simvastatin/PLGA/HAp microspheres enhances bone repair.* International journal of nanomedicine, 2013. **8**: p. 3895.
54. Uematsu, K., et al., *Cartilage regeneration using mesenchymal stem cells and a three-dimensional poly-lactic-glycolic acid (PLGA) scaffold.* Biomaterials, 2005. **26**(20): p. 4273-4279.
55. Cohen-Sela, E., et al., *A new double emulsion solvent diffusion technique for encapsulating hydrophilic molecules in PLGA nanoparticles.* Journal of controlled release, 2009. **133**(2): p. 90-95.

56. Zweers, M.L.T., et al., *Release of anti-restenosis drugs from poly (ethylene oxide)-poly (DL-lactic-co-glycolic acid) nanoparticles.* Journal of controlled release, 2006. **114**(3): p. 317-324.
57. Westedt, U., et al., *Poly (vinyl alcohol)-graft-poly (lactide-co-glycolide) nanoparticles for local delivery of paclitaxel for restenosis treatment.* Journal of controlled release, 2007. **119**(1): p. 41-51.
58. Chung, H.J., et al., *Heparin immobilized porous PLGA microspheres for angiogenic growth factor delivery.* Pharmaceutical research, 2006. **23**(8): p. 1835-1841.
59. Wang, X., et al., *Growth factor gradients via microsphere delivery in biopolymer scaffolds for osteochondral tissue engineering.* Journal of Controlled Release, 2009. **134**(2): p. 81-90.
60. Danhier, F., et al., *PLGA-based nanoparticles: an overview of biomedical applications.* Journal of controlled release, 2012. **161**(2): p. 505-522.
61. Galeska, I., et al., *Controlled release of dexamethasone from PLGA microspheres embedded within polyacid-containing PVA hydrogels.* Aaps Journal, 2005. **7**(1): p. E231-E240.
62. Gu, B., Y. Wang, and D.J. Burgess, *In vitro and in vivo performance of dexamethasone loaded PLGA microspheres prepared using polymer blends.* International Journal of Pharmaceutics, 2015. **496**(2): p. 534-540.
63. Ju, Y.M., et al., *A dexamethasone‐loaded PLGA microspheres/collagen scaffold composite for implantable glucose sensors.* Journal of Biomedical Materials Research Part A, 2010. **93**(1): p. 200-210.
64. Hickey, T., et al., *In vivo evaluation of a dexamethasone/PLGA microsphere system designed to suppress the inflammatory tissue response to implantable medical devices.* Journal of biomedical materials research, 2002. **61**(2): p. 180-187.
65. Hickey, T., et al., *Dexamethasone/PLGA microspheres for continuous delivery of an anti-inflammatory drug for implantable medical devices.* Biomaterials, 2002. **23**(7): p. 1649-1656.
66. Kumari, A., et al., *Biodegradable polymeric nanoparticles based drug delivery systems.* 2010. **75**(1): p. 1-18.
67. Bhardwaj, U., et al., *Controlling acute inflammation with fast releasing dexamethasone-PLGA microsphere/pva hydrogel composites for implantable devices.* J Diabetes Sci Technol, 2007. **1**(1): p. 8-17.
68. Patil, S.D., F. Papadimitrakopoulos, and D.J. Burgess, *Dexamethasone-loaded poly(lactic-co-glycolic) acid microspheres/poly(vinyl alcohol) hydrogel composite coatings for inflammation control.* Diabetes Technol Ther, 2004. **6**(6): p. 887-97.
69. Patil, S.D., F. Papadmitrakopoulos, and D.J. Burgess, *Concurrent delivery of dexamethasone and VEGF for localized inflammation control and angiogenesis.* J Control Release, 2007. **117**(1): p. 68-79.
70. Bobak, D.A., et al., *Modulation of FcR function by complement: subcomponent C1q enhances the phagocytosis of IgG-opsonized targets by human monocytes and culture-derived macrophages.* The Journal of Immunology, 1987. **138**(4): p. 1150-1156.

71. Nepomuceno, R.R., et al., *C1qRP Is a Heavily O-Glycosylated Cell Surface Protein Involved in the Regulation of Phagocytic Activity.* The Journal of Immunology, 1999. **162**(6): p. 3583-3589.
72. Green, T., et al., *Polyethylene particles of a 'critical size'are necessary for the induction of cytokines by macrophages in vitro.* 1998. **19**(24): p. 2297-2302.
73. Chono, S., et al., *Uptake characteristics of liposomes by rat alveolar macrophages: influence of particle size and surface mannose modification.* 2007. **59**(1): p. 75-80.
74. Yue, H., et al., *Particle size affects the cellular response in macrophages.* 2010. **41**(5): p. 650-657.
75. Doshi, N. and S.J.P.o. Mitragotri, *Macrophages recognize size and shape of their targets.* 2010. **5**(4): p. e10051.
76. Champion, J.A., A. Walker, and S. Mitragotri, *Role of Particle Size in Phagocytosis of Polymeric Microspheres.* Pharmaceutical Research, 2008. **25**(8): p. 1815-1821.
77. Murray, P.J. and T.A.J.N.r.i. Wynn, *Protective and pathogenic functions of macrophage subsets.* 2011. **11**(11): p. 723.
78. Scott, R.S., et al., *Phagocytosis and clearance of apoptotic cells is mediated by MER.* Nature, 2001. **411**(6834): p. 207-211.
79. Savill, J.S., et al., *Macrophage phagocytosis of aging neutrophils in inflammation. Programmed cell death in the neutrophil leads to its recognition by macrophages.* Journal of Clinical Investigation, 1989. **83**(3): p. 865-875.
80. Fraser, D.A., et al., *C1q differentially modulates phagocytosis and cytokine responses during ingestion of apoptotic cells by human monocytes, macrophages, and dendritic cells.* 2009. **183**(10): p. 6175-6185.
81. Bobak, D., et al., *Modulation of FcR function by complement: subcomponent C1q enhances the phagocytosis of IgG-opsonized targets by human monocytes and culture-derived macrophages.* 1987. **138**(4): p. 1150-1156.
82. Webster, S.D., et al., *Antibody-mediated phagocytosis of the amyloid ß-peptide in microglia is differentially modulated by C1q.* 2001. **166**(12): p. 7496-7503.
83. Fraser, D.A., et al., *C1q and MBL, components of the innate immune system, influence monocyte cytokine expression.* 2006. **80**(1): p. 107-116.
84. Avgoustakis, K., *Pegylated poly (lactide) and poly (lactide-co-glycolide) nanoparticles: preparation, properties and possible applications in drug delivery.* Current drug delivery, 2004. **1**(4): p. 321-333.
85. Vila, A., et al., *Transport of PLA-PEG particles across the nasal mucosa: effect of particle size and PEG coating density.* Journal of Controlled Release, 2004. **98**(2): p. 231-244.
86. Park, J., et al., *PEGylated PLGA nanoparticles for the improved delivery of doxorubicin.* 2009. **5**(4): p. 410-418.
87. Vij, N., et al., *Development of PEGylated PLGA nanoparticle for controlled and sustained drug delivery in cystic fibrosis.* Journal of nanobiotechnology, 2010. **8**(1): p. 22.
88. Betancourt, T., et al., *PEGylation strategies for active targeting of PLA/PLGA nanoparticles.* Journal of Biomedical Materials Research Part A: An Official Journal of The Society for Biomaterials, The Japanese Society for Biomaterials, and The Australian Society for Biomaterials and the Korean Society for Biomaterials, 2009. **91**(1): p. 263-276.

89. Danhier, F., et al., *Paclitaxel-loaded PEGylated PLGA-based nanoparticles: in vitro and in vivo evaluation.* Journal of controlled release, 2009. **133**(1): p. 11-17.
90. Kamaly, N., et al., *Development and in vivo efficacy of targeted polymeric inflammation-resolving nanoparticles.* Proceedings of the National Academy of Sciences, 2013. **110**(16): p. 6506-6511.
91. Anderson, J.M., *Biological responses to materials.* Annual Review of Materials Research, 2001. **31**: p. 81-110.
92. Hu, W.-J., et al., *Molecular basis of biomaterial-mediated foreign body reactions.* Blood, 2001. **98**(4): p. 1231-1238 %@ 0006-4971.
93. Kim, J.-Y., et al., *The use of PEGylated liposomes to prolong circulation lifetimes of tissue plasminogen activator.* Biomaterials, 2009. **30**(29): p. 5751-5756.
94. Roux, E., et al., *Serum-stable and long-circulating, PEGylated, pH-sensitive liposomes.* Journal of controlled release, 2004. **94**(2-3): p. 447-451.
95. Fishburn, C.S., *The pharmacology of PEGylation: balancing PD with PK to generate novel therapeutics.* Journal of pharmaceutical sciences, 2008. **97**(10): p. 4167-4183.
96. Verhoef, J.J. and T.J. Anchordoquy, *Questioning the use of PEGylation for drug delivery.* Drug delivery and translational research, 2013. **3**(6): p. 499-503.
97. Rosenblum, M.D., et al., *CD200 is a novel p53-target gene involved in apoptosis-associated immune tolerance.* Blood, 2004. **103**(7): p. 2691-2698.